5-2017

Translational Pharmacokinetic-Pharmacodynamic Modeling and Simulation in the Development of Spectinamides, a Novel Class of Anti-Tuberculosis Agents

Chetan Rathi
University of Tennessee Health Science Center

Translational Pharmacokinetic-Pharmacodynamic Modeling and Simulation in the Development of Spectinamides, a Novel Class of Anti-Tuberculosis Agents

ORCID
http://orcid.org/0000-0003-1015-5199

DOI
10.21007/etd.cghs.2017.0428

Translational Pharmacokinetic-Pharmacodynamic Modeling and Simulation in the Development of Spectinamides, a Novel Class of Anti-Tuberculosis Agents

A Dissertation
Presented for
The Graduate Studies Council
The University of Tennessee
Health Science Center

In Partial Fulfillment
Of the Requirements for the Degree
Doctor of Philosophy
From The University of Tennessee

By
Chetan Rathi
May 2017

DEDICATION

To my family, friends and teachers for their endless love and support.

ACKNOWLEDGEMENTS

The journey of obtaining my Doctorate in Philosophy could not have come true without the tremendous support and encouragement from so many people. First and foremost, I would like to express my deepest gratitude to my mentor Dr. Bernd Meibohm for providing me the opportunity to work on challenging projects in a multidisciplinary environment. This allowed me to apply and expand my scientific skill set and in the process learn more about different aspects of drug discovery and development. His teachings also helped me in laying out a strong foundation in pharmacokinetics and pharmacodynamics of small molecules and biologics. Dr. Meibohm provided me with a lot of flexibility to try out different approaches and this helped me to think independently in finding solutions to the challenges encountered during experiments. I would also like to extend my sincere thanks to all my committee members, Drs. Richard E. Lee, Andrea N. Edginton, Charles R. Yates, and P David Rogers for their suggestions, guidance and assistance over the years.

I greatly appreciate the help of Dr. Richard E. Lee at the Department of Chemical Biology and Therapeutics, St. Jude Children's Research Hospital for his insights as well as his lab members Drs Jiuyu Liu, Samanthi Waidyarachchi and David Bruhn for synthesizing the compounds required for the pharmacokinetic studies and generating the MIC data.

I am also extremely thankful to our collaborators Dr. Anne Lenaerts, Dr. Mercedes Gonzalez-Juarrero, Michael S. Scherman and Dr. Gregory T. Robertson at the Department of Microbiology, Immunology and Pathology, Colorado State University for conducting intratracheal PK study and *in vivo* studies in TB infected mice, and providing me with the data required for PK/PD modeling. I would especially like to thank Dr. Andrea N. Edginton for introducing me to PK-Sim software and proving me the guidance required for learning PBPK modeling and simulation.

A special thanks to my friends and colleagues, Dr. Dorababu Madhura, Dr. Ashit Trivedi, Dr. Josiah Ryman, Dr. Pradeep Lukka, Santosh Wagh, Dr. Dorina van der Mey and Dr. Andrew Nishimoto for their wonderful company and enlightening discussions over all these years. I also extend my gratitude to rest of my friends for all their friendship and for making my stay in Memphis an enjoyable experience. I would like to thank the National Institutes of Health and the American Lebanese Syrian Associated Charities for providing the financial support to do my research work.

I would also like to thank all administrative staffs, Shelley Cannioto, Brenda Thornton, Corliss Finlay, Benita Williams and Lisa Schaffer for their suggestions and administrative helps to make my work go smoothly.

I would like to thank my parents and my sister; no words would be enough to thank their support and patience during the completion of this dissertation. Finally, I would like to thank God for everything that I have today.

ABSTRACT

New chemotherapeutic agents are urgently needed to control the spread of multidrug-resistant (MDR) and extensively drug-resistant (XDR) forms of tuberculosis, which still remains an important public health challenge globally. Recently, spectinamides have emerged as a novel class of anti-tuberculosis agents that overcome the native drug efflux. Spectinamides bind to the 30S bacterial ribosomal subunit which interferes with ribosomal translocation, and ultimately results in inhibition of protein synthesis. They have potent *in vitro* activity against drug resistant *Mycobacterium tuberculosis* (*Mtb*), and also demonstrated sustained efficacy in *Mtb*-infected mouse models. Pharmacokinetic (PK)/ pharmacodynamic (PD) analyses play a critical role in identifying the optimum dosing regimen for new treatments. In this dissertation, I hypothesized that the application of translational PK/PD modeling and simulation techniques would facilitate rational dosage regimen design for spectinamides.

To characterize the dose-exposure-response of Lee 1810, a dose-fractionation study was performed in BALB/c mice infected with a low dose aerosol of *Mtb*. Dosing with different dosing regimens was continued for 4 weeks with two blood samples obtained from each mice in the last week, followed by a washout period after which the mice were sacrificed and the lungs removed for measurement of colony forming units (CFU). Drug concentrations in plasma were analyzed with a validated LC-MS/MS method followed by a population PK analysis which also included as anchor point the data of a PK study in healthy mice with intensive sampling. A model for natural bacterial growth in *Mtb* infection in untreated mice was built from data on the natural history of *Mtb* infection in mice obtained from previously performed studies and from the literature. Based on the individual *post hoc* estimates from the population PK modeling, a sequential PK/PD analysis was performed by linking the PK model with the bacterial growth model via an exposure-dependent bacterial kill function that included a sigmoid E_{max} model for describing the overall rate of change in lung CFU with different dosing regimens. A two-compartment model with first-order absorption was used to describe the pharmacokinetics of Lee 1810. The average absorption rate constant (K_a), clearance (CL/F), volume of the central compartment (V_c/F), intercompartmental clearance (Q/F), and volume of the peripheral compartment (V_p/F) was estimated to be 2.31 h^{-1},1.17 L/h/kg, 0.435 L/kg, 0.0191 L/h/kg, and 0.161 L/kg, respectively. The inter-individual variability in CL/F was estimated as 19.9 %. The pharmacokinetics of Lee 1810 was found to be different between healthy and infected mice with the later having 56.5% lower CL/F, 69% lower V_c/F and 69.6% lower Q/F. The two-subpopulation model could successfully describe the natural bacterial growth. The replication rate constant (K_{rep}) of *Mtb* was calculated as 0.0327 h^{-1} which is consistent with values reported in the literature. The death rate constant induced by the immune system (K_{ir}) was 0.00303 h^{-1}, cell count of fast growing population at the initiation of the infection ($N_{1,0}$) was 1.93 Log CFU and maximum number of bacteria (N_{max}) was 6.44 Log CFU. The inter-individual variability in K_{rep} and N_{max} was estimated as 70.8 % and 54.7%, respectively. The bacterial kill induced by the drug was described using a sigmoid E_{max} model. The drug effect

parameters (EC_{50}), maximum kill rate (E_{max}) and Hill coefficient (γ), were estimated as 239 μg/mL, 11.9 h^{-1} and 2.40 respectively. A Hill coefficient substantially greater than 1 is a typical characteristic of concentration-dependent killing. The concentration-dependent killing characteristic of Lee 1810 supports its intermittent dosing.

Poor permeability of spectinamides across the gut limits its oral use. Additionally, since the lungs are the main site of infection in pulmonary TB, the efficacy of lead spectinamide Lee 1599 was evaluated after intratracheal (IT) administration in a mouse model of *Mtb* infection. A dose of 200 mg/kg TIW (3 days a week) for 28 days resulted in excellent efficacy with 2.2 Log CFU reduction in the lungs. Based on these observations, a comparative biodistribution study of Lee 1599 was performed after IT and SC administration in mice. Plasma and tissue samples were collected at pre-specified time points. The drug was extracted from plasma and homogenized tissues after protein precipitation and analyzed with an LC-MS/MS assay. The rate and extent of absorption was almost two times higher with IT as compared to SC administration. As expected, the highest exposure of Lee 1599 after IT administration was attained in the lungs, which was 2.5 times higher than in plasma. This is highly desirable as lungs are the main site of infection in pulmonary tuberculosis. Overall, this study supports the pulmonary route as a potential pathway for the treatment of tuberculosis with Lee 1599.

Physiologically-based pharmacokinetic (PBPK) modeling and simulation is a powerful methodology used in support of dose selection for first-in-human studies. The objective was to develop a PBPK model for describing pharmacokinetics of Lee 1599 in rats and mice, and to extrapolate this PK behavior to humans. 10 mg/kg of Lee 1599 was administered intravenously to rats and 200 mg/kg subcutaneously to mice. The PBPK model was developed based on the observed rat plasma concentrations, physicochemical properties of Lee 1599, and *in vitro* data from its metabolism, protein binding and permeability. The concentration-time profile of Lee 1599 in rats was well described by the optimized PBPK model. The model was prospectively qualified by PBPK scaling from rats to mice and comparing predicted murine concentration-time profiles to observed plasma concentrations. This model was also successful in predicting murine PK with observed PK parameters within two-folds of predicted values. The model predicted, weight normalized human clearance of 0.25 L/h/kg was as expected less than the values in rats (0.666 L/h/kg) and mice (1.25 L/h/kg). The PBPK model predicted, a dose of 7.5 mg/kg and 27.5 mg/kg administered once daily via intravenous administration will be required to attain similar exposure as observed in mice after subcutaneous administration of 50 mg/kg and 200 mg/kg respectively. This model suggests that an efficacious systemic exposure can be achieved with daily doses feasible in humans, and may be useful during drug development for understanding the dose requirements for future human studies.

In conclusion, translational PK/PD approaches have been successfully used for the further development and characterization of spectinamides leads Lee 1599 and Lee 1810. The results from the above studies will be helpful in identifying and optimizing the dosing regimens which can strike a balance between bacterial reduction, adverse effects, and emergence of resistance.

TABLE OF CONTENTS

LIST OF TABLES

LIST OF FIGURES

LIST OF ABBREVIATIONS

AAG	α1 acid glycoprotein
ADME	Absorption, distribution, metabolism, and excretion
AUC	Area under the curve
BDDCS	Biopharmaceutical Drug Disposition and Classification System
BID	Twice daily
BIW	Twice weekly
BSL	Biosafety level
BSV	Between-subject variability
CF	Cystic fibrosis
CFU	Colony forming unit
cLogP	Calculated partition-coefficient
FDA	Food and Drug Administration
FOCE	First-order conditional estimation
HILIC	Hydrophilic interaction chromatography
HPLC	High performance liquid chromatography
IT	Intratracheal
IV	Intravenous
LC-MS/MS	Liquid chromatography-mass spectrometry
LDA	Low dose aerosol
LTBS	Log-transform both sides
MDR	Multidrug-resistant
MIC	Minimum inhibitory concentration
Mtb	*Mycobacterium Tuberculosis*
m/z	Mass/Charge ratio
OADC	Oleic acid-albumin-dextrose-catalase
OBJ	Objective function value
PAE	Post antibiotic effect
PBPK	Physiologically-based pharmacokinetic modeling
PD	Pharmacodynamic
PK	Pharmacokinetic
PK/PD	Pharmacokinetics/Pharmacodynamics
PZA	Pyrazinamide
QD	Once daily
QW	Once weekly
RSE	Relative standard error
RUV	Residual unexplained variability
SC	Subcutaneous
TB	Tuberculosis
TIW	Thrice weekly
VPC	Visual predictive check
XDR	Extremely drug-resistant

CHAPTER 1. TRANSLATIONAL PK/PD OF ANTI-INFECTIVE THERAPEUTICS*

Introduction

The treatment options available to combat infectious diseases are becoming increasingly limited due to a rising incidence of resistance among bacteria against the currently used antibiotics. Additionally, the discovery and development of new antibiotics has slowed down because of limited incentives for the pharmaceutical industry in this therapeutic area and a high benefit-risk ratio of existing antibiotics [1]. This necessitates prudent use of the currently clinically available as well as newly developed antibiotics. One of the key requirements for preserving clinical efficacy of antibiotics and avoiding tolerance development is to identify the optimum dosing schedule for maximum bacterial kill and minimal emergence of resistance [2]. Although standard pharmacokinetic (PK)/ pharmacodynamic (PD) indices have been used for this purpose with some clinical success, this approach is associated with several drawbacks. One of them is the high dependence upon the minimum inhibitory concentration (MIC), which is limited to a single efficacy endpoint that does not take into account the entire time course of effect and may vary between treated individuals and bacterial strains [3].

Translational PK/PD modeling and simulation has emerged as an alternative strategy to characterize the relationship between dose, exposure and response for identifying the most suitable dosing regimen. For example, infections with *Mycobacterium tuberculosis* are usually characterized by the presence of both multiplying and non-multiplying bacteria, and most antibiotics are usually more effective in killing multiplying rather than non-multiplying microorganisms. Mechanistic PK/PD models have successfully been applied to delineate the independent drug effects associated with killing of the multiplying and the non-multiplying bacterial populations [4]. In another example, different dosing regimens with similar exposure to colistin resulted in greater emergence of resistance with longer dosing intervals. Based on this observation, PK/PD models have subsequently been used for simulating untested dosing scenarios and developing an optimum dosing regimen for colistin [5].

It is the purpose of this review to provide an overview on the mechanism-based PK/PD models applied in translational PK/PD modeling for antibiotics.

PK/PD Indices

For decades, the PK/PD relationships of antibiotics have been categorized with three different PK/PD indices, which rely on a summary measurement of *in vivo* drug

*This chapter adapted with permission. Rathi, C., R.E. Lee, and B. Meibohm, *Translational PK/PD of anti-infective therapeutics.* Drug Discov Today Technol, 2016. **21-22**: p. 41-49[6].

exposure relative to the MIC, determined *in vitro* using serial dilution steps [7]. Usually, only free rather than total drug concentrations are considered as only free drug which is not bound to plasma proteins exerts the pharmacological activity. Standardized notations for these PK/PD indices are AUC/MIC, C_{max}/MIC and T>MIC. AUC/MIC is the ratio of area under the free plasma concentration-time curve relative to MIC, C_{max}/MIC is the ratio of free peak plasma concentration relative to MIC, and T>MIC is the cumulative percentage of a time period that the free concentration is above MIC. Antibiotics that are classified as having their efficacy driven by T>MIC show time-dependent killing which suggests that the antibacterial effect is at its maximum with concentrations just above the MIC and no further improvement in killing is obtained by further increasing the concentrations. C_{max}/MIC best describes antibiotics which follow concentration-dependent killing and require maximum peak antibiotic concentration for maximum efficacy, whereas AUC/MIC is representative of the antibiotics which elicit both time- and concentration-dependent killing [3]. Although the MIC based approach has been widely used by clinicians for designing dosing regimens and can be useful to predict the effect of dose fractionation on antibacterial activity, this approach is associated with several limitations.

PK/PD indices rely heavily on MIC. Measurement of MIC is associated with substantial uncertainty and variability because of the two-fold dilution technique used for its assessment and the interpretation as implied binary response, which considers efficacy only above MIC and no killing below MIC. Furthermore, MIC varies across patient populations and bacterial strains, and may change with time in the same patient [8]. Thus, MIC-based approaches ignore the dynamics of bacterial killing with time. It is typically assumed that a PK/PD index determined in a preclinical species or population can be extrapolated to another patient population. However, PK/PD indices have been found to vary among different patient populations, species, and disease conditions, and one of the reasons is associated with differences in the pharmacokinetics of the antibiotic in these groups [9, 10]. For example, in case of β-lactam antibiotics, the PK/PD index has been observed to change from T>MIC to AUC/MIC as the half-life increases in renally impaired patients. Similarly, decreases in half-life will shift the PK/PD index from AUC/MIC to T>MIC [11]. Thus, the value for PK/PD indices as guiding tool for dosage regimen design seems questionable.

One approach to overcome these drawbacks is the use of mechanism-based PK/PD modeling. Rather than relying on point estimates that integrate PK and PD factors of the host, the drug and the microorganism into one index, a mechanism-based PK/PD model has sufficient granularity to allow adjustment to changes in one of several of the PK and PD parameters as needed by changing clinical situations. In addition, PK/PD models reflect the gradual killing effect on bacteria with changing drug exposure rather than dichotomous all-or-nothing effects as implied by MIC values. Finally, PK/PD models consider the time-courses of bacterial growth and killing in relation to time courses of drug concentrations rather than time-integrated measures as used for the indices. Overall, these advantages allow for a more flexible, realistic and dynamic interplay of drug, host and microorganism-related factors that are ultimately predictive of bacterial killing and therapeutic efficacy.

Mechanism Based PK/PD Modeling

Mechanism based PK/PD models take into consideration the time course of bacterial count based on *in vitro*, *in vivo* and clinical information. These models are composed of three basic components: (i) a component that describes the bacterial growth kinetics, (ii) a component that describes the pharmacokinetics of the drug, and (iii) a component that integrates the effect of the drug concentration on bacterial turnover.

Bacterial growth kinetics

The simplest model component used for describing the bacterial growth kinetics consists of a single bacterial compartment with a first-order rate constant for bacterial K_{rep} replication (K_{rep}) and a first order rate constant for death of the bacteria (K_{rep}). **Equation 1-1** and **Figure 1-1A** describe the mono-exponential increase in microbial number seen in the absence of drug treatment [12], where N is the number of bacteria.

$$\frac{dN}{dt} = K_{rep} \times N - K_{dt} \times N \qquad \textbf{Eq. 1-1}$$

Quite often only the net process between bacterial growth and kill is quantified, with a first-order rate constant $K_{growth} = K_{rep} - K_{dt}$, also called K_{net}, since it is difficult to separately estimate both the replication and death rate constants with limited data [13]. The underlying assumption of this model is that the microbial population is homogenous having the same turnover rate constants, which is an oversimplification of the real scenario as microbial populations are usually known to be heterogeneous with multiple subpopulations with distinct metabolic states and drug resistance profiles [8].

In the absence of antibiotics, the bacterial number N eventually approaches a maximum N_{max} when limitation in nutrients and bacterial density limit further growth. In this steady-state condition there is no net change in the microbial population. There are three ways to describe these capacity limited growth curves:

Using a logistic growth function [14, 15]:

$$\frac{dN}{dt} = K_{growth} \times \left(1 - \frac{N}{N_{max}}\right) \times N \qquad \textbf{Eq. 1- 2}$$

Using a saturable, non-linear function [16]:

$$\frac{dN}{dt} = \left(\frac{VG_{max}}{N_{50}+N}\right) \times N \qquad \textbf{Eq. 1- 3}$$

where VG_{max} is the bacterial maximum growth in bacterial count per time, and N_{50} is N at which the bacterial growth is half-maximal.

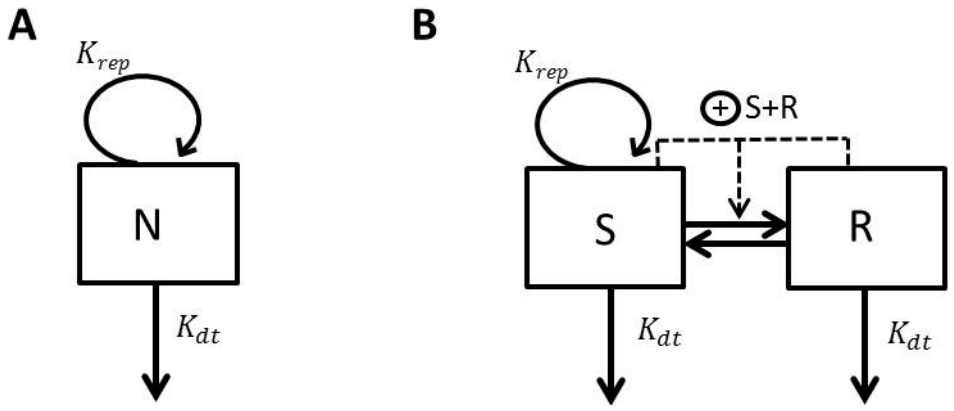

Figure 1-1. Models for bacterial growth kinetics
A) One cell population model, B) Two cell population model with different cell growth status.

Abbreviations: N, Number of bacteria; K_{rep}, first-order replication rate constant; K_{dt}, first-order death rate constant; S, Number of bacteria in growing state; R, Number of bacteria in resting state.

Using a model where transformation from the growing (S) to the resting stage (R) occurs when the total microbial count approaches the stationary phase [17] (**Figure 1-1B**).

$$\frac{dS}{dt} = = K_{rep} \times S - K_{dt} \times S - (K_{rep} - K_{dt}) \times \left(\frac{S+R}{N_{max}}\right) \times S + K_{rs} \times R \quad \textbf{Eq. 1- 4}$$

$$\frac{dR}{dt} = (K_{rep} - K_{dt}) \times \left(\frac{S+R}{N_{max}}\right) \times S - K_{rs} \times R - K_{dt} \times R \quad \textbf{Eq. 1- 5}$$

where S and R are the number of growing and resting bacteria, respectively. A high total bacterial load is assumed to potentiate the transformation from S to R. The transfer back to the growing stage (K_{rs}) is usually assumed to be negligible during *in vitro* time-kill experiments and therefore in those cases fixed to 0.

In some instances, additional delay functions have been introduced to characterize the growth delay observed during the first hours after the initiation of growth experiments when the microbes have not yet reached the logarithmic growth phase. For example, inverse mono-exponential functions with asymptotic increase such as $1\text{-}e^{-\delta \times t}$ have been used as multiplier for K_{rep} or K_{growth}, where δ is a first-order rate constant characterizing the dissipation of the delay [18, 19].

Pharmacokinetics

The pharmacokinetic model component is used for characterizing the concentration profile of a drug over a time period. Traditional compartmental modeling approaches are generally used to describe the pharmacokinetics with one- or multi-compartment systems. For example, in an *in vitro* chemostat-based PK/PD model system [19], the drug concentration can be described with a one-compartment model with mono-exponential decrease with time according to

$$\frac{dC}{dt} = -K_e \times C \quad \textbf{Eq. 1-6}$$

where C is the concentration of the drug and K_e is the first-order elimination rate constant of the drug.

The pharmacokinetic profile of a new drug is usually established in healthy subjects during the initial clinical phase of drug development. The pharmacokinetics may however be altered under pathophysiologic conditions in a diseased population. For example, drugs which are primarily renally cleared may reach higher systemic exposure in patients with renal impairment compared to healthy individuals. In these cases, creatinine clearance is typically found to be a significant covariate and can be used to guide patient customized dosing [20]. Disease conditions can also cause changes in the body fluids and protein binding which may ultimately affect tissue distribution and the

free fraction of the drug [21], and may thus need to be considered in the pharmacokinetic model component of mechanism based PK/PD models.

Many microbial infections are localized in extravascular tissues rather than blood or plasma [22]. The concentration at the site of infection may in these cases be different from plasma concentrations due to drug distribution processes and may thereby complicate the accurate assessment of optimal dosing regimens [23]. For example, concentration-time profiles of antibiotics in epithelial lining fluid in the lungs was found to be different from plasma with concentration ratios ranging from <0.1 to 3 [24]. In addition to efficacy, organ or tissue concentrations may also be of interest with regard to toxicity [25]. Techniques like microdialysis have been used for measurement of drug concentrations in tissue/organs [26]. Tissue distribution of antibiotics may be predicted using physiologically-based pharmacokinetic (PBPK) modeling [27, 28]. Recently, a PBPK model incorporating a multi-compartment permeability-limited lung model was used to simulate the pharmacokinetics of anti-tuberculosis agents in plasma, lungs and its sub-compartments where the mycobacteria reside in the host [29]. This model also provides a framework for predicting the lung concentrations of novel anti-tuberculosis agents.

Pharmacodynamics

The drug effect E can be modeled to either inhibit bacterial replication or potentiate bacterial killing. The relationship between drug concentration and its antimicrobial effect is usually described using an ordinary ($\gamma=1$) or a sigmoidal ($\gamma\neq1$) inhibitory E_{max} model. The general expression for the bacterial growth kinetics is then modified to **Equation 1-7**:

$$\frac{dN}{dt} = E_{rep} \times K_{rep} \times N - E_{dt} \times K_{dt} \times N \qquad \textbf{Eq. 1-7}$$

Drug effect decreasing the replication rate can then be modeled as

$$E_{rep} = 1 - \frac{I_{max} \times C^{\gamma 1}}{IC_{50}^{\gamma 1} + C^{\gamma 1}} \qquad \textbf{Eq. 1-8}$$

Drug effect increasing the death rate can be modeled as

$$E_{dt} = 1 + \frac{E_{max} \times C^{\gamma 2}}{EC_{50}^{\gamma 2} + C^{\gamma 2}} \qquad \textbf{Eq. 1-9}$$

Here E_{max} and I_{max} represent the maximum increase or decrease in effect, EC_{50} and IC_{50} represent the concentrations of drug that produce half of E_{max} and I_{max}, and γ_1 and γ_2 are the sigmoidicity coefficients. In **Equation 1-8** and **Equation 1-9**, the effect corresponds to a unitless fractional change in the rate constant with E_{max} and I_{max} representing the maximum achievable fractional change.

Alternatively to these proportional effect models, the increase in the death rate can also be modeled as an additive effect (**Figure 1-2A**):

$$\frac{dN}{dt} = K_{rep} \times N - K_{dt} \times N - \frac{I_{max} \times C^{\gamma}}{IC_{50}^{\gamma} + C^{\gamma}} \times N \qquad \textbf{Eq. 1-10}$$

In **Equation 1-10**, the effect corresponds to an additional kill-rate constant contributed by the drug with I_{max}, representing the maximum achievable drug-imposed kill-rate constant having the unit 1/time.

Combination Therapy

Combination therapy of antibiotics has been found to be useful as it may improve efficacy, increase patient compliance by optimizing dosing schedules, reduce toxicity, and suppress the emergence of resistance [30]. There is high potential for pharmacodynamic drug-drug interactions when antibiotics of a combination therapy act on the same or different molecular targets (serial or parallel) in the same pathogen, resulting in additive, synergistic or antagonistic interaction [31]. The concentration-effect relationship for two-drug combinations results in a three-dimensional response surface which is usually characterized quantitatively using the response surface analysis as described by **Equation 1-11** [32, 33]:

$$\mathbf{1} = \frac{C_1}{IC_{50,1} \times \left(\frac{I}{I_{max} - I}\right)^{\frac{1}{\gamma_1}}} + \frac{C_2}{IC_{50,2} \times \left(\frac{I}{I_{max} - I}\right)^{\frac{1}{\gamma_2}}} + \frac{\omega \times C_1 \times C_2}{IC_{50,1} \times IC_{50,2} \times \left(\frac{I}{I_{max} - I}\right)^{\frac{1}{2\gamma_1} + \frac{1}{2\gamma_2}}} \qquad \textbf{Eq. 1-11}$$

where C_1 and C_2 are the concentrations of drug 1 and drug 2 in the combination therapy; $IC_{50,1}$ is the concentration for which the effect is half maximal for drug 1 when present alone; $IC_{50,2}$ is the concentration for which the effect is half maximal for drug 2 when present alone; γ_1 and γ_2 are the sigmoidicity coefficients for drug 1 and drug 2, respectively; I_{max} is the maximum bacterial killing rate constant; ω is the interaction parameter; and I is the combined effect of both the drugs. The summation of the first and second term on the right side of the equation defines the additive effect whereas the third term is the drug interaction term. The combination effect is additive when $\omega = 0$, is synergistic when $\omega >> 0$, and is antagonistic when $\omega << 0$.

The kinetics of bacterial killing for the combination therapy can then be described using **Equation 1-12** with modification of the drug effect term by taking a similar approach as described above for the response surface analysis [34].

$$\frac{dN}{dt} = K_{rep} \times N - K_{dt} \times N - \left(\frac{I_{max} \times \left(\frac{C_1}{IC_{50,1}} + \frac{C_2}{IC_{50,2}} + \omega \times \frac{C_1 \times C_2}{IC_{50,1} \times IC_{50,2}} \right)^{\gamma}}{1 + \left(\frac{C_1}{IC_{50,1}} + \frac{C_2}{IC_{50,2}} + \omega \times \frac{C_1 \times C_2}{IC_{50,1} \times IC_{50,2}} \right)^{\gamma}} \right) \times N \qquad \textbf{Eq. 1-12}$$

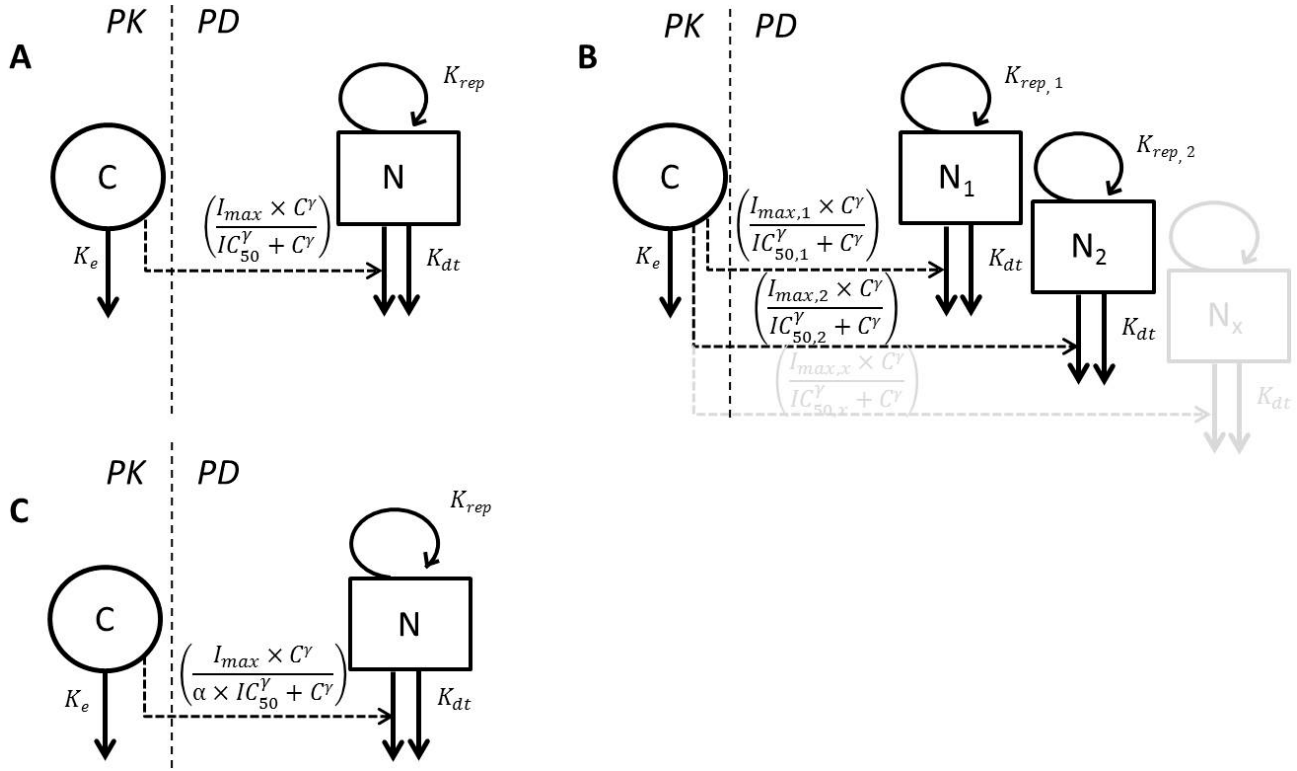

Figure 1-2. PK/PD models consisting of pharmacokinetic component, bacterial growth model, and pharmacodynamic link
A) One bacterial population with additive effect on death rate. B) Subpopulation approach for antibiotic resistance with two or more bacterial populations each having different drug sensitivity. C) Adaptation approach for drug resistance with adaptation factor modulating drug sensitivity.

Abbreviations: C, drug concentration; $N/N_1/N_2/N_x$, number of bacteria in different bacterial populations; K_e, first order drug elimination rate constant; K_{rep}, first-order replication rate constant; K_{dt}, first-order death rate constant; I_{max}, maximum achievable effect (subscripts indicate different values for different bacterial populations); IC_{50}, drug concentration producing 50% of I_{max} (subscripts indicate different values for different bacterial populations); γ, is the sigmoidicity factor; α , adaptation factor.

when ω is the interaction parameter; and γ is the sigmoidicity coefficient for the combination therapy, under the assumption that in the response surface analysis, $\gamma_1 = \gamma_2$.

Antibiotic Resistance

Antibiotic resistance can be mathematically explained either by an increase in IC_{50} or decrease in I_{max}. Prior knowledge about the mechanism of resistance can be used as a rationale for choosing the appropriate model. When reduced drug sensitivity can completely be overcome with a higher dose, an increase in IC_{50} is suggested as the probable mechanism for resistance. If even high doses are unable to achieve the maximum effect, however, then a decrease in I_{max} might be the more appropriate mechanism [13].

A variety of PK/PD models have been proposed for describing antibiotic resistance. These models can be broadly categorized into subpopulation approaches and adaptation approaches.

Subpopulation approaches

The more commonly used subpopulation approaches assume that the total bacterial population is composed of several discrete subpopulations with different drug susceptibility as shown in **Figure 1-2B**. These subpopulations are considered to be present even in the initial inoculum. Subsequent treatment with antibiotic leads to predominant killing of susceptible subpopulations along with selective replication of the less susceptible subpopulations resulting overall in regrowth. More than one differential equation is used simultaneously with each equation representing one bacterial subpopulation (often with different drug susceptibilities) [35]. A variation of the subpopulation model is one in which new drug resistant mutants are formed from the growing subpopulation with a first-order mutation rate during the experiment resulting in regrowth [36].

A modification of the sub-population approach could potentially be used to facilitate development of new generation anti-infectives which do not necessarily kill the bacteria. For example, Bezlotoxumab, a fully human monoclonal antibody, was found to decrease the rate of recurrence of *Clostridium difficile* infection in patients treated with standard-of-care antibiotics [37]. Bezlotoxumab acts by neutralizing the exotoxin B thereby averting its interaction with colonic cells and the associated inflammation. One of the possible approaches to characterize the PK/PD in this scenario could be a modified subpopulation model where the Bezlotoxumab induced toxin neutralization is modeled in parallel with the killing effect imposed by the standard-of-care treatment on the susceptible *Clostridium difficile* population.

Adaptation approaches

An alternative to the subpopulation model in which the total bacteria are assumed to be a mixture of different populations is the adaptive resistance mechanism in which the initial drug susceptible population is gradually considered to evolve into a drug resistant population as shown in **Figure 1-2C**. Only one differential equation is used to describe the rate of change of the total bacterial population. An adaptation factor (α) is introduced which may be dependent on time and concentration:

$$\alpha = 1 + \beta \times (1 - e^{-C \times t \times \tau}) \qquad \textbf{Eq. 1-13}$$

where β describes the maximum adaptation factor and τ represents the rate of adaptation. Dependent on how the adaptation function is implemented in the PK/PD model, a gradual increase in time and concentration may result in an increase in IC_{50}, decrease in I_{max}, or decrease in bacterial replication rate [38].

Identification of the true resistance mechanism based only on total bacterial counts and statistical modelling criteria have failed in the majority of cases. Quantification of resistant populations will help in distinguishing between competing models and support the selection of the most appropriate model for bacterial resistance [39].

Inoculum Effect

The phenomenon that when a higher bacterial density of initial inoculum in an experiment leads to a reduced antibacterial effect is referred to as inoculum effect [40] Some of the potential mechanisms for this phenomenon are (i) enzymatic inactivation of the drug, (ii) non-specific binding to the bacteria, and (iii) increased likelihood of the preexistence of subpopulations of resistant bacteria if the density of the inoculum is higher than the natural mutation rate of the bacteria. For example, the pharmacodynamic effect of ceftazidime, a β-lactam antibiotic, changed from time-dependent killing to concentration-dependent killing when inoculum density was increased [41]. This conversion in the PK/PD-index has been linked to the distribution and accumulation of β-lactamase in the biofilm of high density inocula which can hydrolyze β-lactam antibiotics.

Bacterial burden shows a wide variation in patients and therefore a PK/PD model which incorporates an inoculum effect might be more predictive in clinical scenarios. One of the models proposed to describe inoculum effects is based on the concept of quorum sensing. It assumes that all bacteria release signal molecules to communicate with each other which consequently results in reduced drug sensitivity [42].

Host Responses

In vivo models of bacterial infection are oftentimes established in immuno-compromised animals as they allow for proper estimation of antibiotic efficacy without any interference from the immune system. In many cases, the PK/PD indices needed to be achieved for efficacy in these models are higher compared to those obtained in immuno-competent animals [43]. *In vivo* infection models in animals with functional immune system, although less common, have also been used for assessing the efficacy of antibiotics. As the immune system of immunocompetent animals has the ability to kill bacteria, it is important to study the time course of this effect independently from antibiotic therapy in order to be able to delineate the intrinsic activity of the drug from that of the immune system. The immune system effect can be assessed by three different approaches:

Modulation of bacterial challenge

In this approach inocula with different initial density were used in the same type of animal infection model to quantify the antimicrobial effect associated with the immune system [44]. The immune system was successful in reducing the bacterial load when the initial inoculum was low; at higher initial inocula, however, the immune system's capacity was overwhelmed resulting in net bacterial growth. This impact of immune system has been described quantitatively using mathematical models where the rate of change in bacterial count is equal to the difference between the growth rate of bacteria and the kill rate contributed by the antibacterial effect of the immune system [44]:

$$\frac{dN}{dt} = K_{growth} \times \left(1 - \frac{N}{N_{max}}\right) \times N - \left(\frac{K_{ir} \times N}{N_{50} + N}\right) \times N \qquad \textbf{Eq. 1-14}$$

Here, K_{ir} is the maximal kill rate induced by the immune system and N_{50} is the number of bacteria per g of tissue at which the immune-system mediated kill rate is half-maximal.

Modulation of immune reactivity

An alternative strategy to quantify the contribution of the immune system towards bacterial reduction is to use animal infection models with different levels of immunosuppression [45]. A pneumonia mouse model with functional immune system was treated with different escalating doses of the immunosuppressant cyclophosphamide, thereby reducing the neutrophil counts by 20, 70 and 90%, respectively. The rate of change in the bacterial count was equal to the difference between the first order growth rate of bacteria and the saturable kill rate attributed to the number of available neutrophils:

$$\frac{dN}{dt} = K_{growth} \times \left(1 - \frac{N}{N_{max}}\right) \times N - \left(\frac{K_{ir} \times ANC}{ANC_{50} + ANC}\right) \times N \qquad \textbf{Eq. 1-15}$$

ANC is the absolute neutrophil count and ANC_{50} is the ANC required to achieve 50% of maximal kill rate.

Natural progression of disease

The effect of the immune system can also be included as a time-dependent first-order kill rate, in addition to the natural death rate as described by **Equation 1-16**, for example when immunocompetent animals are treated with vehicle control and establish adaptive immunity over time. This assessment may result in a slight overestimation of the impact of the immune system, however, if comparative data in immunocompetent and immune-compromised animals are not available to delineate the real immune system effect from natural bacterial death:

$$\frac{dN}{dt} = K_{rep} \times \left(1 - \frac{N}{N_{max}}\right) \times N - \left(\frac{K_{ir} \times t^{\gamma}}{{t_{50}}^{\gamma} + t^{\gamma}}\right) \times N - K_{dt} \times N \qquad \textbf{Eq. 1-16}$$

Here K_{ir} is the maximum death rate constant induced by the immune system, t is the time, t_{50} is the time when the death rate constant is half of its maximum value, and γ is the sigmoidicity factor that determines the shape of the curve. The effect of the immune system is thus modeled as a gradual, time-dependent increase of the death rate constant until it reaches its maximum K_{ir}.

Bench to Bedside Translation of PK/PD Models for Anti-Infectives

The current paradigm for translation of antibacterial PK/PD from preclinical species to humans requires integration of the PK/PD index determined in animal models with human pharmacokinetics [46]. Stochastic simulation of human drug exposure using population pharmacokinetic models generates concentration-time profiles which are then used to compute the PK/PD index for each simulated subject. Based on the proportion of subjects with the desired value of the PK/PD index, probability of attaining the therapeutic target is predicted. This approach helps in making decisions regarding the choice of dosing regimens to be implemented in the clinic.

The use of mechanistic PK/PD models for translation from preclinical to clinical scenarios has been limited. PK/PD models based on *in vitro* static and dynamic kill curves have been successful in the prediction of *in vivo* effects in animal models [9]. However, there is still a knowledge gap regarding translation of PK/PD parameters from preclinical to clinical settings. For example, recently a multistate tuberculosis pharmacometric model describing different bacterial states of *Mycobacterium tuberculosis* was developed based on *in vitro* data [4]. For clinical implementation of this model [47], most of the parameters pertaining to the natural bacterial growth were fixed to the *in vitro* estimates; however the exposure-response parameters related to drug effect had to be estimated from clinical data and were different from the *in vitro* drug effect parameters. More research efforts are needed in this area to better facilitate the quantitative translation of mechanistic PK/PD models to clinical situations.

Development of a Translational PK/PD Model for Antibiotics

Mechanism-based models for antibiotics are usually established in a stepwise fashion, in which the different model components are individually developed and integrated (**Figure 1-3**). The typical steps include the following:

1. Development of a pharmacokinetic model in the studied population (animal models or humans), that captures the time course of free, pharmacologically active concentrations of the antibiotic, preferably in the relevant target tissue.

2. Development of a bacterial growth model that captures the bacterial growth kinetics and potential host response effects.

3. Integration of the bacterial growth model and the pharmacokinetic model component into a PK/PD model with a pharmacodynamic model component that links the dynamics of drug concentrations to bacterial turnover. This may include drug combination models, inocula effects, and resistance development.

Once the model has been established, it can be used for simulations to interpolate and extrapolate the observed experimental data to other, untested scenarios, such as different dosing regimens, or different patient populations [3, 48]. It can also be used for quantitative comparisons of multiple drug candidates to identify lead candidates and support go-no go decisions [8].

Conclusions

Mechanism-based PK/PD models are increasingly been used in developing dosing strategies for antibiotics in drug development and clinical application. Although these models are simplified depictions of rather complex interactions of drug, microbe and host physiologic processes, they are able to capture the time course and magnitude of antibacterial effect in relation to bacterial growth, the pharmacokinetic and pharmacodynamic properties of the drug, and the chosen dosing regimen. Complicating factors such as resistance development, combination therapy, or host responses can be incorporated in the modeling approach. In situations where only limited data are available, system specific parameters describing for example growth characteristics may also be implemented based on prior knowledge [4]. With these tools at hand, translational PK/PD modeling and simulation may play a pivotal role in identifying the right balance between bacterial killing, adverse effects, and appearance of resistance, and may help identifying and optimizing dosing regimens for novel and established antibacterial agents.

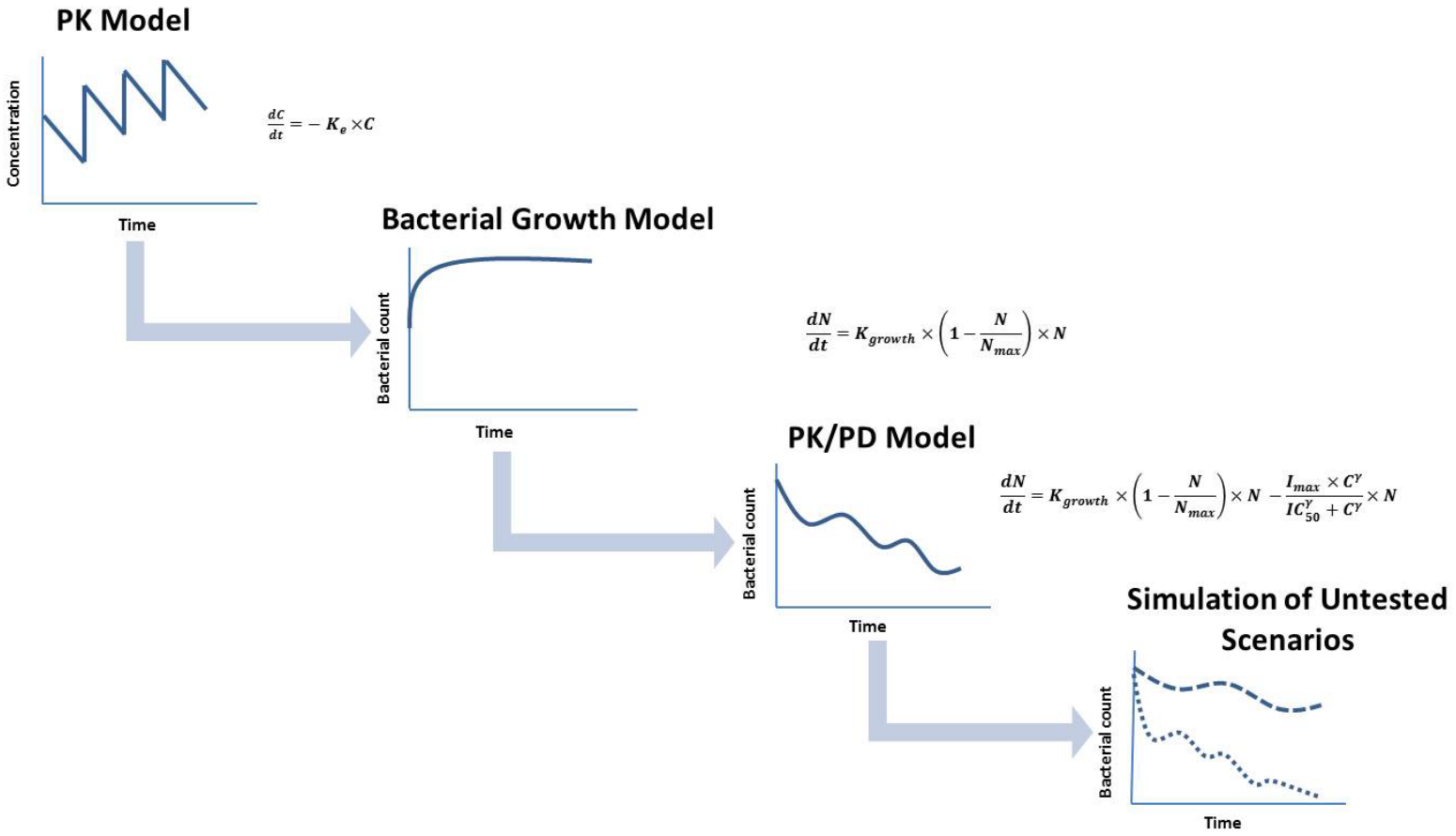

Figure 1-3. Steps involved in the development and application of a translational PK/PD model for antibiotics

CHAPTER 2. HYPOTHESIS AND SPECIFIC AIMS

Tuberculosis (TB) is a serious life threatening disease resulting in 1.4 million deaths per year. Multidrug resistant (MDR) TB (resistant to first line agents: Rifampin and Isoniazid) causes an estimated 300,000 deaths per year. To further exacerbate the situation, extensively drug resistant (XDR) TB (resistant to first line agents and at least one second line agent) and totally drug resistant TB (resistant to all first and second line agents) infections are increasing at an alarming rate in the developing world.

The devastating socioeconomic and public health impact of tuberculosis and the known toxicity of many existing treatments motivated our research team to develop spectinamides, a series of semi-synthetic analogues of the antibiotic spectinomycin, into a novel class of antitubercular drugs. Spectinomycin historically has been used as a second-line agent to treat gonorrheal infections; however, it has only limited activity against *Mycobacterium tuberculosis* (*Mtb*). Yet, its high safety margin and its distinct ribosomal binding site make it a preferred lead structure. By modifying its structure, our research team generated spectinomycin analogues with excellent *in vivo* antitubercular activity which bind to a unique site within the 30S mycobacterial ribosome subunit, and block ribosome translocation. Furthermore, it was also demonstrated that spectinamides, in spite of being highly hydrophilic, are extremely efficacious because in contrast to spectinomycin they are able to evade the efflux transporter Rv1258c expressed in *Mtb*. These findings for the first time challenged the previous view in the field that *Mtb* is intrinsically resistant to many polar antibiotics because of its waxy coating around the cell membrane.

Spectinamides have undergone a comprehensive lead optimization process which included refining the chemical structure to obtain optimum pharmacological, biopharmaceutic and pharmacokinetic characteristics using an iterative approach. Based on these evaluations, Lee 1599 and Lee 1810 have emerged as lead candidates with excellent antitubercular activity against both drug susceptible as well as MDR- and XDR-drug resistant *Mtb* strains, a high safety margin, narrow anti-microbial spectrum, lack of cross-resistance with other protein synthesis inhibitor, low synthesis cost, and favorable pharmacokinetic characteristics. The overall objective of my dissertation work is to utilize translational PK/PD approaches for the further advancement of spectinamide lead candidates, Lee 1599 and Lee 1810, into the late discovery stage. I hypothesize that translational PK/PD approaches facilitate the drug development process in the late discovery stage by providing information on optimal dose selection, rationales for route-specific efficacy differences, and the feasibility of reaching efficacious drug exposures in humans.

Specific Aim 1

Identifying the main driver for antibiotic efficacy is essential for designing its optimum dosing schedules. In Specific Aim 1 (Chapter 3), I hypothesize that the *in vivo*

anti-mycobacterial activity of Lee 1810 follows a defined dose-exposure-response relationship. In order to prove this hypothesis and characterize the dose-exposure and exposure-response relationships for Lee 1810, I will develop a semi-mechanistic PK/PD modeling approach and apply it on concentration and efficacy data obtained from a dose fractionation study in a mouse model of chronic *Mtb* infection.

Specific Aim 2

Spectinamides are highly water soluble and poorly permeable resulting in limited oral bioavailability; hence are usually administered through the subcutaneous route in mice. Since lungs are the main site of infection in pulmonary TB, the efficacy of lead spectinamide Lee 1599 was also evaluated after intratracheal administration in a mouse model of *Mtb* infection. Intratracheal administration of lead spectinamide Lee 1599 was shown to be significantly more efficacious than subcutaneous administration at comparable doses. In Specific Aim 2 (Chapter 4), I hypothesize that this higher efficacy is caused by a higher exposure of Lee 1599 to the target organ, the lungs, after intratracheal compared to subcutaneous administration. I address this hypothesis in a comparative biodistribution assessment of Lee 1599 after subcutaneous and intratracheal administration in mice.

Specific Aim 3

The translation from the preclinical stage to the clinical stage is one of the most critical steps in a drug development program as it requires extrapolation of results for efficacy, safety, PK/PD and toxicology from preclinical species to humans. Physiologically-based pharmacokinetic (PBPK) modeling and simulation is one of the powerful methodologies which is increasingly used for predicting drug exposure in humans based on the pharmacokinetic behavior observed in preclinical species. In Specific Aim 3 (Chapter 5), I hypothesize that systemic exposures to Lee 1599 found to be efficacious in mice are also feasible to be reached in humans. I address this hypothesis by developing and applying a PBPK model for Lee 1599 to predict pharmacokinetics and dose requirements of Lee 1599 in humans. This includes the development of a PBPK model for describing the pharmacokinetics of Lee 1599 in rats and mice, and the subsequent use of the model for prediction of human pharmacokinetics of lead spectinamide Lee 1599.

CHAPTER 3. DOSE-EXPOSURE-RESPONSE ANALYSIS OF SPECTINAMIDE ANTIBIOTIC LEE 1810 IN *MYCOBACTERIUM TUBERCULOSIS* INFECTED MICE

Introduction

Tuberculosis (TB) is a serious life-threatening disease resulting in 1.4 million deaths per year [49]. Multidrug-resistant (MDR) TB (resistant to the first line agents rifampin and isoniazid) causes an estimated 300,000 deaths per year [50]. To make matters worse, extensively drug-resistant (XDR) TB (resistant to first line agents and at least one second line agent) and totally drug-resistant TB (resistant to all first and second line agents) infections are increasing at an alarming rate in the developing world. To address the increasing prevalence of MDR and XDR infections, several novel scaffolds of antibiotics are currently being investigated in various stages of pre-clinical and clinical development [51].

Our research group has recently discovered novel antitubercular agents known as spectinamides. Spectinamides are semi-synthetic derivatives of spectinomycin, an aminocyclitol that inhibits bacterial protein synthesis by binding to a site within the bacterial 30S ribosome (helix 34 of 16SrRNA) distinct from that of other protein synthesis inhibitors. This property provides the necessary selectivity, narrow spectrum antitubercular activity and lack of cross-resistance with other antibiotics. In multiple murine infection models, spectinamides were successful in significantly reducing lung mycobacterial burden and also improving survival. Unlike aminoglycosides, spectinamides do not inhibit human mitochondrial translation and do not exhibit off-target effects which are linked to aminoglycosides-related ototoxicity [52].

Based upon *in vitro* screening assays, pharmacokinetic studies, and preliminary *in vivo* efficacy studies in rodents, Lee 1810 emerged as one of the lead candidate molecules from the class of synthesized spectinamide compounds. Lee 1810 has a minimum inhibitory concentration (MIC) of 1.6 μg/mL [53], a favorable pharmacokinetic profile with high microsomal metabolic stability and renal excretion as the primary elimination pathway. In mouse models of chronic *Mycobacterium tuberculosis* (*Mtb*) infection, Lee 1810 monotherapy reduced the lung bacterial load comparable to streptomycin.

Given the long cycle time involved in new drug development coupled with the limited pipeline of antitubercular agents under development, it is essential to use novel antibiotics for this indication in the most appropriate way. To maximize efficacy, and minimize toxicity and emergence of resistance associated with spectinamides, it is critical to use optimum dosing strategies which are based upon pharmacokinetic /pharmacodynamic (PK/PD) principles. The main objective of the work summarized in this chapter is to develop a semi-mechanistic PK/PD model to characterize the dose-exposure-response of lead spectinamide Lee 1810 based on a dose-fractionation study in a mouse model of chronic *Mtb* infection. The PK/PD relationship established in this model will further support dose selection in preclinical development and will eventually

facilitate translation of preclinical information to humans by informing clinical trial designs and determining clinically optimum dosing regimens.

Materials and Methods

Chemicals and reagents

Spectinamide antibiotic Lee 1810 (2-(5-hydroxypyridin-2-yl)-N-((2R,4R,4aS,5aR,6S,7S,8R,9S,9aR,10aS) -4a,7,9-trihydroxy-2-methyl-6,8-bis(methylamino)decahydro-2H-benzo[b]pyrano[2,3-e][1,4]dioxin-4-yl)acetamide) as shown in **Figure 3-1** was synthesized in Dr. Richard E. Lee's Lab at St. Jude Children's Research Hospital, Memphis, TN as previously described [54]. Acetonitrile, methanol, HPLC grade water, formic acid and nonafluoropentanoic were purchased from Fisher Scientific (Pittsburgh, PA). Drug free BALB/c mouse plasma was purchased from Innovative Research (Novi, MI).

Dose-fractionation study in a chronic mouse model of *Mtb*

6-8 week old BALB/c female mice (150 total) were infected with *Mtb* Erdman with a Low Dose Aerosol (LDA) infection as previously described [49], using an inoculum concentration of 2.0×10^6 CFU/ml to achieve deposition of ~100 CFU in the lungs for the BALB/c mice. At Day 34 post infection, subcutaneous (SC) administration with Lee 1810 was initiated with different dosing regimens as described in **Table 3-1** and continued for 4 weeks with drug holidays on weekends. The spectinamides were formulated in Plasma-Lyte (Baxter, Deerfield, IL) and water with different ratios for each group in order to maintain ideal osmotolerance close to physiological values, and 0.2 ml of the formulation was administered subcutaneously using a 29 gauge insulin syringe. To assess the pharmacokinetics of Lee 1810 under multiple dosing in infected mice, two blood samples were taken per mice by submandibular bleed collected in BD Microtainer plasma separator tubes containing lithium-heparin (BD, Franklin Lakes, NJ): one at 0.25 h post SC administration ($C_{0.25}$) and another at the 8 h post SC administration during the last week of dosing (C_8). Plasma was separated immediately by centrifugation (10,000g for 10 min at 4 °C) and stored at −70 °C until analysis. After 4 weeks of treatment followed by 2 days of washout period, lungs were harvested and homogenized for dilution and plated on Middlebrook 7H11 agar plates supplemented with oleic acid-albumin-dextrose-catalase (OADC). Plates were incubated at 37°C and colonies (CFU) were enumerated after at least 21 days of incubation. To enumerate the bacterial uptake from the LDA infection, 6 BALB/c mice were sacrificed day 1 post-infection. On Day 34 post-infection, 5 BALB/c mice were sacrificed to determine bacterial load at the start of therapy. On Day 62 post-infection, 5 BALB/c untreated mice and 7 BALB/c mice dosed with vehicle were sacrificed to determine bacterial load in the untreated group and placebo group respectively. This information was used for describing the natural bacterial growth. The viable CFU counts were logarithmically converted for further data analysis.

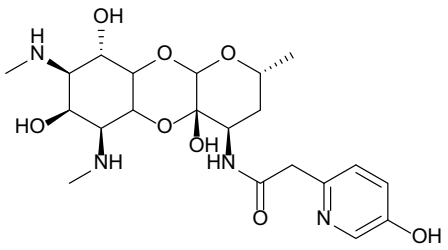

Figure 3-1. Structure of Lee 1810

Table 3-1. Dosing regimens evaluated in the dose-fractionation study

Dosing frequency	Total weekly dose (mg/kg)															
	20	**40**	**60**	**80**	**100**	**120**	**200**	**300**	**400**	**500**	**600**	**1000**	**1200**	**2000**	**3000**	**4000**
5x per week (m-f) twice					10 BID		20 BID			50 BID		100 BID		200 BID	300 BID	400 BID
5x per week (m-f)					20 QD		40 QD			100 QD		200 QD		400 QD	600 QD	
3x per week (m,w,f)			20 TIW			40 TIW		100 TIW			200 TIW		400 TIW			
2x per week (m,r)		20 BIW		40 BIW			100 BIW		200 BIW							
1x per week (m)	20 QW	40 QW			100 QW											

Abbreviations: m, Monday; t, Tuesday; w, Wednesday; r, Thursday; f, Friday; BID, Twice daily; QD, Once daily; TIW, Thrice weekly; BIW, Twice weekly; QW, Once weekly.

The dose-fractionation study was conducted in the dedicated BSL-3 facility by the research group of Dr. Anne Lenaerts at Colorado State University according to the guidelines of the Colorado State University Institutional Animal Care and Use Committee. As the plasma samples were collected from *Mtb* infected mice, it was necessary to sterilize them before bioanalysis. A validated approach with γ-irradiation at a radiation dose of 1 Mrad using a Cobalt-60 gamma irradiator was used for sterilization of the plasma samples. To account for degradation of drug during the irradiation process, quality control samples of known concentrations (10 ng/mL (low), 1 µg/mL (medium), and 10 µg/mL (high)) were simultaneously irradiated. After sterilization, the sample concentrations were quantified and the concentrations were corrected for the drug lost during the irradiation procedure.

Pharmacokinetic study in healthy mice

To assess the pharmacokinetics in healthy compared to infected mice and to provide an anchor point for a population pharmacokinetic analysis of the limited samples obtained in the mouse model of chronic *Mtb* infection, female BALB/c mice (6–8 weeks old, ~20 g, n = 15) were dosed with 200 mg/kg of Lee 1810 subcutaneously. Blood samples were collected at 0.083, 0.25, 0.5, 1, 2, 3, 5, 8, 12 and 24 h after administration. Each mouse provided two blood samples, one by a one-time retro-orbital bleed under isoflurane anesthesia and the other by cardiac puncture under isoflurane anesthesia followed by euthanasia through cervical dislocation. This pharmacokinetic study was performed at the University of Tennessee Health Science Center following approval by the Institutional Animal Care and Use Committee. Plasma was separated immediately by centrifugation as described above and stored at −70°C until LC-MS/MS analysis.

Quantification of Lee 1810 concentrations in plasma

The plasma samples were processed by protein precipitation. To 25 µL aliquots of specimens 100 µL methanol containing the internal standard Lee 1369 (3′-dihydro-3′-deoxy-3′(R)-isopropylacetylamino spectinomycin) was added. This was followed by vortexeing for 1 min and centrifugation at 10,000g for 10 min at 4ºC. The supernatant was separated and 5 µL of supernatant was analyzed using high-performance liquid chromatography coupled with tandem mass spectrometry (LC-MS/MS). Chromatographic separations were carried out using a Shimadzu Nexera XR (LC-20ADXR) liquid chromatograph (Shimadzu Corporation, Kyoto, Japan) consisting of two pumps, online degasser, system controller and an autosampler. Liquid chromatography was performed on Waters Symmetry® 3.5 µm C8, 50 × 2.1 mm column (Waters, Milford, MA). The mobile phase was solvent A (water with 1.6% nonafluoropentanoic acid and 0.7 % formic acid) and solvent B (90% acetonitrile with 0.8% nonafluoropentanoic acid and 0.35% formic acid) in the gradient mode as follows: 0–0.5 min, 20% B; 0.5–1.6 min, 20–90% B; 1.6–2 min, 90% B; 2-2.5 min, 90-20% B, 2.5–3 min, 20% B at a flow rate of 0.5 mL/min. Analytes were detected with a API 5500 triple-quadruple mass spectrometer (Applied Biosystems, Foster City, CA) with electrospray

ionization in multiple reaction monitoring mode using the compound-specific mass transfers of m/z 469.2/ 207.1 for Lee 1810 and m/z 418.3/207.1 for Lee 1369.

Two calibration curves ranging from 1.95 to 2,000 ng/mL and 1.95 to 1000 µg/mL were constructed and validated with spiked samples of mouse plasma. Samples with concentrations above 2000 ng/mL were analyzed with the higher calibration range. The peak area ratios of analyte to internal standard was linear over the concentration range tested for both compounds, with correlation coefficients (weighted least-square linear regression analyses) >0.997. Accuracy (deviation of the analyzed quality control samples from nominal values) was within ±3% over the entire range of the calibration curve, and precision (coefficient of variation of repeated measurements of the quality control samples) was <2%.

Dose proportionality assessment

The assessment of dose linearity and dose proportionality was performed by power regression modeling on log-transformed data for $C_{0.25}$ and C_8. 95% confidence intervals for the slopes were determined from the power regression analysis. The dose proportionality was considered linear when the lower confidence limits were ≥ 0.8 and upper confidence limits were ≤ 1.25 [55].

Population pharmacokinetic model development

A population pharmacokinetic model was used to simultaneously describe the plasma concentration measurements from both healthy and infected mice by nonlinear mixed-effects modeling. The concentration data were natural log transformed and modeled using a log-transform-both-sides (LTBS) approach [56]. The evaluation of the structural pharmacokinetic model was undertaken by visual exploratory data analysis. The densely sampled concentration-time points in the healthy mice were primarily used to guide base model development. Once the base model could adequately describe the data in healthy mice with physiologically plausible parameter estimates, the model was expanded to include the sparse pharmacokinetic data from the dose-fractionation study. Based upon the biphasic distribution of Lee 1810 after SC administration, a two-compartment model with first-order absorption was used to describe the pharmacokinetics of Lee 1810 (**Figure 3-2**).

For all models evaluated in this population analysis, between-subject variability (BSV) was modeled as a log-normal distribution,

$$P_i = P_{pop} \times e^{\eta i} \qquad \textbf{Eq. 3-1}$$

where P_i is the parameter estimate for mouse i, P_{pop} represents the typical population value for the parameter, and η_i is the independent random variable in mouse i, described

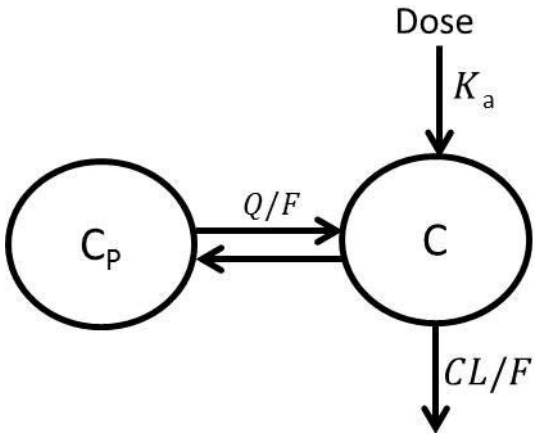

Figure 3-2. Two-compartment pharmacokinetic model for characterizing the pharmacokinetics of Lee 1810

Abbreviations: C, concentration in the central compartment; C_P, concentration in the peripheral compartment; Q/F, intercompartmental clearance corrected for bioavailability; CL/F, clearance corrected for bioavailability; K_a, first-order absorption rate constant.

by a normal distribution with mean zero and variance ω^2, which corresponds to a log-normal distribution for the parameter.

The residual unexplained variability (RUV) was characterized as an additive error, which relates to a proportional error when using an LTBS approach, such that:

$$Ln(C_{ij}) = Ln\left(\hat{C}_{ij}\right) + \varepsilon_{ij} \quad \textbf{Eq. 3-2}$$

where $Ln(C_{ij})$ is the natural logarithm of the j^{th} observed concentration in the mouse i, $Ln(\hat{C}_{ij})$ is the natural logarithm of the model predicted concentration for the j^{th} observation in the mouse i, and ε_{ij} is the residual error characterized by normal distribution with mean zero and variance σ^2.

Following the development of the base model, disease effect was tested as a categorical covariate coded as power model on clearance (CL/F), central volume of distribution (V_c/F) and intercompartmental clearance (Q/F) using the following relationship:

$$P = \theta_1 \times (\theta_2)^{Status} \quad \textbf{Eq. 3-3}$$

where P represents the typical value of parameter in the population, Status is an indicator variable equal to 0 for healthy mice and 1 for infected mice, θ_1 is the typical value of P for healthy mice, and θ_2 is the multiplicative factor describing the increase or decrease in P as a result of the infection.

To account for the more than dose-proportional increase in $C_{0.25}$ above doses of 100 mg/kg as observed in the data, a higher absorption rate for these groups was tested using the following relationship:

$$PopK_a = \theta_3 \times (\theta_4)^{HD} \quad \textbf{Eq. 3-4}$$

where $PopK_a$ represents the typical value of K_a in the population, HD is an indicator variable equal to 0 for dose ≤100 mg/kg and 1 for dose >100 mg/kg, θ_3 is the typical value of K_a for dose ≤100 mg/kg, and θ_4 is the multiplicative factor describing the increase in K_a for dose >100 mg/kg.

Semi-mechanistic PK/PD model development

The semi-mechanistic PK/PD model developed to describe the effect of Lee 1810 on *Mtb* in the murine infection model takes into consideration the time course of bacterial count based on *in vivo* information. The model was composed of three basic components: (i) a component that describes the bacterial growth kinetics, (ii) a component that describes the pharmacokinetics of Lee 1810, and (iii) a component that integrates the effect of the drug concentration on bacterial turnover.

The natural bacterial growth of *Mtb* in the control group of untreated immunocompetent mice was characterized based on time courses of CFU data obtained from this study, previously performed studies by Dr. Anne Lenaerts' research group at Colorado State University using the same mouse and bacterial strains, and from the scientific literature (**Figure 3-3**) [57-59]. The growth kinetics in untreated groups of mice was found to be independent of the bacterial or mouse strain used in the study (**Table 3-2**). This is consistent with the observations made previously where mice infected intravenously or aerogenically with *Mtb* strains of CDC 1551, Erdman, H37Rv developed almost identical infections in the lungs and spleen [60].

The model for natural mycobacterial growth in the untreated group of immunocompetent mice was developed by implementing the idea of phenotypic heterogeneity, where a fast growing bacterial population (N_1) switches into a slow growing population (N_2) as a result of stochastic or induced expression of persister genes as shown in **Figure 3-4** [61]. The implementation of this model was inspired from the 2-subpopulation approach used for describing the *in vitro* growth kinetics of *Streptococcus pyogenes* [17]. In the early exponential growth phase, N_1 is assumed to constitute the majority of total bacteria with a first-order replication rate of K_{rep}.The conversion from the fast growing stage to the slow growing stage was assumed to be triggered by a high total bacterial population. In the model, the N_2 have the ability to revert back to the fast growing bacteria once the conditions become favorable. However, during initial model evaluation, the transfer from N_2 to N_1 was negligible and was therefore fixed to 0 in further model development. The mice used in the dose-fractionation study were immunocompetent. Interferon-γ producing T-cells, which regulate the adaptive immune system, are recruited to the lungs post-infection in aerosol infected mouse models [59]. In order to account for the role of host immune reaction in killing bacteria, a first-order death rate constant K_{ir} was introduced on both bacterial subpopulations. The CFU readout from the agar plates was considered to represent the sum of both bacterial subpopulations. The initial number of bacteria in the fast growing subpopulation ($N_{1,0}$)in the starting inoculum was estimated during the model fit. Since the mice were challenged with a low-dose aerosol inoculum of bacteria in the early logarithmic phase, the initial number of N_2 was fixed to 0.

$$\frac{dN_1}{dt} = K_{rep} \times N_1 - K_{ir} \times N_1 - (K_{rep} - K_{ir}) \times \left(\frac{N_1+N_2}{N_{max}}\right) \times N_1 \qquad \textbf{Eq. 3-5}$$

$$\frac{dN_2}{dt} = (K_{rep} - K_{ir}) \times \left(\frac{N_1+N_2}{N_{max}}\right) \times N_1 - K_{ir} \times N_2 \qquad \textbf{Eq. 3-6}$$

Once the natural bacterial growth model had been developed, the next step was to integrate it with the drug effect. Based on the individual *post hoc* estimates from the population pharmacokinetic modeling, a sequential PK/PD analysis was performed by linking the pharmacokinetic model with the bacterial growth model via an exposure-dependent kill function associated with the effect of Lee 1810 as shown in **Figure 3-5**. The parameters related to the natural bacterial growth model were fixed during the drug evaluation and only the drug effect parameters were estimated during the PK/PD analysis.

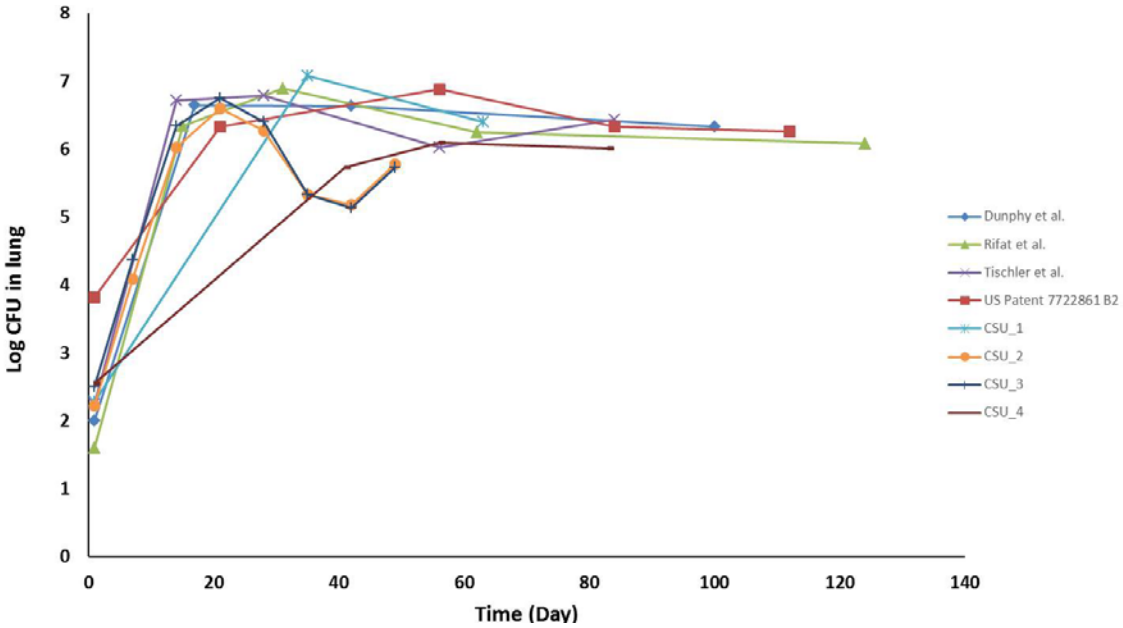

Figure 3-3. Natural bacterial growth of *Mycobacterium tuberculosis* in the untreated group of immunocompetent mice

Dunphy *et al.* [58], Rifat *et al.* [57], Tischler *et al.* [59] and US Patent 7722861B2 [62] represents the literature sources from which the data was extracted. CSU_1 represents the data obtained from the current dose fractionation study of Lee1810 and CSU_2, CSU_3 and CSU_4 are the time courses of CFU data obtained from previously performed studies by Dr. Anne Lenaert's research group at Colorado State University using the same mouse and bacterial strains.

Table 3-2. Information about the bacterial and mouse strain reported in the literature sources from which the data was extracted for the natural bacterial growth of *Mycobacterium tuberculosis* in the untreated group of immunocompetent mice

Literature source	Bacterial strain	Mouse strain
Dunphy *et al.*	H37Rv	C57BL/6
Rifat *et al.*	CDC1551	BALB/c
Tischler *et al.*	Erdman	C57BL/6
US Patent 7722861B2	H37Rv	C57BL/6
CSU_1, _2, _3, _4	Erdman	BALB/c

Dunphy *et al.* [58], Rifat *et al.* [57], Tischler *et al.* [59] and US Patent 7722861B2 [62] represents the literature sources from which the data was extracted. CSU_1 represents the data obtained from the current dose fractionation study of Lee1810 and CSU_2, CSU_3 and CSU_4 are the time courses of CFU data obtained from previously performed studies by Dr. Anne Lenaerts' research group at Colorado State University using the same mouse and bacterial strains.

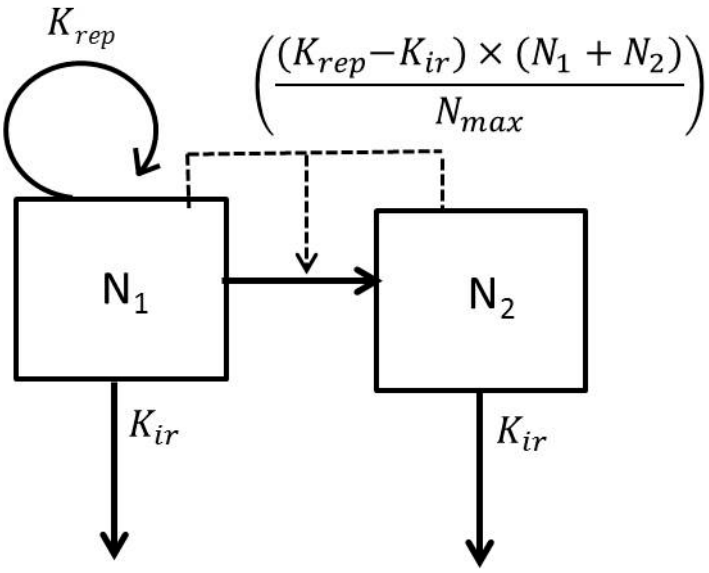

Figure 3-4. Two-subpopulation *Mycobacterium tuberculosis* growth model

Abbreviations: N_1, cell count of fast growing population; N_2, cell count of slow growing population; K_{rep}, first-order replication rate constant; N_{max}, maximum number of bacteria; K_{ir}, first-order death rate constant induced by the immune reaction.

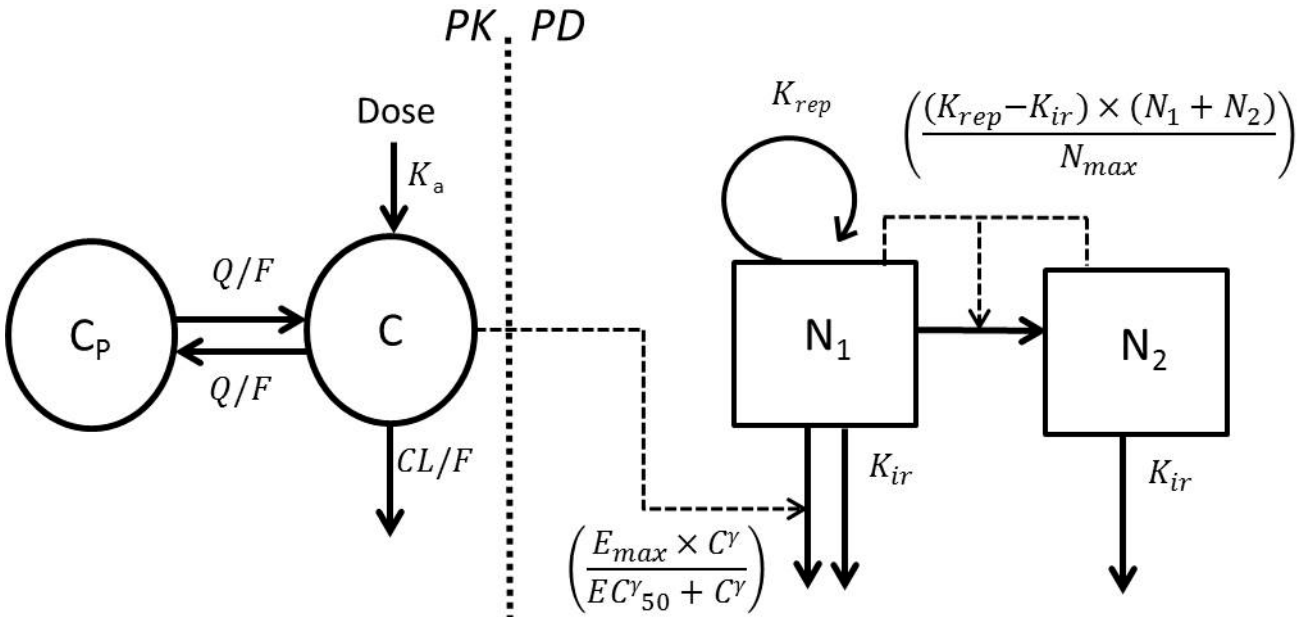

Figure 3-5. PK/PD model of Lee 1810 consisting of a two-compartment pharmacokinetic model and *Mycobacterium tuberculosis* growth model integrated with additive drug effect

Abbreviations: N_1, cell count of fast growing population; N_2, cell count of slow growing population; K_{rep}, first-order replication rate constant; N_{max}, maximum number of bacteria; K_{ir}, first-order death rate constant induced by the immune reaction; E_{max}, maximum kill rate induced by Lee1810; C, is concentration of Lee 1810 at time t; EC_{50}, concentration of Lee1810 at half of E_{max} and γ is the sigmoidicity factor.

The drug effect was evaluated as an additive effect. The additive model describes the drug effect as an additional kill rate as described by **Equation 3-7**.

$$\frac{dN_1}{dt} = K_{rep} \times N_1 - K_{ir} \times N_1 - (K_{rep} - K_{ir}) \times \left(\frac{N_1+N_2}{N_{max}}\right) \times N_1 - \left(\frac{E_{max} \times C^{\gamma}}{C^{\gamma} + EC_{50}^{\gamma}}\right) * N \qquad \textbf{Eq. 3-7}$$

In the **Equation 3-7** and **Figure 3-4**, the effect corresponds to an additional kill-rate constant contributed by the drug with E_{max} representing the maximum achievable drug-imposed kill-rate constant having the unit 1/time and γ is the sigmoidicity factor, which determines the shape of the concentration-effect relationship.

The CFU data were log transformed by taking Log base 10 to Log CFU. Similar to the pharmacokinetic analysis, a LTBS approach was also used for the PK/PD model, and the unexplained residual variability was characterized using as an additive error. As a single sample was available per animal, it was not feasible to separately estimate BSV and residual variability [63]; hence only the RUV characterized as additive error was estimated in the model.

Model qualification

In order to comprehensively characterize the dose-exposure-response relationship for Lee 1810, the adequacy of the developed semi-mechanistic PK/PD model was evaluated by performing a Visual Predictive Check (VPC) in which the parameters derived from the final model were used to simulate data and compare them for their consistency with the observed data [64]. Monte Carlo simulation was performed with a total of 1000 replicates to obtain the dose-response curves ranging from weekly dose of 0 mg/kg to 5000 mg/kg with QW, BIW, TIW, QD and BID. The primary endpoint here was the bacterial count at the end of drug treatment. The median value of simulations was plotted as a line while the 80%, 70% and 60% prediction intervals were represented as pink, purple and green shaded bands respectively.

Numerical simulations for the two subpopulations

The extent of change in each of the bacterial subpopulation was simulated based on the final PK/PD model for all the groups tested in this study. This simulation provides an overview of the quantitative dynamics in bacterial population growth with different dosing regimens

Data analysis and software

The PK/PD data analysis and simulations were performed in the nonlinear mixed effects modeling software NONMEM (version VII, level 2.0; Icon, Hanover, MD) using the first-order conditional estimation (FOCE). The software suite R (version 3.2; R Foundation for Statistical Computing) was used for data management and graphical as

well as statistical assessment of models. Models were evaluated based on goodness-of-fit plots, objective function value, parameter precision and scientific plausibility. Model comparison for hierarchical models was performed using the likelihood ratio test. The differences in the objective function value are approximately Chi-square distributed with n degrees of freedom (n is the difference in the number or parameters between the full and the reduced model). The differences in objective function of 3.84 for 1 degree of freedom, corresponding to a significance level of $p < 0.05$, was used to discriminate two hierarchical models.

Results and Discussion

The overall goal of this study was to characterize the dose-exposure-response relationship of lead spectinamide candidate Lee 1810 in *Mtb* infected mice using a PK/PD modelling approach. In order to separately tease out the impact of dose and dosing regimen on the response, a dose-fractionation study was conducted over a wide range of weekly doses, including 20-4000 mg/kg using different dosing frequencies. There were in total 24 dose groups with 5 mice per group (except for groups of Day 1 post-infection with 6 mice, Day 34 post-infection with 5 mice and Day 62 post-infection with 7 mice). BALB/c mice were infected with a low dose aerosol of *Mtb*, followed by a gap of 5 weeks to allow infection to establish and subsequently treated with different dosing regimens of Lee 1810 as described in **Table 3-1**. Dosing was continued for 4 weeks with 2 blood samples at 0.25 h and 8 h from each mice in the last week, followed by a washout period after which the mice were sacrificed, and the lungs removed for measurement of CFU. The study was successfully completed in 116 mice, resulting in 226 concentration measurements and 116 lung CFU measurements. 4 were lost during the conduct of the study for non-drug related issues.

Dose proportionality

The concentrations at 0.25 h and 8 h increased consistently with increase in dose as shown in **Figure 3-6**. For the same dose level, the concentrations at 0.25 h and 8 h were similar for different dosing frequencies suggesting minimal accumulation. Dose proportionality was evaluated by using the power regression model on the log-transformed data for $C_{0.25}$ and C_8 across the dose range evaluated in the dose-fractionation study. Plots of log-transformed $C_{0.25}$ and C_8 along with the regression lines are displayed in **Figure 3-7**. Results from the power regression analysis of the $C_{0.25}$ and C_8 are summarized in **Table 3-3**.The concentrations at $C_{0.25}$ increased in a dose-proportional fashion until 100 mg/kg, and were more than dose-proportional between 200 – 400 mg/kg. However, concentrations at C_8 were found to be dose-proportional across the entire dose range. The more than dose-proportional increase observed in $C_{0.25}$ above the dose of 100 mg/kg may be caused by an increased absorption rate associated with faster diffusion at the subcutaneous site of administration at higher concentrations. This information was useful for characterizing the nonlinearity for the subsequently developed population pharmacokinetic model.

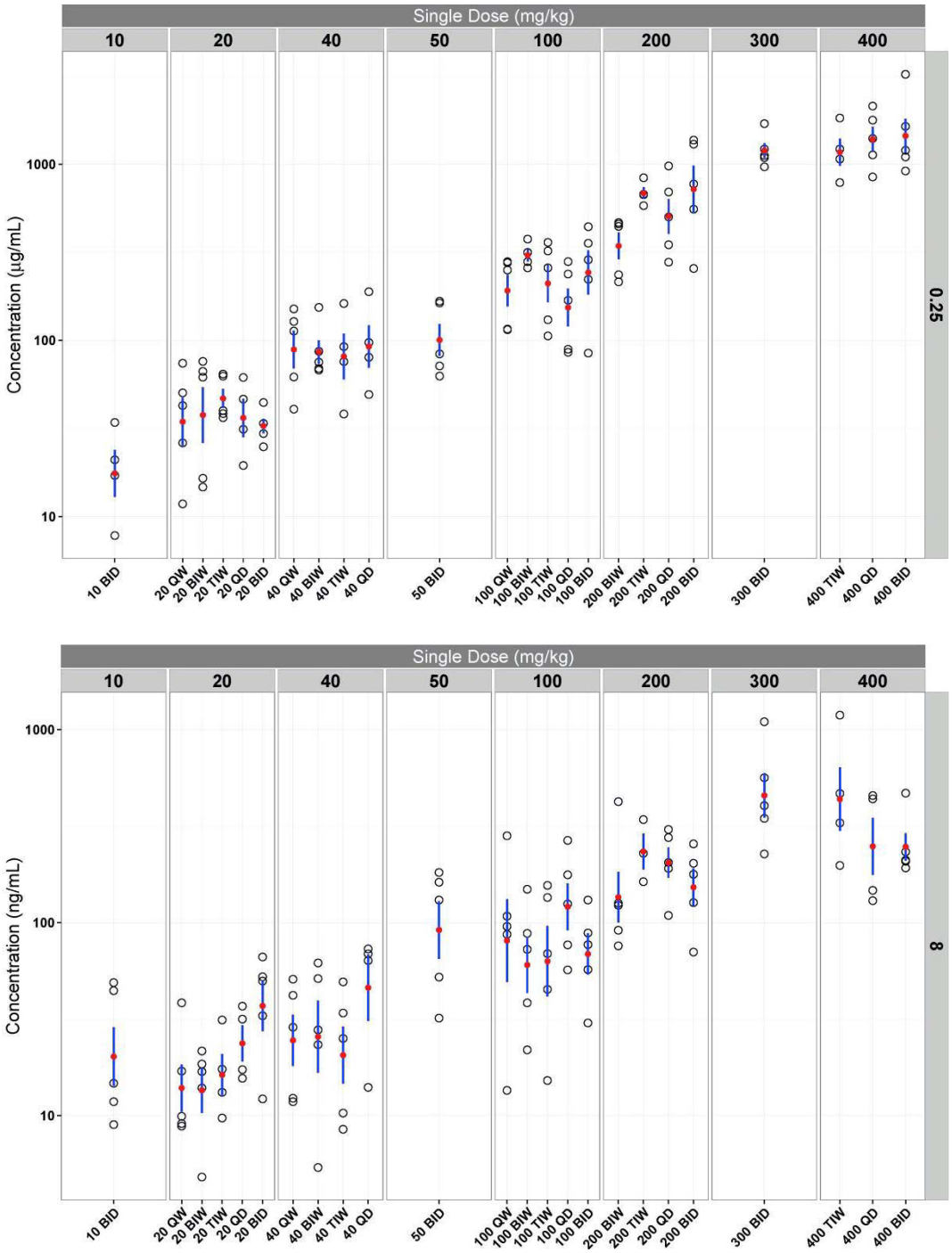

Figure 3-6. Concentration of Lee 1810 at 0.25 h (top panel) and 8 h (bottom panel) for the different dosing regimens evaluated in the dose-fractionation study
Each column heading represents the amount of single dose in mg/kg. The open black circles indicate observed data, red points indicate the mean and blue lines indicate the standard error of the observed data.

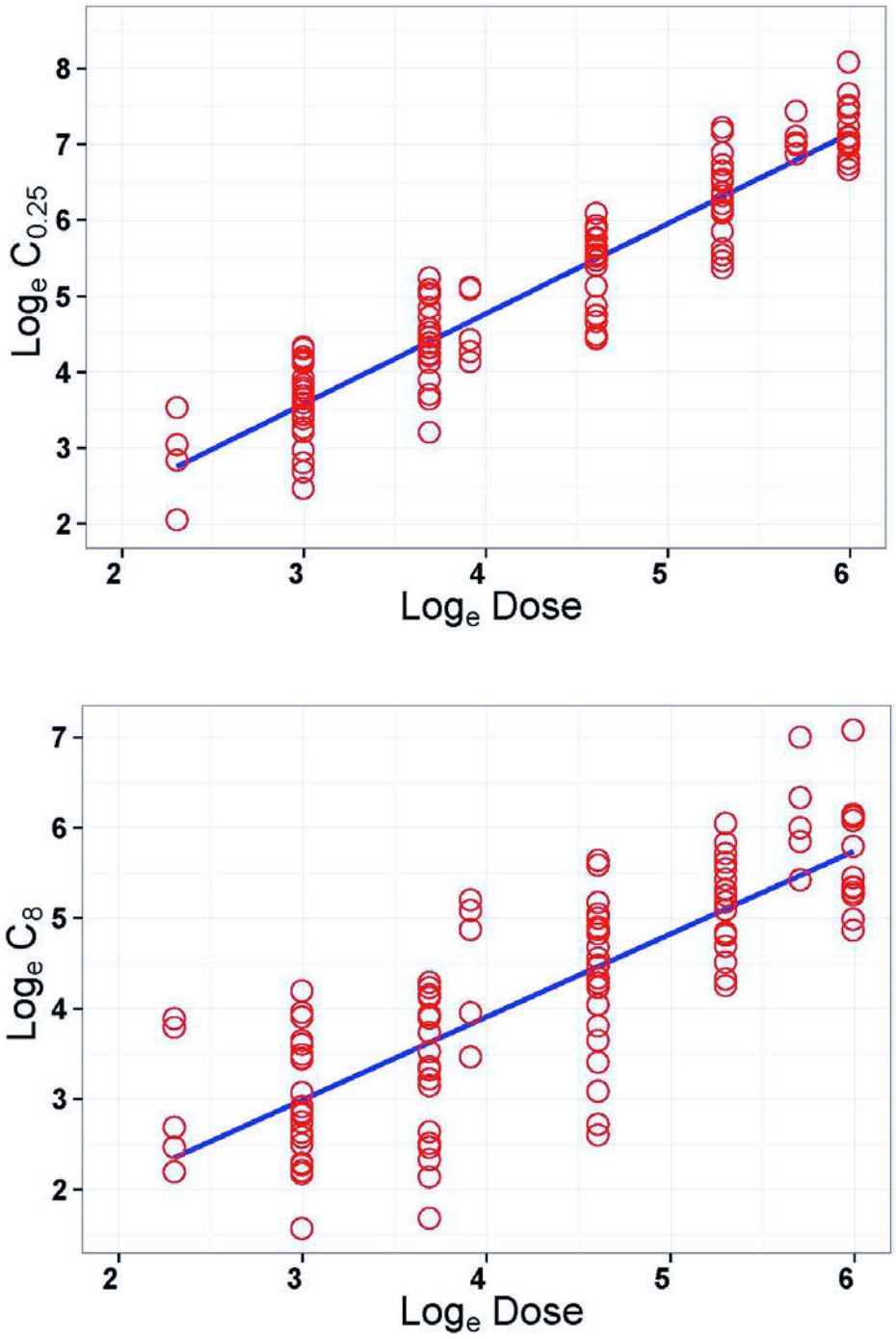

Figure 3-7. Dose proportionality assessment of $C_{0.25}$ (top panel with concentration units in µg/mL) for a dose range of 10 - 100 mg/kg and C_8 (bottom panel with concentration units in ng/mL) for a dose range of 10 - 400 mg/kg
The blue line represents the regression line and red open circles represent the observed data.

Table 3-3. Dose proportionality test using power regression model for Lee 1810.

Parameter	Dose range (mg/kg)	Slope	95% confidence limit	
			Lower	Upper
$C_{0.25}$	10 - 400	1.19	1.10	1.27
$C_{0.25}$	10 - 100	1.08	0.92	1.24
C_8	10 - 400	0.918	0.792	1.04

Population pharmacokinetic analysis of Lee 1810

The population pharmacokinetic modeling approach has been extensively used for characterizing preclinical and clinical pharmacokinetics especially in cases involving sparse sampling per individual/animal [65]. The non-linear mixed effects modeling approach was successfully applied for simultaneous modeling of the pharmacokinetics of Lee 1810 in healthy mice with intensive pharmacokinetic data as shown in **Figure 3-8** and in infected mice with sparse sampling data. A two-compartment model with first-order absorption and linear elimination from the central compartment was used to characterize the plasma concentration–time profile of Lee 1810 (**Figure 3-9**). The model was parameterized in terms of first-order absorption rate constant (K_a), clearance (CL/F), central volume of distribution (V_c/F), inter-compartmental clearance (Q/F) and peripheral volume of distribution (V_p/F). The parameter estimates along with their precision are given in **Table 3-4**. The drug undergoes rapid absorption from the subcutaneous site with an absorption rate constant of 2.31 h^{-1}, which corresponds to a short absorption half-life of 18 min. Lee 1810 displayed a biphasic pharmacokinetic profile with its volume of distribution mainly limited to the extracellular fluid volume with some peripheral distribution. Similar to other cationic amphiphilic drugs, Lee 1810 may also have high binding affinity towards intracellular phospholipids, and slow release from these sites could be the potential reason for its prolonged terminal elimination half-life [66].

To account for the potentially increased absorption above the dose of 100 mg/kg, a separate absorption rate was included for these groups, which resulted in a significant drop in the objective value function (ΔOBJ = - 8.99).The groups with doses above 100 mg/kg had a mean absorption rate of 5.89 h^{-1} which was ~2.5-times higher than the mean absorption rate of 2.31 h^{-1} for groups with doses less than 100 mg/kg.

Health status as a covariate on V_c/F, CL/F and Q/F improved model fits and resulted in a significant drop in objective value function (ΔOBJ = - 7.38 for V_c/F , ΔOBJ = - 7.00 for CL/F and ΔOBJ = - 12.8 for Q/F). The pharmacokinetics were found to be different between healthy and infected mice with the later having a 56.5% lower CL/F, 69% lower V_c/F and 69.6% lower Q/F The reason for the reduced clearance is not clear, particularly since Lee 1810 is largely eliminated by renal excretion without major metabolic conversion. A 2.5- to 3-fold lower clearance, however, was also observed with dihydrostreptomycin in TB infected mice as compared to healthy mice [67]. In some human patient populations, reduced clearance has also been observed for rifampin [68], which is typically known to exhibit increased clearance due to autoinduction during chronic therapy [69]. One of the potential explanations for lower CL/F in infected mice could be an alteration in protein binding of Lee1810. Lee 1810 is a basic drug and is found to have a protein binding of 40% in rat plasma. With its two ionizable basic moieties, Lee 1810 could possibly bind to α1 acid glycoprotein (AAG) which is an acute-phase plasma protein that predominantly binds to basic drugs and increases in reaction to bacterial infections and other inflammatory stimuli [70]. For example, the plasma AAG concentration was found to be significantly higher in patients with plasmodium filarial malaria infection as compared to healthy individuals, resulting in a lower free fraction of antimalarial drug quinine [71]. Additionally, patients with Crohn's disease, inflammatory

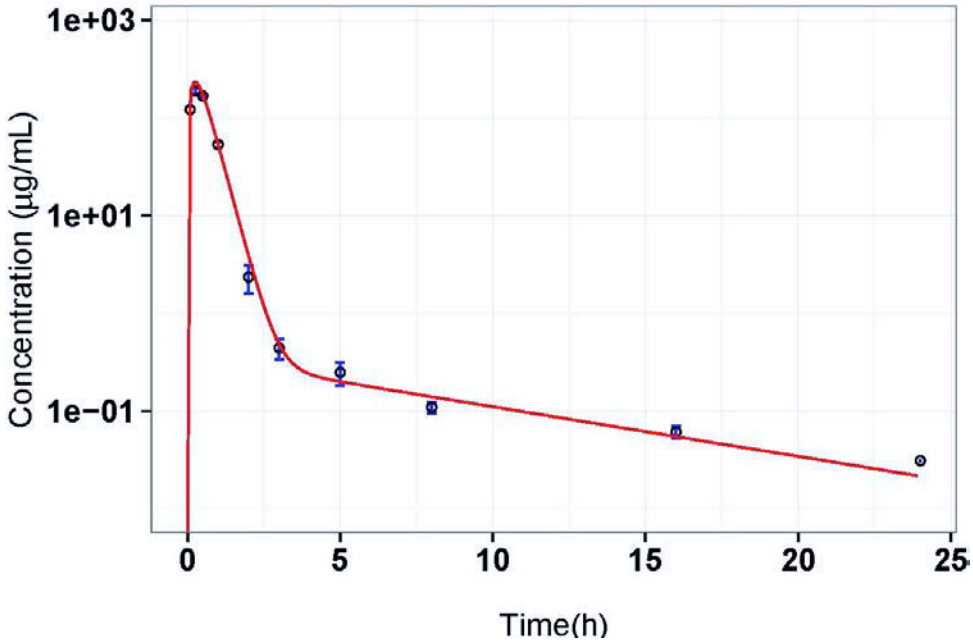

Figure 3-8. Concentration–time profile of Lee 1810 for a single dose of 200 mg/kg by subcutaneous administration in healthy BALB/c mice

The red line indicate the population prediction, black points indicate the mean and the blue error bars indicate the standard error of the observed data at each time point (n=3).

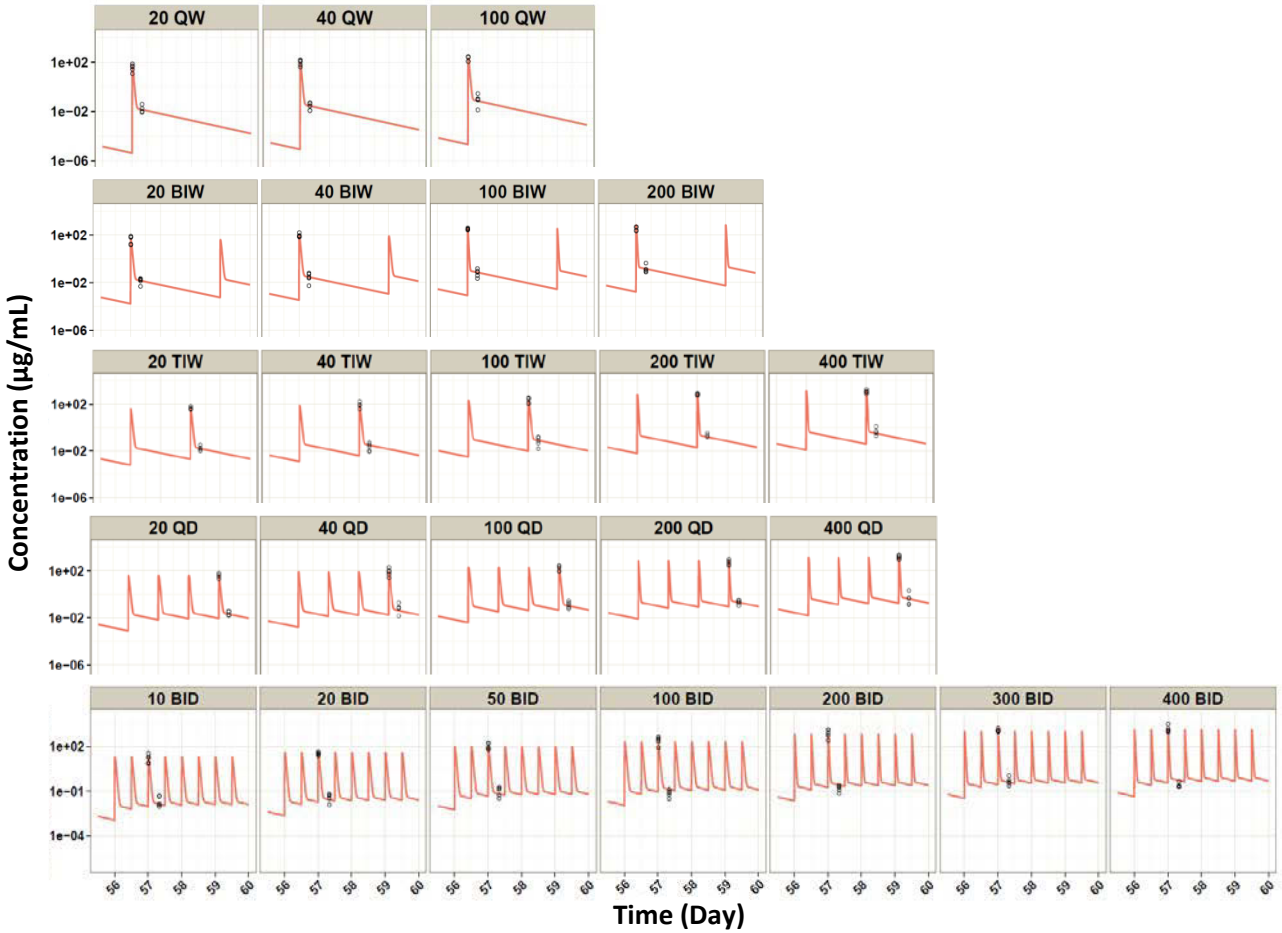

Figure 3-9. Individual Lee 1810 concentration-time profiles for the different treatment groups tested in the dose-fractionation study

The observed concentrations (open black circles) and population predictions (thick red line) are depicted for the time period of 56 to 60 days after initiation of infection (equivalent to 22 to 26 after initiation of dosing).

Table 3-4. Population pharmacokinetic model parameter estimates

Parameters	Typical value (%RSE)	%BSV (%RSE)
K_a (h^{-1})	2.31 (17.8)	
V_c/F (L/kg)	0.435 (21.6)	
V_p/F (L/kg)	0.161 (22.2)	
CL/F (L/h/kg)	1.17 (9.30)	19.9 (53.7)
Q/F (L/h/kg)	0.0191 (21.5)	
Effect of disease on CL/F	0.435 (19.5)	
Effect of disease on V_c/F	0.310 (24.2)	
Effect of disease on Q/F	0.304 (29.3)	
K_a > 100mg/kg	5.89 (15.8)	
RUV(%CV)	49.3 (7.3)	

Abbreviations: K_a, absorption rate constant; V_c/F, volume of central compartment corrected for bioavailability; V_p/F, volume of peripheral compartment corrected for bioavailability; CL/F, clearance corrected for bioavailability; Q/F, intercompartmental clearance corrected for bioavailability; Effect of disease on parameter was determined using the following relationship: $P=\theta_1\times(\theta_2)^{Status}$, where P represents the typical value of parameter in the population, Status is an indicator variable equal to 0 for healthy mice and 1 for infected mice, θ_1 is the typical value of P for healthy mice, and θ_2 is the multiplicative factor describing the increase or decrease in P as a result of the infection ; K_a > 100 mg/kg, absorption rate constant for dose above 100 mg/kg; RUV, Residual Unexplained Variability

arthritis, and chronic renal failure also had increased levels of AAG and reduced free fraction of basic drugs like propranolol and chlorpromazine [72]. Based on these observations, it is possible that TB infected mice may have elevated levels of AAG which reduces the free fraction of Lee 1810 and this ultimately results in reduction of its renal clearance. Increase in plasma protein binding of Lee 1810 could also result in reduced V_c/F. Reduced V_c/F of Lee 1810 in infected mice could potentially be explained by dehydration in infected mice which resulted in reduction in average body weight from 21 g on Day 1 of treatment to 20.3 g on the final day of study leading to reduced volume of distribution. Lee1810 based on its physico-chemical characteristics is mainly limited to the extra-cellular space which decreases with decrease in body weight. The distribution of Lee1810 via the diffusion process would also be reduced by the decreased fluid content and this could also explain the reduction in Q/F observed in infected animals. Similar observations were also seen in dehydrated goats which lost on an average 10-13% of their body weight resulting in significant changes in distribution and elimination parameters of oxytetracycline [73]. Further research needs to be conducted to better understand the reason for the differences in pharmacokinetics between healthy and chronically infected mice.

Effect of dosing regimen on the bacterial counts

After four weeks of therapy in mice chronically infected with *Mtb*, Lee 1810 exhibited a dose-dependent decrease in the bacterial counts with saturation at doses above 200 mg/kg as shown in **Figure 3-10**. **Figure 3-11** indicates the concentration-dependent rather than time-dependent killing characteristics of Lee 1810 as suggested for the spectinamides similar to Lee 1810 [52]. For example, a weekly dose of 500 mg/kg when given as 100 mg/kg QD resulted in better efficacy compared to 50 mg/kg BID. Similar trends were also observed with dose fractionation of other weekly doses where intermittent dosing provided improved efficacy relative to more frequent dosing regimens. Drugs with concentration-dependent bacterial killing characteristics are associated with a dramatic reduction in bacterial count as a consequence of a rise in drug concentrations [74].This could potentially be explained by the ability of spectinamides to accumulate inside the macrophages [75] promoted by lysosomal trapping and attain high concentration to kill the intracellular form of *Mtb*. This intracellular accumulation would likely be facilitated by high concentration gradients that drive drug molecules across the bacterial cell wall into the intracellular compartment.

Model-based characterization of the natural growth of *Mtb* in infected mice

In the immunocompetent mouse chronic infection model, TB infection undergoes a transition from an initial exponential growth phase to a long-term stationary phase, where the overall growth rate diminishes markedly [76, 77]. This may be conceptualized as a manifestation of phenotypic variants which evolved within this isogenic population in response to the various physiological stresses like immune response, starvation,

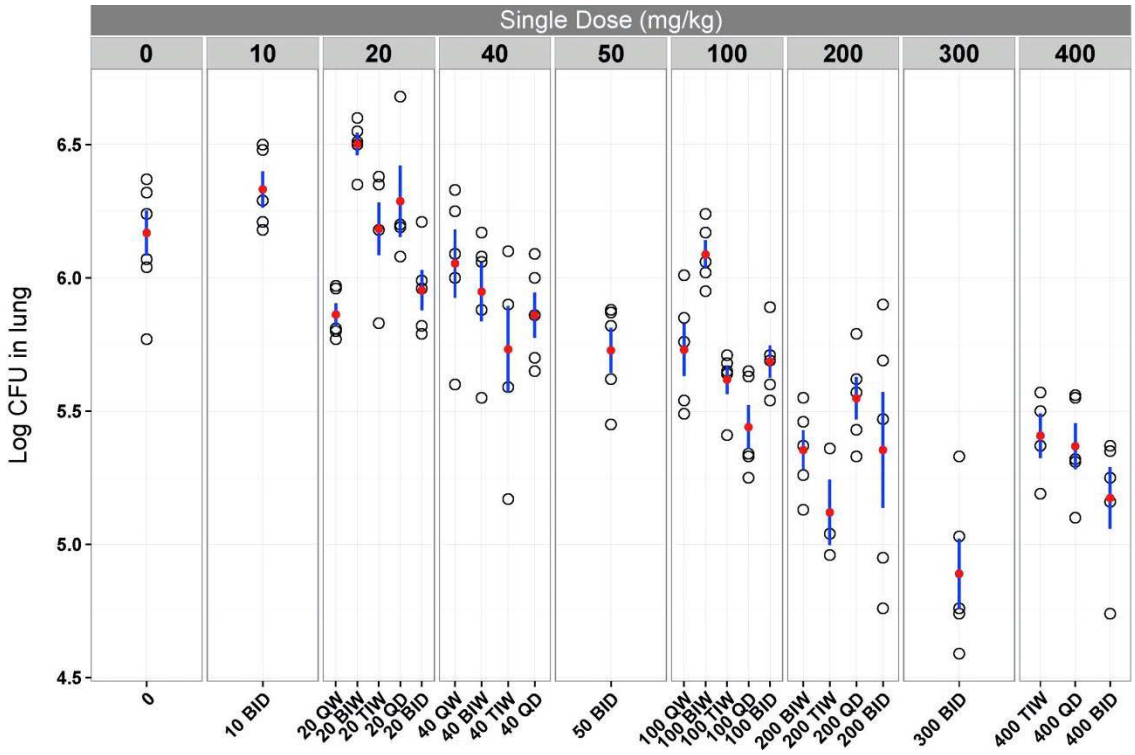

Figure 3-10. Bacterial burden (Log CFU) in the lungs of *Mycobacterium tuberculosis* infected mice for the different dosing regimens evaluated in the dose-fractionation study

Each column represents the amount of single dose in mg/kg. Open black circles indicate the observed data, red points indicate the mean and blue lines indicate the standard error.

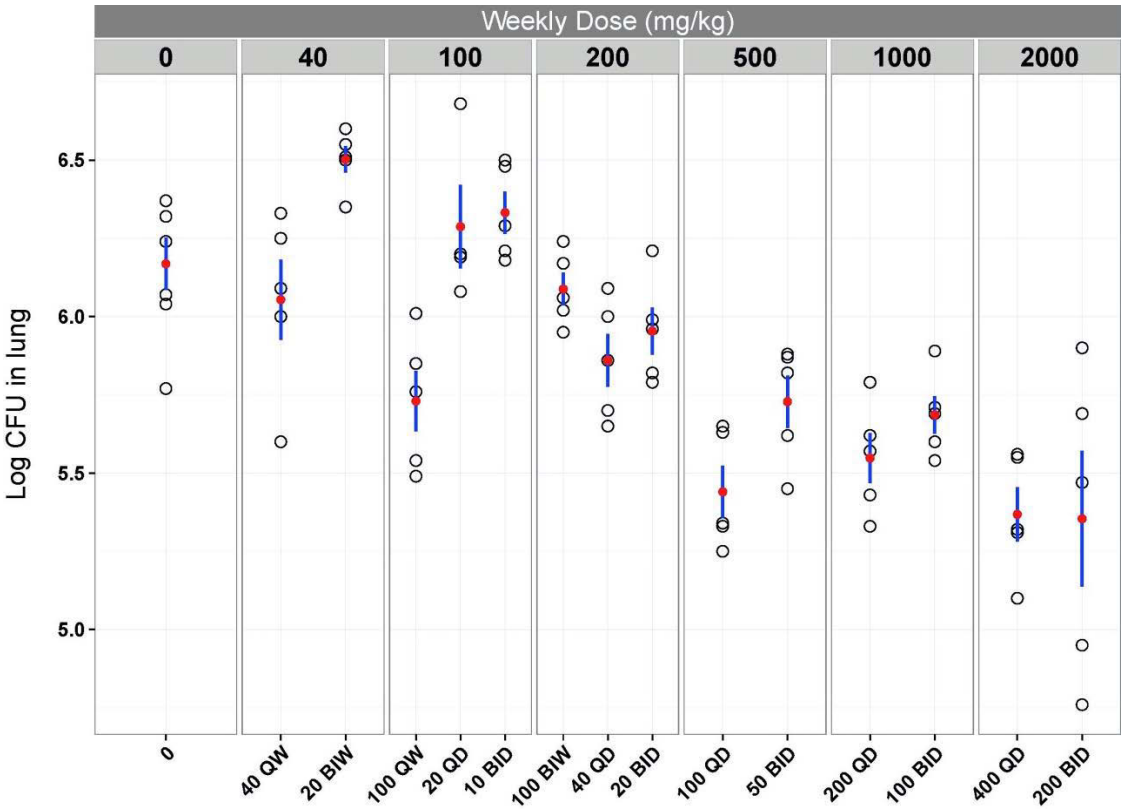

Figure 3-11. Bacterial burden (Log CFU) in the lungs of *Mycobacterium tuberculosis* infected mice for the different dosing regimens with same weekly dose evaluated in the dose-fractionation study

Each column heading represents the total weekly dose amount in mg/kg. Open black circles indicate the observed data, red points indicate the mean and blue lines indicate the standard error.

acidification and hypoxia [78]. The developed two-subpopulation bacterial growth model adequately described this phenotypic switching from the fast growing metabolic state to the slow growing/non-replicating state. **Figure 3-12** for the natural bacterial growth in the untreated group predicts that during the early phase of infection, most of the total microbial population consists of the fast growing subpopulation (N_1) which results in exponential growth. Under the pressure of host immune response and other stresses, the system gradually shifts into the stationary phase with increasing number of bacteria in the slow growing subpopulation (N_2), which are better equipped to sustain themselves in the unfavorable conditions [79]. Recently, it was also demonstrated that the slow growing subpopulation retains their metabolic activity [80], and also have the ability to reactivate growth upon detection of a favorable signal or environment [81, 82].

The replication rate constant for the fast growing population (K_{rep})was found to be 0.0327 h^{-1} (**Table 3-5**) and the corresponding doubling time was calculated as 21.2 h, which is within the range reported in the literature (13–80 h) [19, 83-86]. This slow *in vivo* growth rate is a hallmark of *Mtb*, a characteristic that may contribute to its persistence in the host without manifestation of clinical symptoms, yet preserving the ability to reactivate and disseminate [87]. Since growth rate of fast growing bacteria when described using a logistic function did not improve the fit of the natural bacterial growth model, a simple first-order growth rate constant was used for describing replication in the fast growing bacteria.

Model-based characterization of the dose-exposure-response relationship for Lee 1810 in *Mtb* infected mice

To account for the killing effect by Lee 1810 exposure, the concentration from the central compartment of the pharmacokinetic model was linked to the natural bacterial growth model. The drug effect was implemented as an additive component to the natural death rate of the bacteria via an E_{max}-type model. (**Equation 3-7**). A sigmoidal E_{max} model resulted in a significantly improved fit as compared to an ordinary E_{max} model (ΔOBJ = - 51.3). The Hill coefficient was substantially greater than 1, which is a typical characteristic that has also been observed for other antibiotics with concentration-dependent killing (**Table 3-6**) like streptomycin and rifampin, which displayed a hill coefficient of 1.9 and 2.5 respectively. A high value of the Hill coefficient is indicative of a steep concentration-effect relationship [74].

The concentration that produced the half-maximal effect EC_{50} (239 µg/mL) was found to be much higher than MIC (1.6 µg/mL) of Lee 1810. This was expected, as EC_{50} describes the effect on the rate constant for drug-induced bacterial killing and is much more realistic parameter to compare potency of compounds with regard to bacterial kill than the MIC. The experimentally determined MIC represents the lowest concentration at which no growth of microorganism is visible to the naked eye. MIC is usually estimated at a fixed concentration and does not resemble the physiological conditions in which the drug concentrations changes with time. Additionally, the inoculum size and percentage contribution of the bacterial sub-population also contribute to the differences between

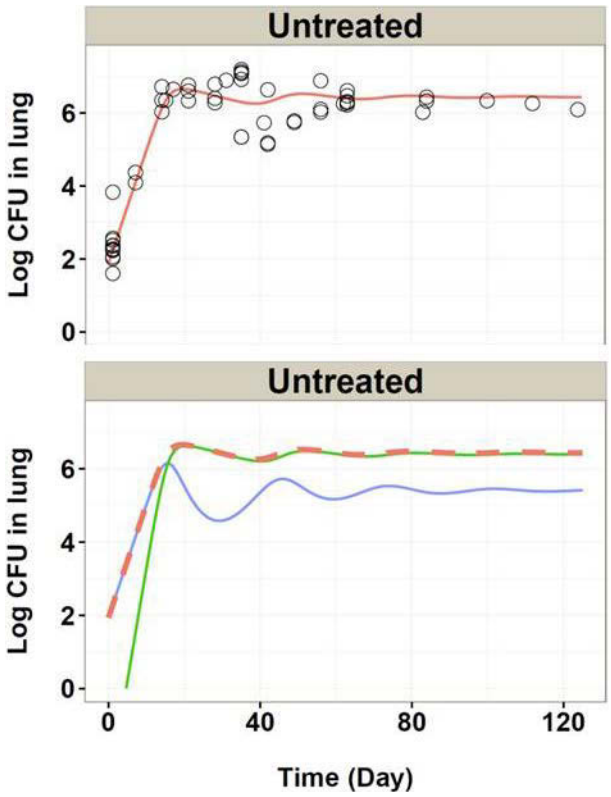

Figure 3-12. Natural growth model fitted typical Log CFU-time profile for the untreated group data obtained from literature and CSU studies
Model predicted Log CFU in the fast growing subpopulation (N_1 , blue line), slow growing subpopulation (N_2 , green line), total population (red dash line) and observed Log CFU (open black circles) are depicted.

Table 3-5. Parameter estimates of the *Mycobacterium tuberculosis* natural growth model

Parameters	Typical value (%RSE)	%BSV (%RSE)
K_{rep} (h^{-1})	0.0327 (33.3)	70.8 (57.7)
$N_{1,0}$ (Log CFU)	1.93 (9)	
N_{max} (Log CFU)	6.44 (1.2)	54.7 (58.5)
K_{ir}(h^{-1})	0.00303 (3.6)	
RUV (% CV)	32.4 (19.6)	

Abbreviations:$N_{1,0}$, cell count of fast growing population at the initiation of the infection; K_{rep}, first-order replication rate constant; N_{max}, maximum number of bacteria; K_{ir}, first-order death rate constant induced by the immune reaction; BSV, Between Subject Variability; RUV, Residual Unexplained Variability.

Table 3-6. Parameter estimates of the final PK/PD model of Lee 1810

Parameters	Typical value (%RSE)
EC_{50} (μg/mL)	239 (0.167)
E_{max} (h^{-1})	11.9 (0.485)
γ	2.40 (0.142)
RUV (% CV)	20.6 (4.2)

Abbreviations: E_{max}, maximum kill rate induced by Lee1810; EC_{50}, concentration of Lee 1810 at half of E_{max}; γ, Hill function.

EC_{50} and MIC [88]. MIC also assumes an all-or-nothing effect on the bacterial growth. In contrast, EC_{50} captures the drug's effect on the rate of bacterial killing. Bacterial killing is already achieved at concentrations much lower than EC_{50}, but at a much lower magnitude than at concentrations above EC_{50}. The effect achieved at EC_{50} is half of the maximum kill rate constant achievable with Lee 1810.

The RUV in the PK/PD model was described using an additive error model. The modeled profiles of bacterial count versus time for all the groups as well as experimentally determined CFU counts are shown in **Figure 3-13**. The figure indicates that the population predictions of the PK/PD model were in close agreement with the observed values.

A VPC was furthermore performed to qualify the established model. The VPC shown in the **Figure 3-14** highlights the ability of the model to reasonably predict the central tendency and the variation in the bacterial count. The impact of dosing frequency on efficacy of Lee 1810 was also captured by the VPC where the rate of reduction in the bacterial load with increasing doses was steeper with decrease in dosing frequency.

Alternative models and model limitations

Alternative PK/PD models could not fit the data as well. A natural bacterial growth model with single population could describe the untreated group data equally well as the two-subpopulation model; however it was not able to describe the dose-exposure-response for all the different dosing regimens as a higher bacterial kill was predicted for groups with more frequent dosing as compared to the ones with intermittent dosing. The addition of drug effect was also tested on the slow growing population but it resulted in over-parameterization with no convergence and poor fits.

The presented model has several limitations. Firstly, the PK/PD model was based on the total bacterial count and no measurements were made to separately identify the percentage of each subpopulation in the two-subpopulation modeling approach. Quantification of each subpopulation could be helpful in distinguishing competing models which can describe the data equally well. Secondly, the model has not been studied for different bacterial strains, inoculum size, and immune status in different preclinical models. For example, the initial inoculum when taken from a stationary-phase culture will most likely have a higher proportion of slow growing bacteria as compared to an inoculum from a log-phase culture, which could eventually have an impact on the entire time course of relative bacterial dynamics. The mycobacterial populations in immunodeficient strains of mice (e.g., IFN-γ-knockout mice) have reduced phenotypic heterogeneity, and higher growth potential as compared to the immunocompetent mouse model used in this study [80]. In these situations, appropriate modification in the natural growth model will be required to describe the bacterial kinetics. Thirdly, there are differences in the pathophysiology and disease progression of *Mtb* between mice and humans. The mouse model used in this study develops granulomas that consist of loose

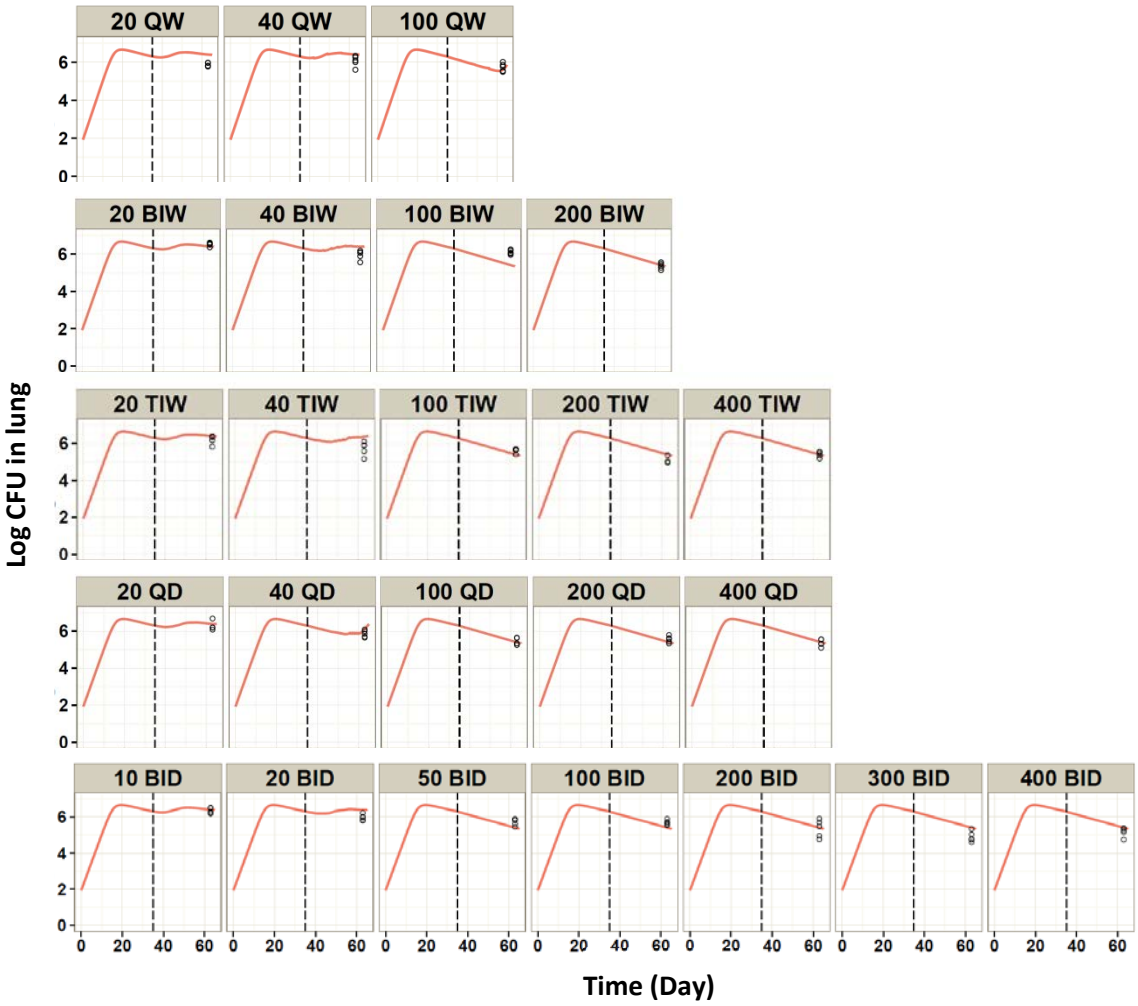

Figure 3-13. Individual Lee 1810 Log CFU-time profiles for the different treatment groups evaluated in the dose-fractionation study

The observed Log CFU (open black circles) and population predictions (thick red line) are depicted. The black dash line indicates the time when treatment was initiated.

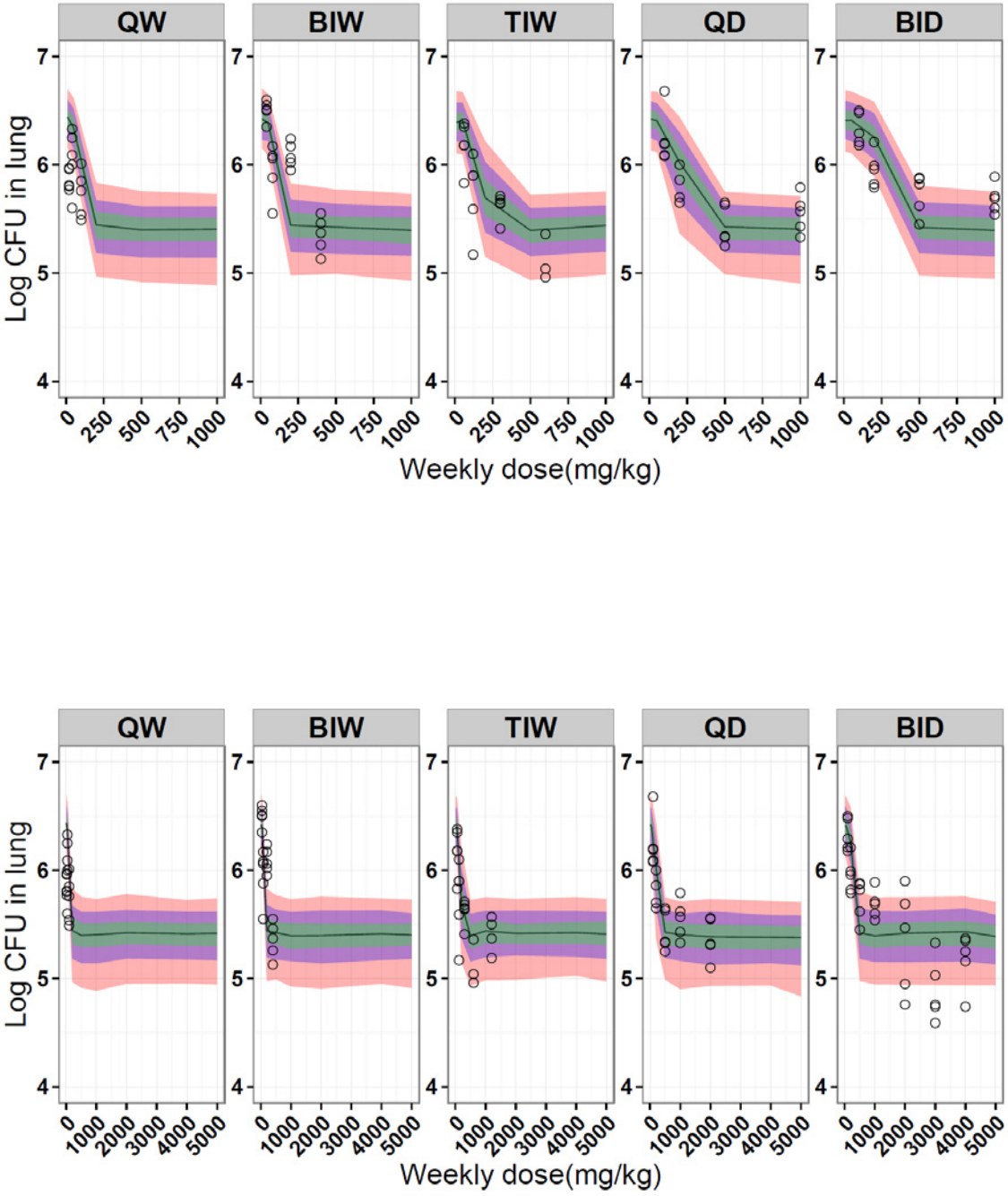

Figure 3-14. Visual predictive check (VPC) of the PK/PD model for the describing the weekly dose-response relationship

Top Panel: Weekly dose range from 0 to 1000 mg/kg. Bottom Panel: Weekly dose range from 0 to 5000 mg/kg. Pink, purple and green bands represent 80% prediction interval, 70% prediction interval and 60% prediction interval of simulated data respectively. The solid black line is the median of simulated data and open circles are the observations.

aggregates of lymphocytes and macrophages which do not progress into the well-formed necrotic granulomas observed in humans [89]. The drug exposure in plasma may not equilibrate homogeneously within the granulomatous lesions, and this could potentially complicate the translation of exposure-response relationship from mice to humans.

PK/PD modeling results in perspective with antitubercular combination therapy

The developed PK/PD model was applied to simulate the relative dynamics of fast growing and slow growing subpopulations as conceptualized in our modeling approach. The simulations presented for different dosing regimens in **Figure 3-15** suggests that weekly doses ranging from 100 mg/kg for twice weekly dosing down to 50 mg/kg for twice daily dosing is sufficient to kill most of the fast growing bacteria and further increases in dose may only result in marginal increases in efficacy. Based on these simulations, it can be speculated that further enhancement in efficacy and shortening of treatment duration could be achieved by combining spectinamides with other anti-tuberculosis agents which are active against the slow growing population including pyrazinamide (PZA) and rifampin. PZA, a first line anti-tuberculosis therapy has unique pharmacological activity as it is less effective against the fast growing tubercle bacilli but more effective against the slow growing/non-replicating bacteria [90]. Pyrazinoic acid, which is the active moiety of pyrazinamide, acts by disrupting the membrane energetics and inhibiting the membrane transport function preferentially against the non-replicating bacilli which are associated with low membrane potential and acidic pH [91]. This could be one of the potential explanations for the significantly improved efficacy observed in a recently conducted combination trial of Lee 1599 (structural analog of Lee1810 and a competing lead spectinamide candidate) along with PZA in a high dose aerosol mice infection model that was performed by Dr. Anne Lenaert's research group at Colorado State University (**Figure 3-16**). Lee 1599 was found to be as efficacious as Lee 1810, whereas PZA had modest activity as a single agent. The combination of Lee 1599 and PZA resulted in a significant reduction in bacterial count compared to the same drugs when used alone. This synergistic effect in combination could possibly be the outcome of each drug's ability to act on a different subpopulation of bacteria.

Looking ahead, this PK/PD model could also be used for simulating untested scenarios and for quantitative comparison of different dosing strategies as well as competing lead candidates. Furthermore, the PK/PD relationship established with this model could be integrated with the information about antibiotic susceptibility, drug associated adverse effects, and pharmacokinetics in different patient populations to perform simulations for identifying clinically optimum dosing regimens and also help in informing clinical trial designs. This semi-mechanistic model-based approach also provides a framework for evaluating the dose-exposure-response analysis of other investigational anti-tuberculosis agents. The differentiation of drug-specific and mycobacterium specific parameters makes it convenient to apply this model for scenarios other than those reported for this drug and study.

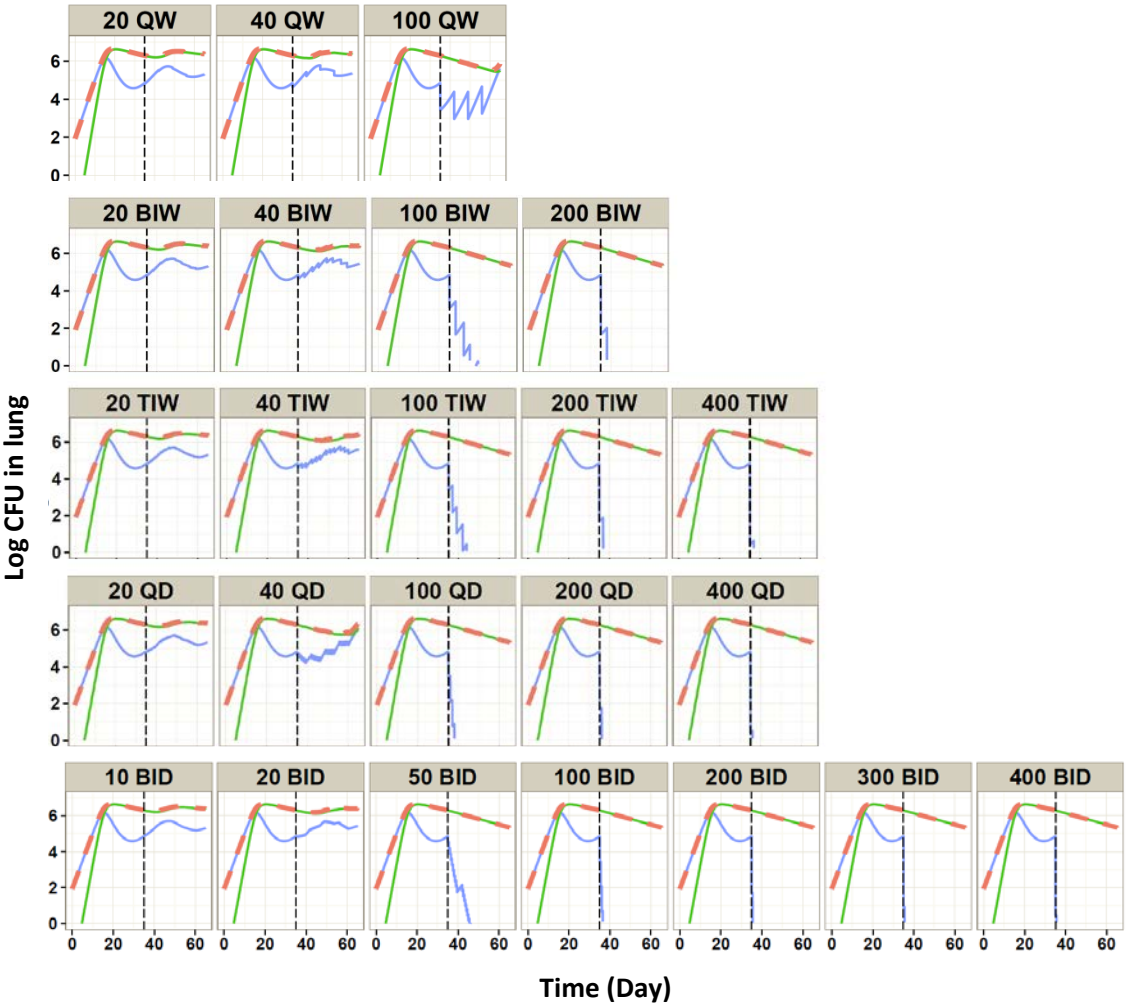

Figure 3-15. PK/PD model predicted Log CFU in the fast growing state, slow growing state and total population for the different treatment groups evaluated in the dose-fractionation study

Model predicted Log CFU in the fast growing subpopulation (N_1, blue line), slow growing subpopulation (N_2, green line) and total population (red dash line) are depicted. The black dash line indicates the time when treatment was initiated.

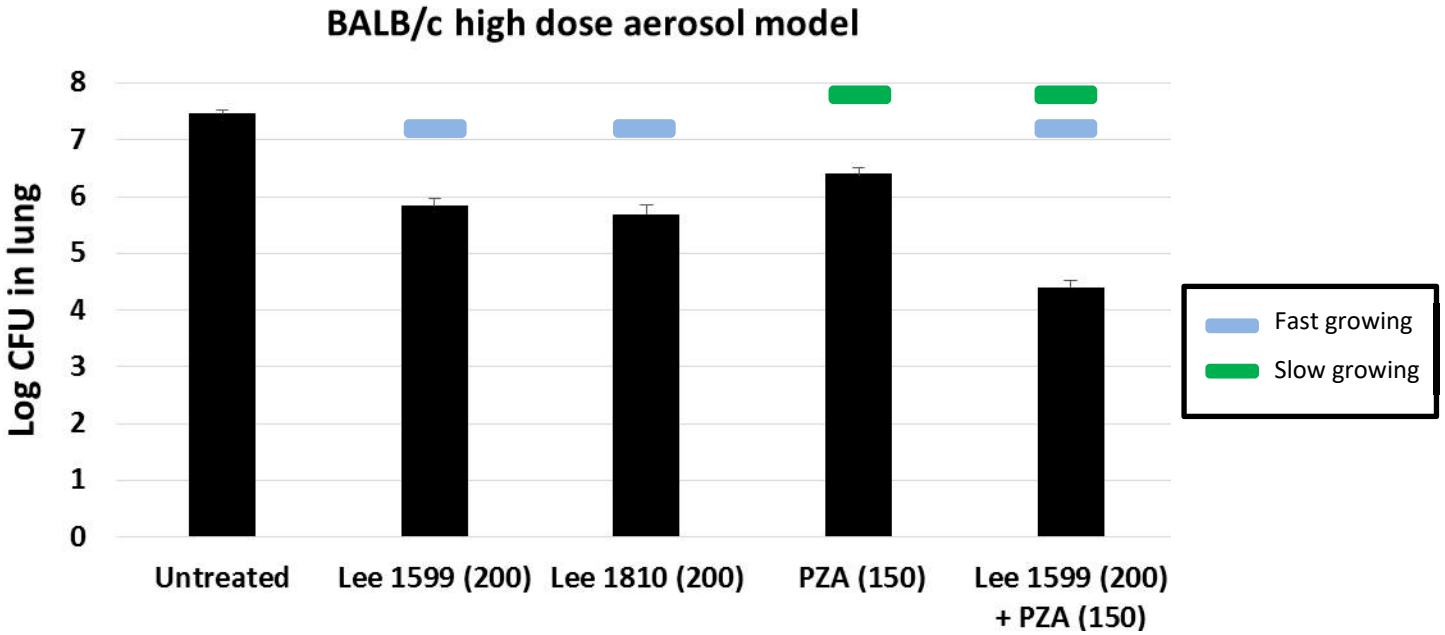

Figure 3-16. ***In vivo*** **efficacy trial showing bacterial burden in the lungs for combination of spectinamides with pyrazinamide in a BALB/c mouse (n=3-6) infection model following high dose aerosol infection of** ***Mycobacterium tuberculosis*** **Erdman (mean ± s.e.m.)**

Lee 1599 /Lee 1810 were subcutaneously dosed at 200 mg/kg and pyrazinamide (PZA) was orally dosed at 150 mg/kg. All treatments were given QD, 5 days a week for 4 weeks.

In summary, the efficacy of Lee 1810 was largely driven by concentration-dependent killing, and this supports the use of intermittent dosing. A two-subpopulation bacterial growth model adequately described the phenotypic heterogeneity associated with *Mtb* infection in immunocompetent mice. This model component was integrated with the pharmacokinetics of Lee 1810 to successfully describe its dose-exposure-response relationship. The semi-mechanistic PK/PD modelling approach allowed for a more comprehensive characterization of drug efficacy as compared to the MIC based PK/PD index approach. Based on the PK/PD model it was hypothesized that improved efficacy could be achieved by combining spectinamides with sterilizing anti-tuberculosis agents. This hypothesis was supported by the synergistic activity obtained with combination of Lee 1599 and PZA. Preclinical PK/PD assessments of Lee1810 will be useful for determining it's preclinically and clinically optimum dosing regimen. This semi-mechanistic model-based approach also provides a framework for investigating the PK/PD relationship of other investigational anti-tuberculosis agents.

CHAPTER 4. COMPARATIVE PHARMACOKINETICS OF SPECTINAMIDE ANTIBIOTIC LEE 1599 AFTER INTRATRACHEAL AND SUBCUTANEOUS ADMINISTRATION FOR THE TREATMENT OF TUBERCULOSIS

Introduction

Spectinamides are a novel semisynthetic series of spectinomycin analogs with excellent narrow-spectrum antitubercular activity. They exhibit selective ribosomal inhibition and are not cross-resistant with the existing tuberculosis therapeutics. Spectinamides maintain activity against Multidrug-resistant (MDR) and extensively drug-resistant (XDR) tuberculosis. Physico-chemically, spectinamides are hydrophilic in nature making them highly water soluble and exhibit low plasma protein binding. However, these analogs have poor permeability across the intestinal barrier, limiting their bioavailability and thus oral use. Consequently, a parenteral route such as subcutaneous (SC) injection was selected for dosing in efficacy studies. The lead spectinamide Lee 1599 upon SC administration in a mouse model of *Mycobacterium tuberculosis* (*Mtb*) infection at a dose of 200 mg/kg QD (5 days a week) for 28 days resulted in 1.57 Log CFU (colony forming unit) reduction in the lungs. This excellent anti-mycobacterial activity of Lee 1599 was similar to streptomycin at similar doses in the lungs [52].

Historically, orally and parenterally administered antibiotics have been used to treat patients with lung infections, but the downside is that they do not directly target the lungs [92]. Therefore in order to deliver even moderate concentrations of antibiotic to the lungs, the primary site of infection, the required overall systemic exposure is usually high and thus increases the potential for the emergence of side effects [93, 94]. The delivery of antibiotics via the inhalation route potentially leads to much higher concentrations of antibiotic in the lungs. It also increases the possibility of targeting alveolar macrophages which may allow the delivery of drugs to the intracellular (phagosomal) compartment. Additionally, inhaled therapies have the potential to stimulate innate bactericidal responses and/or antigen presenting functions more efficiently [95]. The development of resistance during antimicrobial therapy stems at least partially from the fact that when administered systemically many antimicrobial drugs fail to reach therapeutically effective concentrations in the lungs or penetrate into the alveolar macrophages, a reservoir for intracellular infections [96, 97]. High local concentrations are consequently needed to prevent amplification of less sensitive pathogens, especially when located intracellularly [98]. Intrapulmonary administration can deliver high concentrations of drug to the lung tissue and macrophage cytosol, potentially sufficient to prevent or overcome drug resistance [97, 98].

Inhalational delivery has revolutionized the treatment of chronic *Pseudomonas aeruginosa* infections in cystic fibrosis (CF) since the FDA approval of TOBI (tobramycin inhalation solution) in 1997 followed by CAYSTON (aztreonam for inhalation solution) in 2010. In Europe, a third antibiotic from the polymyxin family is approved in CF, colistimethate sodium, a prodrug of colistin, but it is not approved in the United States [94]. Use of inhaled antibiotics in CF has been shown to decrease

Pseudomonas aeruginosa colonization, delay onset of chronic infection, increase lung function, improve the quality of life, and correlates with a reduction in morbidity, the number of exacerbations and the number of hospital admissions when compared to systemic administration [94].

Based on the experiences described above, the efficacy of Lee 1599 had been evaluated after intratracheal (IT) administration in the same mouse model of *Mtb* infection as used in our previous studies [99]. A dose of 200 mg/kg TIW (3 days a week; Monday, Wednesdays and Fridays) for 28 days demonstrated excellent efficacy with a 2.2 Log CFU reduction in the lungs. This antitubercular activity was comparable to that of rifampin (administered orally at 10 mg/kg, 5 days per week) [52].

It was hypothesized that the excellent efficacy following intrapulmonary delivery of Lee 1599 may be a result of extensive distribution of the free drug within the lungs. In this chapter, we test this hypothesis by performing a comparative tissue distribution study of Lee 1599 in BALB/c mice following SC and IT administration. In addition to the lungs, distribution in other organs such as spleen, liver and kidneys were also evaluated to better understand the impact of tissue distribution on overall efficacy of Lee 1599.

Material and Methods

Animal study

Healthy female BALB/c mice (n= 15) were administered a dose of 200 mg/kg of Lee 1599.2HCl by IT aerosol delivery with a PennCentury MicroSprayer PennCentury Inc. (Wyndmoor, PA) as previously described [99]. The tip of the device was inserted up to the first bronchial bifurcation of the trachea of the anesthetized animal, bypassing the nose and throat and making it easier to precisely control the delivered dose. This is in contrast to metered-dose inhalers and dry powder inhalers and/or nebulizers in animal studies, which filter the aerosol through the nasopharynx, are prone to between-subject variability and are not capable of targeting a desired, predetermined area of the lungs. At pre-dose and 0.25, 1, 3, and 8 h after administration, mice (n=3) were sacrificed humanely. Lungs, spleen, liver, and kidneys were immediately harvested and frozen in liquid nitrogen. Blood obtained by cardiac puncture was collected in heparinized collection tubes, and plasma was separated immediately by centrifugation (10,000 g for 10 min at 4°C). All the plasma and tissue samples were stored at -70°C until analysis.

For comparison of plasma pharmacokinetics of Lee 1599, healthy BALB/c female mice (n=15) were dosed via the SC route at 200 mg/kg of Lee 1599.2HCl. Blood and tissue samples were collected and processed as described for IT administration.

All animal experiments were conducted in accordance with the Animal Welfare Act and the Public Health Service Policy on Humane Care and Use of Laboratory Animals. The study protocols were approved by the Institutional Animal Care and Use

Committees of Colorado State University and the University of Tennessee Health Science Center, respectively.

Bioanalysis

Concentrations of Lee 1599 in plasma and tissues were determined by a validated liquid chromatography tandem mass spectrometry assay. The frozen tissues were thawed at room temperature and weighed. For every 1 g of tissue 4 mL of water was added for homogenization using an Ultra Turrax homogenizer (IKA, Wilmington, NC). To prevent cross contamination between two samples, the plunger of the homogenizer was washed with methanol and water after each sample. Samples were further prepared by protein precipitation with methanol (spiked with the internal standard 3′-dihydro-3′-deoxy-3′(R)-isopropylacetylamino spectinomycin) followed by centrifugation at 10,000 g for 10 min at 4°C. Chromatographic separation of the supernatant was carried out on a Luna 3 µm hydrophobic interaction liquid chromatography (HILIC) 100 × 4.6 mm column (Phenomenex, Torrance, CA) using a gradient mobile phase of methanol and 10 mM ammonium formate, pH 2.75, at a flow rate of 0.4 mL/min. Detection was performed with an API 4500 triple-quadruple mass spectrometer (ABI-Sciex, Foster City, CA) with electrospray ionization in multiple reaction monitoring mode using the mass transfers of m/z 487.2/207.1 for Lee 1599 and m/z 418.3/207.1 for the internal standard (Lee 1369). Calibration curves were constructed for each test compound and validated with spiked samples of mouse plasma or respective homogenized tissue.

Pharmacokinetic analysis

Pharmacokinetic profiles of Lee 1599 were analyzed by standard non-compartmental procedures using Phoenix WinNonlin 6.3 (Pharsight Corporation, Mountain View, CA) in plasma and tissues. Penetration of drug in tissues was estimated from the ratios of the area under the concentration-time curve from time 0 to infinity ($AUC_{0-\infty}$) for tissues compared to the $AUC_{0-\infty}$ in plasma. Total plasma clearance was calculated as ratio of dose and resulting plasma $AUC_{0-\infty}$.

Results and Discussion

After IT and SC administration Lee 1599 demonstrated very rapid absorption into plasma (**Figure 4-1**). The maximum plasma concentration C_{max} was two times higher after IT than SC administration (**Table 4-1** and **Table 4-2**). This is in line with the fact that the lungs are well known to be naturally permeable to small molecule drugs [100]. Although the mechanism of absorption of molecules after pulmonary deposition is still being researched, it seems that the lung's tremendous surface area, very low surface fluid volume, thin diffusion layer and paracellular transport are some of the factors which contribute towards the rapid absorption of Lee 1599 into the systemic circulation. For

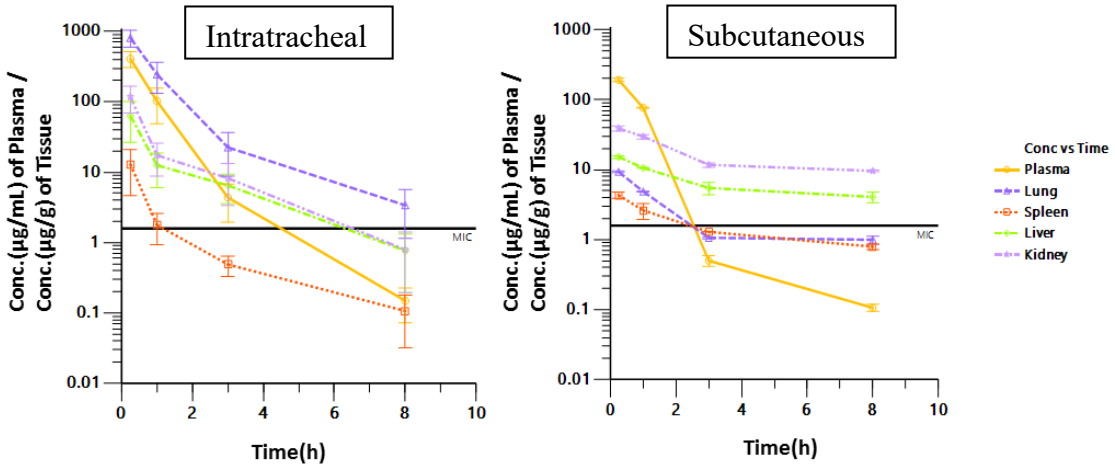

Figure 4-1. Measured concentration-time profiles (mean ± s.e.m) in different tissues/plasma relative to the minimum inhibitory concentration (MIC) after intratracheal (IT) (Left Panel) and subcutaneous (SC) administration (Right Panel) of Lee 1599 in mice at a dose of 200 mg/kg (n=3 at each time point)

Table 4-1. Penetration ratios after intratracheal (IT) administration of Lee 1599 in mice at a dose of 200 mg/kg

Sample	*$AUC_{0\text{-}8h}$	^C_{max}	#Penetration ratio
Plasma	284	406	1
Lung	695	805	2.45
Spleen	9.36	12.9	0.0330
Liver	65	63.4	0.229
Kidney	95.9	117	0.338

Abbreviations: $AUC_{0\text{-}8h}$: Area under the curve from time zero to 8 h; C_{max}, Peak concentration.
*AUC units for plasma (h.µg/mL) and for tissues (h.µg/g)
^ C_{max} units for plasma (µg/mL) and for tissues (µg/g)

$$\#\ Pentration\ ratio = \frac{AUC_{sample}}{AUC_{plasma}}$$

Table 4-2. Penetration ratios after subcutaneous (SC) administration of Lee 1599 in mice at a dose of 200 mg/kg

Sample	*$AUC_{0\text{-}8h}$	^C_{max}	#Penetration ratio
Plasma	149	192	1
Lung	21.8	9.31	0.146
Spleen	17	4.31	0.114
Liver	84.1	15.2	0.564
Kidney	191	38.7	1.28

Abbreviations; $AUC_{0\text{-}8h}$: Area under the curve from time zero to 8 h; C_{max}, Peak concentration.

*AUC units for plasma (h.µg/mL) and for tissues (h.µg/g)

^ C_{max} units for plasma (µg/mL) and for tissues (µg/g)

$$\#\ Pentration\ ratio = \frac{AUC_{sample}}{AUC_{plasma}}$$

small molecule drugs which are not dissolution rate-limited, including Lee 1599, the intrinsic absorption rates across the lungs are usually fast with absorption half-lives of ≤1 h, and are independent of lipophilicity or involvement of transporters [101]. The absorption rate also varies within the respiratory track between the epithelial cells and alveolar cells. There is experimental evidence that absorption of small molecules through the peripheral region is twice as fast compared to the central region of the lungs [102]. In this pilot study for Lee 1599, the disposition pattern of the formulation in the lungs was not evaluated. However, the rapid pulmonary absorption rate of Lee 1599 suggests that the drug is being delivered to the peripheral region of the lungs. This is desirable as *Mtb* usually resides in the deeper regions of the lungs [103].

The systemic relative bioavailability after IT versus SC administration was 1.91(**Table 4-3**). This suggests that the drug is permeable across the lung barrier to a larger extent compared to absorption from the SC route. The high systemic plasma exposure of Lee 1599 after IT administration (**Figure 4-2**) also suggests that close to the total inhaled dose was actually deposited in the lungs and that there was negligible first-pass metabolism. Most of the small molecule drugs currently used for inhalation, including bronchodilators and tobramycin, are not dissolution rate-limited, and have approximately 100% bioavailability for the fraction of the dose deposited in the lungs irrespective of their permeability characteristics [101]. The relatively lower bioavailability after SC administration has also been observed with other aminocyclitol antibiotics like trospectinomycin which was 75% bioavailable in rats following SC administration [104]. This could potentially be explained by the incomplete and slow absorption from the subcutaneous site of administration. Similar to IV administration, the high clearance of Lee 1599 predominantly through renal excretion limits the systemic exposure to a relatively short duration [52].

Information about tissue distribution is very important for the evaluation of efficacy and potential toxicity. As expected, the highest exposure of Lee 1599 after IT administration was attained in the lungs which was 2.5 times higher than plasma (**Figure 4-2** and **Table 4-1**). This is highly desirable as the lungs are the main site of infection in pulmonary TB. Dibasic compounds such as Lee 1599 usually have longer lung retention as compared to neutral and cationic compounds, which may be explained by the phenomenon of 'lysosomal trapping' where the basic drug accumulates in the acidic environment of lysosomes, which acts as a reservoir [105]. Additionally, spectinamides also have the ability to penetrate inside the macrophage, which is one of the main sites for intracellular survival and replication of *Mtb* [75]. Macrophage uptake of spectinamide Lee 1329 was found to be significantly higher than spectinomycin, the parent compound of Lee 1329, and streptomycin, a second line anti-tuberculosis agent [75].

Inhalation delivery allows easier accessibility of Lee 1599 to alveolar macrophages, which are the predominant form of infected cells in TB, thereby creating high localized concentrations of the drug that can kill the intracellular *Mtb* [89]. The circulation of alveolar macrophages also promotes drug distribution into the poorly-ventilated areas of the lungs which are often a safe-haven for *Mtb* [106]. Experimental evidence from rat studies involving IT administration of soluble compounds indicates

Table 4-3. Pharmacokinetic parameters for plasma concentration-time profiles after subcutaneous (SC) and intratracheal (IT) administration of Lee 1599 in mice at a dose of 200 mg/kg

Route	Dose (mg/kg)	$AUC_{0\text{-}8h}$ (h.µg/mL)	CL/F (L/h/kg)	$t_{1/2}$ (h)	F (Relative to SC)
IT	200	284	0.704	0.785	1.91
SC	200	149	1.38	0.847	1

Abbreviations; $AUC_{0\text{-}8h}$: Area under the curve from time zero to 8 h; CL/F, Total body clearance corrected for bioavailability, t ½, Half-life; F, Bioavailability.

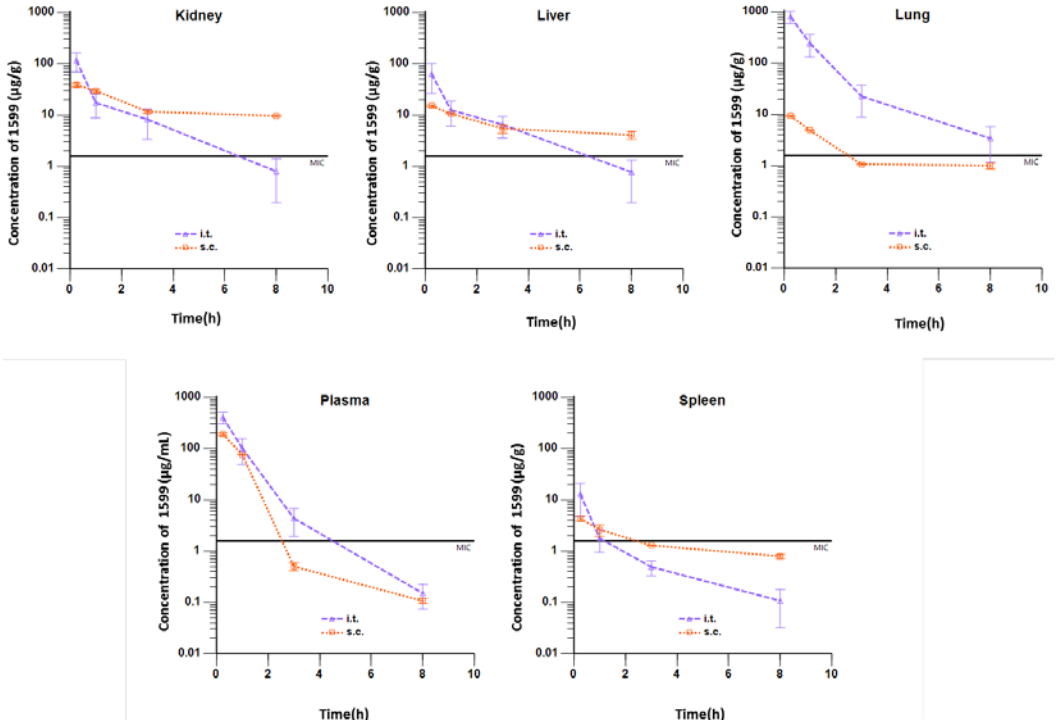

Figure 4-2. Measured concentration-time profiles (mean ± s.e.m) in different tissues relative to the minimum inhibitory concentration (MIC) after intratracheal (IT) and subcutaneous (SC) administration at a dose of 200 mg/kg of Lee 1599 in mice (n=3 at each time point)

that $t_{1/2}$ observed in lungs often mimics the apparent $t_{1/2}$ observed in plasma [100]. This is consistent with the observations in our study.

Although Lee 1599 is getting rapidly cleared from the lungs and plasma, excellent efficacy was still observed by thrice a week IT administration in mice. The potential explanation could be its concentration-dependent killing pattern and lengthy post-antibiotic effect (PAE) of 133 h at 10×MIC [52]. The concentration of a drug is one of the major determinants of PAE. For example, the PAE of penicillin G gradually increases with increase in its concentration [107, 108]. In case of Lee 1599, higher concentrations achieved in the plasma and lungs after IT administration could potentially be associated with longer PAE as compared to SC administration.

Following IT administration, Lee 1599 distributes to a similar extent in the kidneys and liver with penetration ratios of 0.338 and 0.229 respectively (**Figure 4-2**), although the C_{max} in the liver was approximately half that in the kidneys. Passive diffusion across the cell membrane is highly unlikely for Lee 1599 as it is very polar (cLog P = -2.5) and based on its pK_a of 8 and 10, it is expected to be largely in ionized form at physiological pH. This strongly suggests an active role of transporters involved in the uptake into kidneys and liver. The Biopharmaceutics Drug Disposition Classification System (BDDCS) classifies compounds into four types based on the solubility and permeability and is useful for predicting the role of transporters in the disposition of novel entities during the early stages of drug discovery. As Lee 1599 exhibits high solubility and poor permeability, it can be categorized as BDDCS Class 3 compound. BDDCS predicts that for class 3 drugs uptake transporters will be important for its entry into the liver [109]. The endocytic receptor complex formed by megalin and cubulin is known to transport aminoglycosides into the renal tubular epithelial cells [110]. Megalin associated uptake transport has also been associated with accumulation of colistin in the kidneys [111]. Similar to the kidneys, accumulation in the liver may also be assisted by hepatic uptake transporters. The highest tissue levels of trospectinomycin were found in the liver [112]. The mechanism behind selective hepatic sequestration was not clear; however it is likely that hepatic uptake transporter may be associated with it.

The lowest penetration ratio was observed in the spleen with both SC and IT administration indicating that Lee 1599 may not be successful in treating TB infections that have disseminated into the spleen (**Figure 4-2**). This was supported by the relatively lower reduction in bacterial load in the spleen as compared to the lungs observed after IT and SC administration of Lee 1599 [52]. This limitation, however, can likely be addressed by using Lee 1599 in combination therapy with other antitubercular agents which have better penetration and efficacy in the spleen.

In the present study, tissue penetration was found to be higher in the kidneys and liver, whereas it was lower in the lungs and spleens. In a previously conducted mass balance study of Lee1329, a structurally similar spectinamides analogue, in rats after IV administration [75], similar drug distribution pattern was observed with highest tissue penetration in the kidneys followed by liver while lower and similar penetration in lungs and spleen.

Conclusions

IT administration of Lee 1599 provides higher exposure in the lungs compared to the SC route. As the lungs are the main site of infection, this could potentially explain the improvement in efficacy with a lower weekly dose followed by IT administration. In spite of being highly hydrophilic, Lee 1599 accumulates in kidney and liver suggesting a potential role of uptake transporters in these organs. Spleen had the lowest exposure among all the tissues investigated following IT and SC administration. Overall, these results are encouraging to further pursue pulmonary delivery as an administration route for spectinamides in the treatment of tuberculosis.

CHAPTER 5. PHYSIOLOGICAL MODEL-BASED PREDICTION OF THE HUMAN PHARMACOKINETICS OF LEE 1599, A NOVEL ANTI-TUBERCULOSIS AGENT

Introduction

The translation from the preclinical stage to the clinic is one of the most critical steps in drug development with an average attrition rate of 30% [113]. Successful human pharmacokinetic prediction based on preclinical data can be highly beneficial for any drug development program for calculating the first-in-human dose. One of the most common approaches used for prediction of human pharmacokinetics is allometric scaling, which typically uses body size based on a power law function to extrapolate clearance and volume of distribution from preclinical species to humans [114]. Allometric scaling adjusted for maximum lifespan potential and brain weight have also been suggested in order to improve its predictive capability [115].

Physiologically based pharmacokinetic (PBPK) modeling is an alternative approach which combines species-specific physiological features along with drug-specific *in silico*/*in vitro* input parameters for prediction of pharmacokinetics in a species [28, 116]. Its mechanistic and more realistic modeling approach compared to empirical compartmental models has led to its wide spread use for studying the disposition of xenobiotics. Because of their intricacy, PBPK models are able to achieve a detailed quantitative assessment of the plasma and tissue disposition of drugs along with ease of scaling up the model to different species since the structural model is relatively common to most mammalian species and only needs size and blood flow related species-specific adjustments [117]. This approach in combination with physiological scaling factors has been successfully used for cross-species extrapolation of drugs like cyclosporine and docetaxel [118, 119], and in combination with pharmacodynamic data, it can also help to guide optimized clinical dosing. These models can also be used for predicting the pharmacokinetics of drugs in complex scenarios which arise as a result of multivariate changes to intrinsic (e.g., disease states, age, pharmacogenomics) and extrinsic (e.g., drug-drug interaction) factors.

Lee 1599 has emerged as one of the potential lead spectinamide candidates based upon its excellent microbiological, safety and efficacy profile for treatment of tuberculosis. It binds to a site within the mycobacterial 30S ribosome and inhibits its protein synthesis with a minimum inhibitory concentration (MIC) of 0.8 μg/mL [53]. It evades the efflux pump Rv1258c upregulated in drug resistant bacteria, thereby gaining significant efficacy in both *in vitro* and *in vivo* models of tuberculosis infection. Unlike aminoglycosides, Lee 1599 does not inhibit human mitochondrial translation which is linked to ototoxicity. In this present study, we present an application of PBPK modelling and simulation to predict human pharmacokinetics of Lee 1599 which was conducted in the following steps:

1. Develop and optimize a PBPK model that can describe the pharmacokinetics of Lee 1599 in rats after intravenous (IV) administration,

2. Prospectively qualify the performance of the model by predicting the pharmacokinetics of Lee 1599 in mouse after subcutaneous (SC) administration, and

3. Extrapolate the PBPK model to predict pharmacokinetics of Lee 1599 in human after IV administration.

Materials and Methods

Chemicals and reagents

Spectinamide antibiotic Lee 1599 (3'-Dihydro-3'-deoxy-3'(R)- (5-chloropyridin-2-yl)acetylamino spectinomycin), as shown in **Figure 5-1** was synthesized in Dr. Richard E. Lee's Lab at St. Jude Children's Research Hospital, Memphis, TN. Acetonitrile, methanol, HPLC grade water, formic acid and nonafluoropentanoic acid were purchased from Fisher Scientific (Pittsburgh, PA). Drug free BALB/c mouse plasma and rat plasma was purchased from Innovative Research (Novi, MI).

Protein binding

The plasma protein binding of Lee 1599 in different species was determined using equilibrium dialysis method with ready-to-use RED device inserts (Thermo Scientific, Rockford, IL) in base plates containing plasma and a buffer chamber for analysis. Two concentrations (0.5 and 5 mg/L) of Lee 1599 were prepared in rat and mouse plasma. 200 µL of the plasma sample was added to the central chamber and 350 µL of blank isotonic phosphate buffer, pH 7.4 to the peripheral chamber of dialysis base plate. The base plate was sealed and then incubated at 37ºC at 100 rpm on an orbital shaker for 4 h to achieve equilibrium. At the end of incubation, the drug concentration was determined in plasma and buffer using an LC-MS/MS assay. The free fraction of the drug was calculated as ratio of the concentrations in the buffer and in plasma. The results are expressed in terms of fraction of drug unbound to plasma proteins (f_u).

Microsomal incubations

In vitro microsomal metabolic stability of the Lee 1599 was performed in pooled rat liver microsomal preparations (BD Biosciences, Woburn, MA). 20 µM stock solution of Lee 1599 and 10 mg/mL of microsomal protein solution were prepared in phosphate buffer solution (pH 7.4). The final reaction mixture (450 µl) consisted of 50 µL of

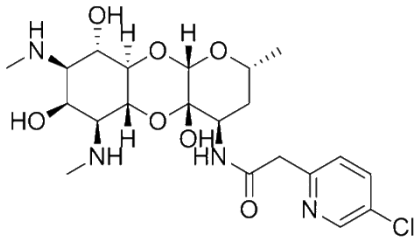

Figure 5-1. Structure of Lee 1599

microsomal protein solution (10 mg/mL), 400 µL of NADPH regenerating solution containing 1.3 mM NADP+, 3.3 mM glucose-6-phosphate, 3.3 mM $MgCl_2$ and 1 unit/mL glucose-6-phosphate dehydrogenase (BD Biosciences, Woburn, MA). Reaction was started by addition of 50 µL of Lee 1599 solution (20 µM) to the reaction mixture and incubated at 37°C for 90 minutes. Then the sample was collected and immediately quenched by the addition of ice-cold methanol containing an internal standard to stop the reaction. The quenched samples were centrifuged and the supernatant was analyzed by LC-MS/MS assay to measure the parent compound (Lee 1599) remaining after 90 min of incubation period. Verapamil with known significant phase I metabolism was used as positive control while deactivated microsomes was used as negative control.

Formulation preparation and administration

A dosing solution of Lee 1599.2HCl (10 mg/kg) was freshly formulated in water (50%) and Plasmalyte A (50%). The IV dose was administered via a femoral vein catheter followed by flushing the catheter with saline followed by heparinized glycerol locking solution to clear the dead space in the catheter. For subcutaneous administration, dosing solution of Lee 1599.2HCl was freshly formulated in water (33.8 %) and Plasmalyte A (66.3%) and was administered subcutaneously using a 29 gauge insulin syringe.

Pharmacokinetic studies in rats and mice

The *in vivo* pharmacokinetic studies presented were performed at the University of Tennessee Health Science Center protocol numbers 13-165 and 15-121, approved by the Institutional Animal Care and Use Committee of the University of Tennessee Health Science Center. Animal studies were conducted according to the guideline of Animal Welfare Act and the Public Health Service Policy on Humane Care and Use of Laboratory Animals. The animals were kept on a 12 h light/ dark cycle with access to food and water *ad libitum*.

Lee 1599 was administered to groups of catheterized (jugular and femoral veins) female Sprague-Dawley rats (8–10 weeks old, 200–225 g, n = 6, Harlan BioScience, Indianapolis, IN) intravenously at a dose of 10 mg/kg body weight. Thirteen serial blood samples (~250 µL) were collected in BD Microtainer plasma separator tubes containing lithium-heparin via the jugular vein catheter at 0.08, 0.25, 0.5, 0.75, 1, 1.5, 2, 4, 6, 8, 10, 24 and 48 h after dosing. Plasma was separated immediately by centrifugation (10,000g for 10 min at 4°C) while cumulative urine samples were collected for 48 h.

Healthy female BALB/c mice (6–8 weeks old, ~20 g) weighing approximately 20-25 g were obtained from Harlan Bioscience (Indianapolis, IN). Lee 1599 was administered to a group of 15 mice by subcutaneous injection at a dose of 200 mg/kg. Blood samples were in BD Microtainer plasma separator tubes containing lithium-heparin collected at 0.083, 0.25, 0.5, 1, 2, 3, 5, 8, 12 and 24 h after administration. Each

mouse provided two blood samples, one by a one-time retro-orbital bleed under isoflurane anesthesia, and the other by cardiac puncture under isoflurane anesthesia followed by euthanasia through cervical dislocation. Plasma was separated immediately by centrifugation as described above and stored at −70 °C until LC-MS/MS analysis.

Bioanalysis

Plasma and urine samples were prepared by protein precipitation with methanol (spiked with the internal standard 3′-dihydro-3′-deoxy-3′(R)-isopropylacetylamino spectinomycin) followed by vortexing for 1 min, and then centrifugation at 10,000g for 10 min at 4°C. The supernatant was separated and 5 µL of supernatant was analyzed using high-performance liquid chromatography coupled with tandem mass spectrometry (LC-MS/MS). Chromatographic separations were carried out using a Shimadzu Nexera XR (LC-20ADXR) liquid chromatograph (Shimadzu Corporation, Kyoto, Japan) consisting of two pumps, online degasser, system controller and an autosampler. Liquid chromatography was performed on Waters Symmetry® 3.5 µm C8, 50 × 2.1 mm column (Waters, Milford, MA). The mobile phase was solvent A (water with 1.6% nonafluoropentanoic acid and 0.7 % formic acid) and solvent B (90% acetonitrile with 0.8% nonafluoropentanoic acid and 0.35% formic acid) in the gradient mode as follows: 0–0.5 min, 20% B; 0.5–1.6 min, 20–90% B; 1.6–2 min, 90% B; 2-2.5 min, 90-20% B, 2.5–3 min, 20% B at a flow rate of 0.5 mL/min. Analytes were detected with a API 5500 triple-quadruple mass spectrometer (Applied Biosystems, Foster City, CA) with electrospray ionization in multiple reaction monitoring mode using the compound-specific mass transfers of m/z of 487.2/ 207.1 for Lee 1599 and m/z of 418.3/207.1 for Lee 1369.

Two calibration curves ranging from 1.95 to 2,000 ng/mL and 1.95 to 1000 µg/mL were constructed and validated with spiked samples of rat and mouse plasma. Samples with concentrations above 2000 ng/mL were analyzed with the higher calibration range. The peak area ratios of analyte to internal standard was linear over the concentration range tested for both compounds, with correlation coefficients (weighted least-square linear regression analyses) >0.997. Accuracy (deviation of the analyzed quality control samples from nominal values) was within ±3% over the entire range of the calibration curve, and precision (coefficient of variation of repeated measurements of the quality control samples) was <2%.

Pharmacokinetic data analysis

Naïve data pooling was performed with the mean values of plasma concentrations in plasma at each time point plotted against time to generate concentration-time profile. The pharmacokinetic parameters were estimated using Phoenix WinNonlin 6.3 (Pharsight Corporation, Mountain View, CA) by noncompartmental analysis.

Overall strategy for development of the PBPK model for cross-species extrapolation

As a first step, a PBPK model was developed for describing the pharmacokinetics of Lee 1599 in rats after IV administration. An independent parameter (cLogP) was manually adjusted to optimize the PBPK model with respect to the IV pharmacokinetics in rats. Before subsequently predicting the pharmacokinetics in humans, a cross-species extrapolation was performed by predicting the pharmacokinetics in mice after SC administration. Once the optimization of the systemic distribution and clearance of Lee 1599 had been completed using the rat IV plasma pharmacokinetics as described above, a first-order absorption was estimated for SC administration by fitting the model to the experimental data obtained from the SC pharmacokinetic study in mice, thereby leaving all other drug-specific parameters unchanged and switching the system specific parameters from the rat to the mouse species. After evaluating its predictive performance in mice, the model was finally used to predict human pharmacokinetics with input for human clearance which was scaled from rat clearance. A virtual human population of 100 individuals was simulated from distributions of anatomical, demographic, and physiological variables derived from real patient populations using a Monte Carlo simulation approach to account for the variability observed in clinical populations [120].

PBPK model structure

The PBPK modeling and simulation was performed using the PK-Sim software platform (Version 6.1, Bayer Technology Services GmbH, Leverkusen, Germany) [121]. The generic PBPK model structure consists of a series of compartments corresponding to different tissues which are connected by the circulation system with a mass balance for each compartment [122].

PBPK model parameterizations are broadly categorized into system-specific and drug-specific parameters. System-specific physiological parameters such as organ volumes, blood flow rates or tissue composition are provided in the software, and were originally collected from large numbers of literature sources [123].

The second set of parameters required for PBPK models are drug-specific, which includes physiochemical data (cLogP, MW and pK_a) listed in **Table 5-1** and ADME properties. cLogP for Lee1599 was estimated using the ChemDraw Ultra software (version 11.0, Cambridge Software Company), while the pK_a was estimated using MarvinSketch 5.10.4 (ChemAxon Lt., Budapest, Hungary). Partition coefficients (K_p) are also an important set of compound-specific parameters which determine the distribution of the drug into different compartments. The K_p value for each tissue is defined as the ratio of total drug exposure in the tissue to the total drug exposure in the plasma at steady state. In the past, K_p values had to be determined experimentally by performing extensive tissue distribution studies. However, recent development of algorithms based on physicochemical and *in vitro* binding characteristics, including molecular weight, lipophilicity and protein binding of the drug, allows prediction of K_p values with reasonable degree of accuracy. The PK-Sim software offers several generic algorithms

Table 5-1. Physicochemical characteristics of Lee 1599

Physicochemical parameter	Estimate
cLog P	-2.5
Molecular Weight (MW)	486.9
pKa	8,10

for calculation of partition coefficients, and amongst those the distribution model by Schmitt was selected for this project.

Knowledge about the ADME characteristics of the compound is also vital for successful prediction by the model. Clearance is one of the key parameters required for PBPK model predictions. For drugs which are predominantly cleared by the liver, the *in vivo* clearance is usually extrapolated from *in vitro* systems including microsomes and hepatocytes using physiological scaling factors. However, for the drugs which are renally cleared, the *in vivo* clearance is used as input or it is predicted using allometric scaling [116]. Spectinamide antibiotic Lee 1599 is metabolically stable and is nearly exclusively cleared by the kidneys via glomerular filtration and active secretion processes. For describing the pharmacokinetics of Lee 1599 in rat and mouse, the *in vivo* clearance was used as an input in the PBPK model. In the absence of human pharmacokinetic data, the clearance in humans had to be determined by scaling from preclinical species. As renal clearance with net active secretion is the main route of elimination for Lee 1599, it requires using scaling approaches which are specifically applicable for drugs which are predominantly actively secreted in urine. Paine *et al.* [124] proposed three different approaches for prediction of human renal clearance from preclinical species for drugs that exhibit active secretion or net reabsorption. These three approaches are as follows:

Direct correlation method: The renal clearance value in humans is estimated from the clearance in rats using the following equation:

$$CL_{r,human} = CL_{r,rat} \times \left(\frac{f_{u,human}}{f_{u,rat}}\right) \times \left(\frac{KBF_{human}}{KBF_{rat}}\right) \quad \textbf{Eq. 5-1}$$

where $CL_{r,human}$ and $CL_{r,rat}$ are the renal clearances in human and rat, $f_{u,human}$ and $f_{u,rat}$ are the unbound fractions in plasma, and KBF_{human} (1.3 L/min) [125] and KBF_{rat} (0.0104 L/min[126] are the respective kidney blood flows. f_u has been found to consistent across rat, mouse and human for most of the other analogs of spectinamide series [127]. As $f_{u,human}$ was not yet available for Lee 1599, it was assumed to be similar to the f_u determined experimentally for Lee 1599 in rat and mouse plasma.

Simple allometry: The unbound clearance is scaled across preclinical species using the following relationship:

$$CL_r = x \times (BW)^y \quad \textbf{Eq. 5-2}$$

where CL_r is renal clearance, BW is body weight, and x and y are the coefficient and exponent of the allometric equation, respectively. Using this established relationship, the human clearance is predicted.

Mahmood's renal clearance scaling method: The simple allometry method was modified by introducing a species scaling factor (SSF) which takes into account the physiological differences in kidney between human and preclinical species.

$$SSF = \left(\frac{GFR \times KBF}{BW \times KW}\right)$$ **Eq. 5-3**

$$Correction\ factor = \left(\frac{SSF_{species}}{SSF_{human}}\right)$$ **Eq. 5-4**

where GFR is the glomerular filtration, KBF is the kidney blood flow, and KW is kidney weight.

The first method is single species scaling approach, whereas the latter two approaches require IV clearance in at least two preclinical species for extrapolation of human clearance. For Lee 1599, IV clearance was only available in rats and therefore, the direct correlation method was used for scaling of human clearance.

Results and Discussion

Pharmacokinetics of Lee 1599 in rats and mice

The concentration-time profile of Lee 1599 displayed bi-exponential decline upon IV administration (10 mg/kg) in rats and SC administration (200 mg/kg) in mice. In agreement with the theory of allometry, the weight normalized clearance in rats was slightly lower than in mice, whereas weight normalized volume of distribution was similar in both species (**Table 5-2** and **Table 5-3**). The protein binding was also comparable in both species with most of the drug available in unbound form (**Table 5-2** & **Table 5-3**). The fraction of drug eliminated in unchanged form (f_e) close to 1 in rats and the minimal loss of the parent drug in the *in vitro* rat microsomal stability study strongly suggests that Lee 1599 is predominantly cleared by the renal route. The excretion ratio (E_{ratio}) was greater than 1 indicating a net active renal secretion process.

The pharmacokinetics of Lee 1599 was similar to that of its parent compound spectinomycin which was also found to be predominantly eliminated by the renal route with a total CL of 0.602 L/h/kg in rats. Spectinomycin has a volume of distribution of 0.756 L/kg which was also comparable to Lee 1599 indicating that it mainly distributes into the extracellular body water [66].

PBPK model development in rats

A PBPK model for Lee 1599 was developed in rats based after IV administration of 10 mg/kg based on the inputs on physicochemical properties listed in **Table 5-1** and rat specific ADME properties including clearance and protein binding listed in **Table 5-2**.

The model predicted pharmacokinetic profile in rat was initially unable to reasonably describe the distribution phase with under-prediction observed at the lower concentrations suggesting poor estimation of partition coefficients (**Figure 5-2**).

Table 5-2. Pharmacokinetic parameters and protein binding of Lee 1599 in rats

Route	Dose (mg/kg)	AUC_{INF} (h·µg/mL)	V_{ss} (L/kg)	CL (L/h/kg)	f_u	E_{ratio}	f_e	Microsomal stability (% Remaining)
IV	10	15.0	0.467	0.666	0.558	2.76	0.883	100

Abbreviations: AUC_{INF}: Area under the curve from time zero extrapolated to infinity; V_{ss}: Volume of distribution at steady state, CL, Total body clearance; f_u, Average of the fraction of drug unbound to plasma proteins at 0.5 and 5mg/L; f_e, Fraction excreted unchanged in the urine; Microsomal Stability, % of Lee 1599 remaining after 90 min incubation; E_{ratio}, Excretion ratio.
All values are shown as the means.

Table 5-3. Pharmacokinetic parameters and protein binding of Lee 1599 in mice

Route	Dose (mg/kg)	AUC_{INF} (h·µg/mL)	V_z/F (L/kg)	CL/F (L/h/kg)	f_u
SC	200	159	0.499	1.25	0.632

Abbreviations: AUC_{INF}: Area under the curve from time zero extrapolated to infinity; V_Z/F, Volume of distribution corrected for bioavailability, CL/F, Total body clearance corrected for bioavailability; f_u, Average of the fraction of drug unbound to plasma proteins at 0.5 and 5mg/L; f_e, Fraction excreted unchanged in the urine; Microsomal Stability, % of Lee 1599 remaining after 90 min incubation; E_{ratio}, Excretion ratio.
All values are shown as the means.

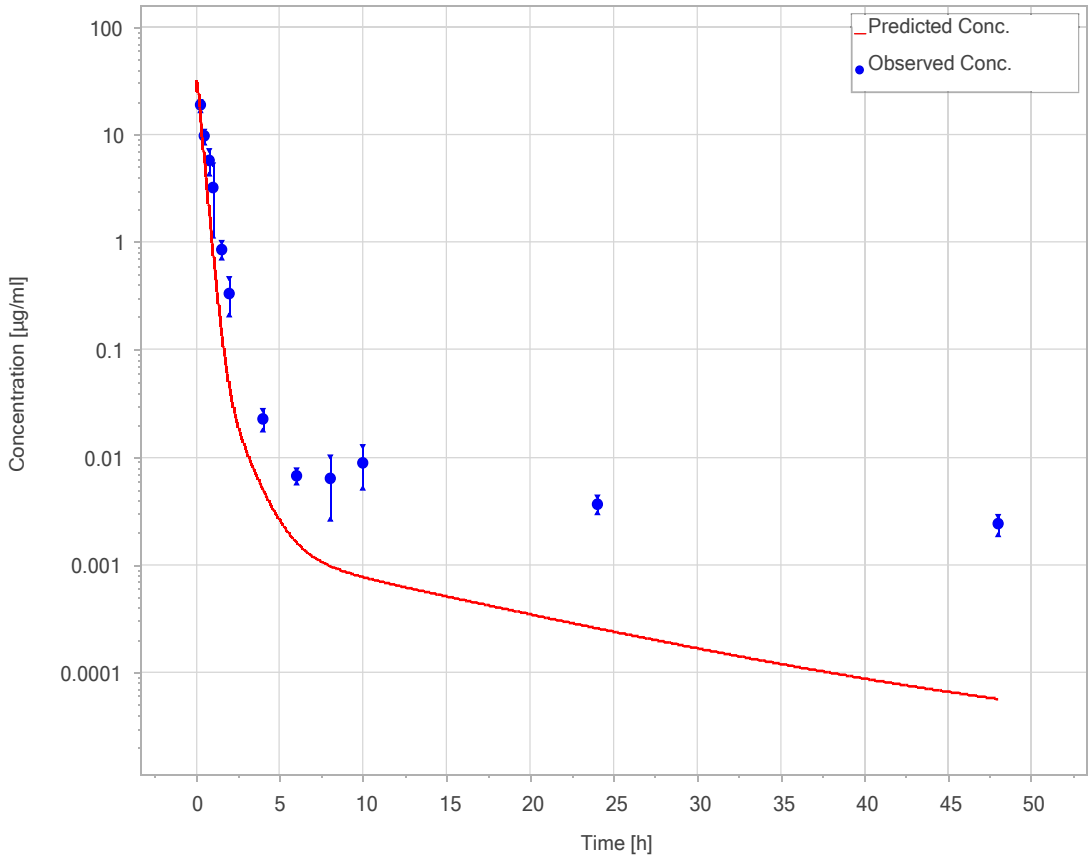

Figure 5-2. Observed and PBPK model-simulated Lee 1599 total plasma concentration-time profile in rats after a single intravenous (IV) dose of 10 mg/kg. Solid red line represents simulation result and blue circles represent mean observed data with standard error bars.

The model was further refined through comparison of PBPK-model predicted and observed concentration-time profiles in rat via optimization of partition coefficients through manual adjustment of cLogP from -2.5 to -0.50. The rationale for modifying the cLogP was based on the premise that software quite often overestimates the hydrophilicity of polar compounds. Additionally, the online database ChemDplus Advanced (http://chem.sis.nlm.nih.gov/chemidplus) reported a LogP of -0.82 for the parent compound spectinomycin, and this supports the modification in the cLogP of Lee 1599. This change resulted in improved model fits with the predicted parameter values within 2 folds of the observed values (**Figure 5-3** and **Table 5-4**) and the final model was updated with cLogP of -0.5.

Application of the PBPK model in mice

The optimized PBPK model developed based on concentration-time data in rats was subsequently prospectively tested to predict the Lee 1599 concentration-time profile in mice after SC dosing. The clearance and plasma protein binding (f_u) were updated with the mouse-specific, experimentally determined values (**Table 5-3**). All other drug-specific parameters remained unchanged. The absorption phase after SC administration was best described by a first-order input to the plasma with an absorption half-life of 13 minutes. Overall, the PBPK model for Lee 1599 optimized in rats was successful in explaining its disposition in mice, with all the predicted pharmacokinetic parameters in mice within less than 10% deviation of the observed values (**Figure 5-4** and **Table 5-5**).

Scaling of human clearance

After prospective qualification of the PBPK model in mice, the final step was to predict the pharmacokinetics of Lee 1599 in humans. Unlike in the case with the rat and mouse model where *in vivo* clearance was used as an input, for the human PBPK model, clearance was predicted using the Direct Correlation Method. Based on this approach, human clearance was estimated to be 0.25 L/h/kg. Renal clearance using this approach assumes that the renal secretion process remains conserved across species [124]. Predictions based on this methodology have been found to correlate well with actual clearance parameters in humans, except for certain organic anions for which under-prediction has been observed because of lower reuptake in human kidneys relative to rats [124]. Additionally, gender differences in urinary excretion have also been reported in rats for substrates of organic anion-transporting polypeptide 1 (oatp1) with higher clearance in females as compared to male rats [128]. Studies are underway to further characterize the transporters involved in the active secretion of Lee 1599, and its relative expression in different preclinical species and humans.

The predicted human CL of Lee 1599 was within two folds of the spectinomycin CL of 0.104 L/h/kg which was observed after IV administration of spectinomycin in healthy volunteers [129]. It is also important to acknowledge, however that as the human clearance prediction was based only upon one species, there is substantial uncertainty

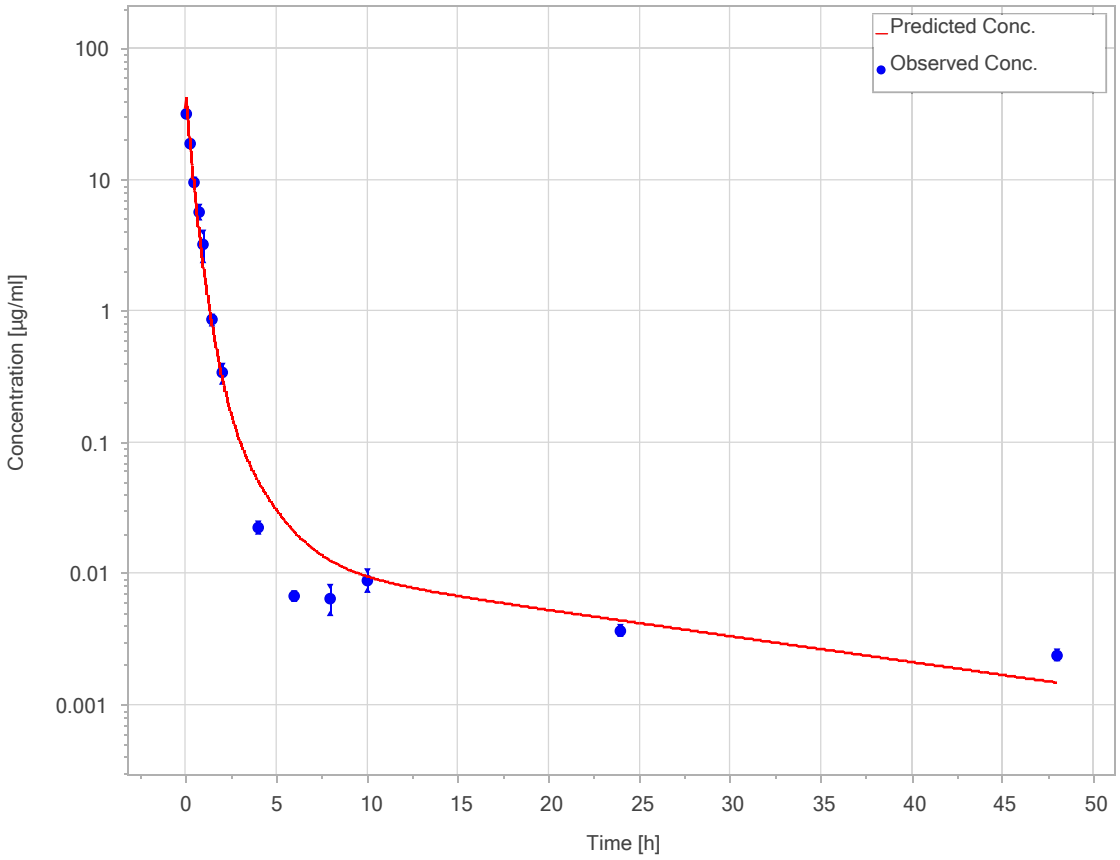

Figure 5-3. Observed and refined PBPK model-simulated Lee 1599 total plasma concentration-time profile in rat after a single intravenous (IV) dose of 10 mg/kg
Solid red line represents simulation result and blue circles represent mean observed data with standard error bars.

Table 5-4. Comparison of observed versus PBPK model predicted pharmacokinetic parameters of Lee 1599 in rats after a single intravenous (IV) dose of 10 mg/kg

Parameter	Observed	Predicted	Ratio of observed / predicted
AUC_{INF} (h·µg/mL)	15.0	15.0	1
V_{ss} (L/kg)	0.467	0.441	1.06
CL (L/h/kg)	0.666	0.666	1

Abbreviations: AUC_{INF}: Area under the curve from time zero extrapolated to infinity; V_{ss}: Volume of distribution at steady state, CL, Total body clearance.

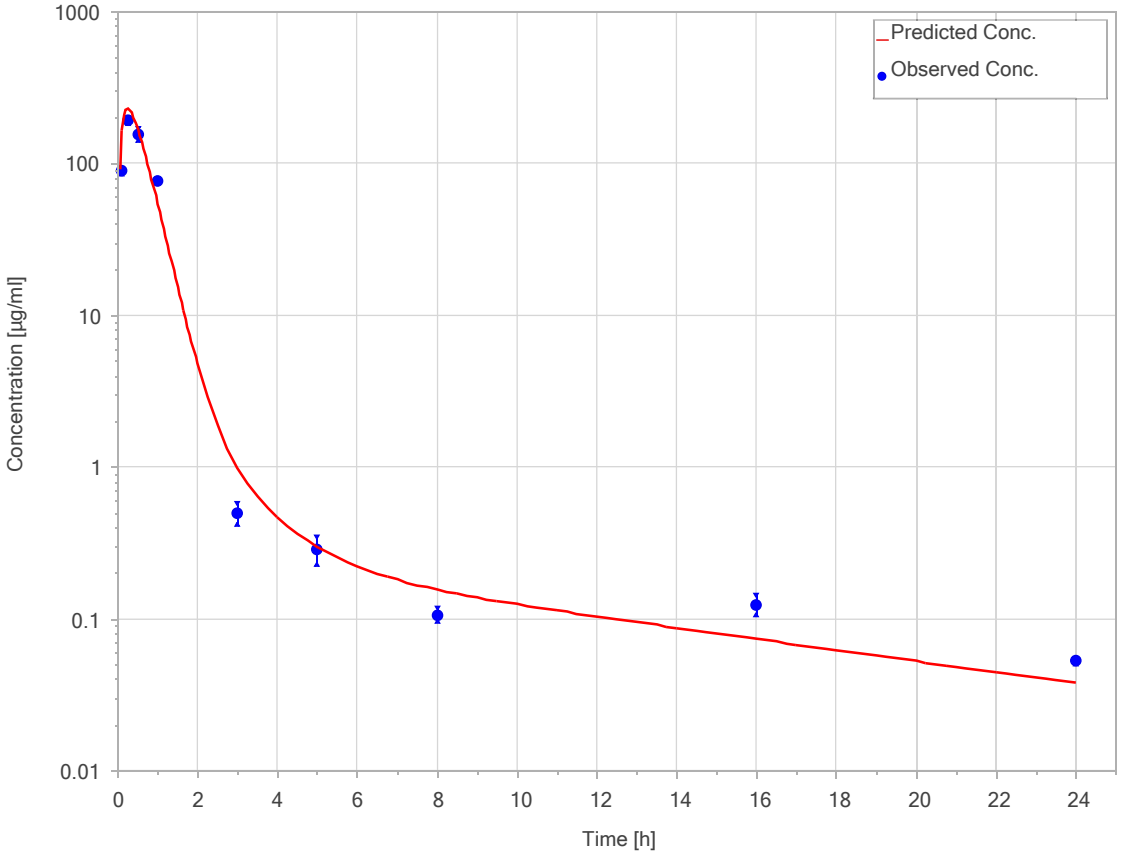

Figure 5-4. Observed and PBPK model-simulated Lee 1599 total plasma concentration-time profile in mice after a single subcutaneous (SC) dose of 200 mg/kg

Solid red line represents simulation result and blue circles represent mean observed data with standard error bars.

Table 5-5. Comparison of observed versus PBPK model predicted pharmacokinetic parameters of Lee 1599 in mice after a single subcutaneous (SC) dose of 200mg/kg

Parameter	Observed	Predicted	Ratio of observed / predicted
AUC_{INF} (h·µg/mL)	159	168	0.946
V_z /F(L/kg)	0.499	0.541	0.922
CL/F (L/h/kg)	1.25	1.19	1.05

Abbreviations: AUC_{INF}: Area under the curve from time zero extrapolated to infinity; V_Z/F, Volume of distribution corrected for bioavailability, CL/F, Total body clearance corrected for bioavailability.

associated with it. As the development of Lee 1599 gradually progresses into the late discovery phase, additional pharmacokinetic data will become available in other pre-clinical species like dogs, which in combination with the existing data could be used for making a more confident prediction.

Prediction of human pharmacokinetics

Using the human clearance estimate from the Direct Correlation Method along with an assumed f_u of 0.55 (similar to rat and mice f_u) in humans, and all other drug specific parameters unchanged, the PBPK model was used to predict the human pharmacokinetics (**Figure 5-5**). The parameters for the simulated virtual pharmacokinetic profile in humans for dose of 7.5 and 27.5 mg/kg are listed in **Table 5-6**. In agreement with the theory of allometry, the predicted weight normalized clearance as well as volume of distribution were lower than those found in rats and mice.

Based on this model, a dose of 7.5 and 27.5 mg/kg administered once daily via IV administration will be required to attain similar exposure as observed in mice after SC administration of 50 mg/kg and 200 mg/kg respectively. This dose range was selected based on the results of the dose-exposure-response analysis of Lee 1810, a structural analog of Lee 1599 and a competing lead candidate, which suggested that reasonable efficacy could be attained within a dose range of 50 mg/kg – 200 mg/kg, dependent on the dosing interval. The feasibility of achieving the projected dose range of Lee 1599 in humans is supported by similar dose recommendation for the parent compound spectinomycin, which is prescribed as single-dose treatment of 2 g spectinomycin administered by intramuscular injection for the treatment of gonococcal infections and other associated conditions [130]. Going forward, the exposure differences in mice for different routes of administration and health status would also need to be studied in order to obtain a more precise prediction of the efficacious dose range in humans. Additionally, the dose projection was based on the premise that Lee 1599 will be used as a single agent. However, in the clinic Lee 1599 will likely be used in combination with other anti-tuberculosis agents, which is assumed to result in a lower dose requirement for Lee 1599.

In summary, the pharmacokinetics of Lee 1599 was described by a PBPK model in rats and mice, and the model was applied to predict the pharmacokinetics and dose requirements of Lee 1599 in humans. This model suggests that an efficacious systemic exposure can be achieved with daily doses feasible in humans, and may be useful during drug development for understanding the dose requirements of future preclinical and clinical studies.

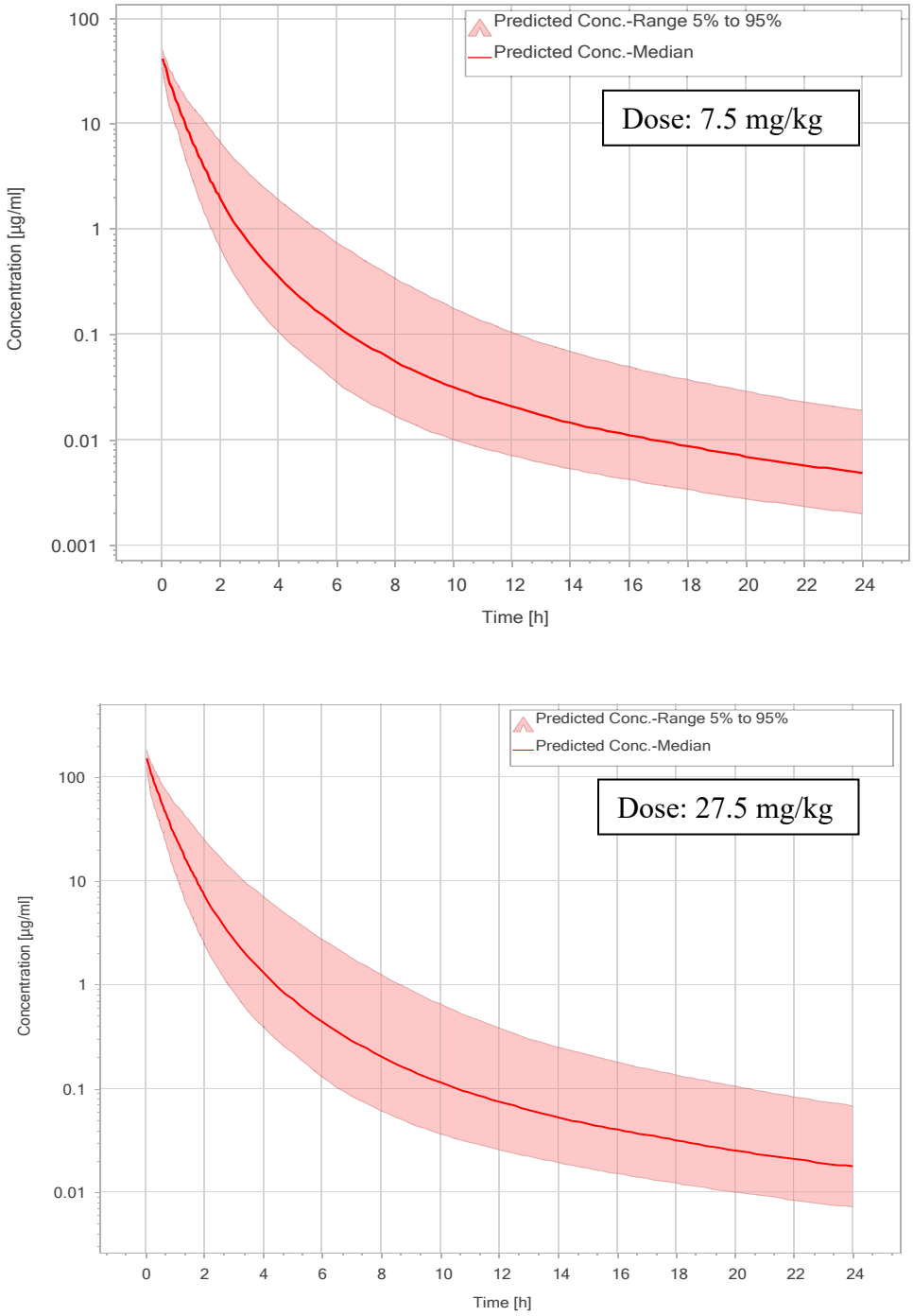

Figure 5-5. Simulated time course of Lee 1599 total plasma concentration after intravenous (IV) dose of 7.5 (top) and 27.5 mg/kg (bottom) in a virtual population human

The solid red line represents the median and the red band represents the range 5% to 95% for the 100 simulated profiles in a virtual human population.

Table 5-6. Model predicted pharmacokinetic parameters of Lee 1599 in humans after intravenous (IV) dose of 7.5 and 27.5 mg/kg, which results in a similar exposure after subcutaneous (SC) injection in mice of 50 and 200 mg/kg respectively

Dose	Parameter	Lower 5% range	Median	Upper 95% range
7.5 mg/kg	C_{max} (µg/mL)	34.6	41.2	56.2
	AUC_{INF} (h·µg/mL)	15	26.6	50.8
	V_{ss} (L/kg)	0.322	0.254	0.239
	CL (L/h/kg)	0.499	0.282	0.148
27.5 mg/kg	C_{max} (µg/mL)	160	165	206
	AUC_{INF} (h·µg/mL)	55.1	97.6	186
	V_{ss} (L/kg)	0.322	0.254	0.239
	CL (L/h/kg)	0.499	0.282	0.148

Abbreviations: C_{max}, Peak concentration, AUC_{INF}: Area under the curve from time zero extrapolated to infinity; V_{ss}: Volume of distribution at steady state, CL, Total body clearance.

CHAPTER 6. SUMMARY

The antibiotic spectinomycin is a bacterial protein synthesis inhibitor with a distinct mechanism of action and a high safety margin, but it is ineffective against *Mycobacterium tuberculosis* (*Mtb*). Using structure-based design, a novel class of amide derivatives of spectinomycin was generated with potent antitubercular activity which blocks native efflux from the tuberculosis cell. I hypothesized that the application of translational PK/PD approaches would facilitate further development of the lead compounds Lee 1599 and Lee 1810.

To identify the main driver for efficacy of lead spectinamide Lee 1810, a dose-fractionation study was performed in BALB/c mice infected with a low dose aerosol of *Mtb* which were treated with different dosing regimens of Lee 1810. Dosing was continued for 4 weeks with blood sampling at 0.25 h and 8 h post dose from each mice in the last week, followed by a washout period after which the mice were sacrificed and the lungs removed for measurement of colony forming units (CFU). The concentrations at 0.25 h increased in a dose-proportional fashion until 100 mg/kg and then increased more than dose-proportional between 200 – 400 mg/kg. However, concentrations at 8 h were found to be dose-proportional across the entire dose range. A simultaneous population pharmacokinetic analysis of sparse data from the dose-fractionation study and intensive data from a pharmacokinetic study in healthy mice was performed using nonlinear mixed effects modeling. A two-compartment model with first-order absorption and linear elimination from the central compartment characterized the plasma concentration–time profile of Lee 1810. The nonlinearity in $C_{0.25}$ above 100 mg/kg was described using a higher absorption rate for those dose levels and can potentially be explained by an increased absorption rate associated with faster diffusion at the subcutaneous site of administration. Healthy mice had 56.5 % lower clearance, 69% lower volume of distribution of the central compartment and 69.6 % lower intercompartmental clearance as compared to infected mice. These differences could be a result of differences in plasma binding protein concentrations, an altered hydration status in infected animal, and/or altered hemodynamics in this chronic disease state.

A two-subpopulation natural bacterial growth model adequately described the dynamic change in bacterial count in the untreated group of mice plus data obtained from previously performed studies and from the literature. *Mtb* is a slow growing bacterium with a growth rate constant K_{rep} estimated by the model as 0.0327 h^{-1}, which is within the range of growth rate constants found in the literature. To account for the bacterial kill by the immune system of mice, a first-order death rate constant (K_{ir}) was introduced for both of the subpopulations.

A sequential PK/PD analysis was performed by integrating the individual *post hoc* parameter estimates from the population pharmacokinetic analysis with the bacterial growth model via an exposure-dependent bacterial kill function characterized by a sigmoid E_{max} model for describing the overall rate of change in lung CFU with different dosing regimens. The PK/PD model could reasonably describe the microbial kill of Lee

1810 with EC_{50}, E_{max} and γ estimated as 239 µg/mL, 11.9 h^{-1} and 2.40, respectively. A high value of the Hill coefficient is a typical characteristic observed for other concentration-dependent killing antibiotics. EC_{50} (239 µg/mL) was found to be much higher than MIC (1.6 µg/mL) of Lee 1810. EC_{50} describes the time course of drug effect and is much more realistic parameter to compare potency of compounds rather than the MIC, which represents the lowest static concentration at which no growth of microorganism is visible to the naked eye. Lee 1810 demonstrated concentration-dependent antibacterial kill which suggests that the higher the peak concentration is above MIC, the better would be the microbial kill. Although Lee 1810 has a short half-life, its concentration–dependent killing characteristics and moderate *in vitro* post antibiotic effect of 20 h support its intermittent dosing which is also commonly used for aminoglycoside antibiotics.

Spectinamides are highly water soluble and poorly permeable resulting in limited oral bioavailability and hence are usually administered through the subcutaneous route in mice. Additionally, since the lungs are the main organ affected in pulmonary tuberculosis, the efficacy of Lee 1599 was evaluated after IT administration in a mouse model of *Mtb* infection. The results of this study suggest significantly improved efficacy compared to SC administration. Based on these observations, I hypothesized that IT delivery of Lee 1599 has better efficacy compared to SC administration in mice due to higher concentrations of drug at the site of infection in the lungs for a longer duration of time. This hypothesis was tested by comparing the biodistribution of Lee 1599 in vital organs, including the lungs, in mice with both routes of administration. The rate and extent of absorption was almost two times higher with IT as compared to SC administration. This can be explained by the natural capacity of lungs to allow permeation of small molecules, and it also suggests that the drug is likely being delivered to the peripheral regions of the lungs which is desirable as *Mtb* usually resides in these regions. As expected, highest exposure of Lee 1599 after IT administration was attained in the lungs which was 2.5 times higher than in plasma. Dibasic compounds including Lee 1599 usually have longer lung retention which may be explained by the phenomena of 'lysosomal trapping' where the basic drug gets accumulated in the acidic compartment of lysosomes of alveolar macrophages and acts as a reservoir. Even though Lee 1599 is highly hydrophilic, it was found to slightly accumulate in tissues such as liver and kidney suggesting the potential role of transporters involved in the uptake into cells in these organs. Overall, this study supports the pulmonary route as a potential pathway for the treatment of tuberculosis with Lee 1599.

The projection of human pharmacokinetics from preclinical species is one of the most challenging steps in drug development. Physiologically-based pharmacokinetic (PBPK) modelling is an approach which has recently gained importance for cross-species extrapolation of pharmacokinetics. It utilizes the anatomical and physiological parameters of the species along with the drug-specific inputs obtained by *in silico*/*in vivo* extrapolation or *in vitro*/*in vivo* extrapolation for prediction of pharmacokinetics. My objective was to develop a PBPK model for describing the pharmacokinetics of Lee 1599 in rats and mice, and perform human pharmacokinetics predictions in order to address the

hypothesis that systemic exposures efficacious in mice are feasible to be achieved in humans.

The pharmacokinetics of Lee 1599 in rats were well described by the optimized PBPK model. The predicted systemic exposure, clearance and volume of distribution were within 10% of their observed values. The model was subsequently qualified by reasonably predicting murine pharmacokinetic behavior. The subsequently predicted, dose normalized human clearance and volume of distribution were as expected lower than those found in rats and mice. An IV dose of 7.5 mg/kg and 27.5 mg/kg administered once daily was predicted to match the efficacious exposure observed in mice after SC administration of 50 mg/kg and 200 mg/kg respectively, and appears to be achievable in patients.

In conclusion, translational PK/PD approaches have been successfully used for further the further development and characterization of the spectinamide lead compounds Lee 1599 and Lee 1810. The results from the above studies will be helpful in identifying and optimizing dosing regimens which can strike a balance between bacterial count reduction, adverse effects, and emergence of resistance. Pulmonary delivery offers an innovative solution to overcome the limitation of poor oral bioavailability of spectinamides, and also opens up new opportunities to further improve efficacy. PBPK-modeling based interspecies scaling suggests that therapeutically effective exposures can be achieved with doses that are feasible to be administered to humans.

LIST OF REFERENCES

1. Ventola, C.L., *The antibiotic resistance crisis: part 1: causes and threats.* P T, 2015. **40**(4): p. 277-83.
2. Ventola, C.L., *The antibiotic resistance crisis: part 2: management strategies and new agents.* P T, 2015. **40**(5): p. 344-52.
3. Nielsen, E.I. and L.E. Friberg, *Pharmacokinetic-pharmacodynamic modeling of antibacterial drugs.* Pharmacol Rev, 2013. **65**(3): p. 1053-90.
4. Clewe, O., et al., *A multistate tuberculosis pharmacometric model: a framework for studying anti-tubercular drug effects in vitro.* J Antimicrob Chemother, 2016. **71**(4): p. 964-74.
5. Bergen, P.J., et al., *Comparison of once-, twice- and thrice-daily dosing of colistin on antibacterial effect and emergence of resistance: studies with Pseudomonas aeruginosa in an in vitro pharmacodynamic model.* J Antimicrob Chemother, 2008. **61**(3): p. 636-42.
6. Rathi, C., R.E. Lee, and B. Meibohm, *Translational PK/PD of anti-infective therapeutics.* Drug Discov Today Technol, 2016. **21-22**: p. 41-49.
7. Trivedi, A., R.E. Lee, and B. Meibohm, *Applications of pharmacometrics in the clinical development and pharmacotherapy of anti-infectives.* Expert Rev Clin Pharmacol, 2013. **6**(2): p. 159-70.
8. Wu, B., S.K.B. Sy, and H. Derendorf, *Principles of Applied Pharmacokinetic–Pharmacodynamic Modeling*, in *Fundamentals of Antimicrobial Pharmacokinetics and Pharmacodynamics*, A.A. Vinks, H. Derendorf, and W.J. Mouton, Editors. 2014, Springer New York: New York, NY. p. 63-79.
9. Nielsen, E.I., O. Cars, and L.E. Friberg, *Pharmacokinetic/pharmacodynamic (PK/PD) indices of antibiotics predicted by a semimechanistic PKPD model: a step toward model-based dose optimization.* Antimicrob Agents Chemother, 2011. **55**(10): p. 4619-30.
10. Craig, W.A., J. Redington, and S.C. Ebert, *Pharmacodynamics of amikacin in vitro and in mouse thigh and lung infections.* J Antimicrob Chemother, 1991. **27 Suppl C**: p. 29-40.
11. Kristoffersson, A.N., et al., *Simulation-Based Evaluation of PK/PD Indices for Meropenem Across Patient Groups and Experimental Designs.* Pharm Res, 2016. **33**(5): p. 1115-25.
12. Vaddady, P.K., R.E. Lee, and B. Meibohm, *In vitro pharmacokinetic/pharmacodynamic models in anti-infective drug development: focus on TB.* Future Med Chem, 2010. **2**(8): p. 1355-69.
13. Czock, D. and F. Keller, *Mechanism-based pharmacokinetic-pharmacodynamic modeling of antimicrobial drug effects.* J Pharmacokinet Pharmacodyn, 2007. **34**(6): p. 727-51.
14. Mouton, J.W. and A.A. Vinks, *Pharmacokinetic/pharmacodynamic modelling of antibacterials in vitro and in vivo using bacterial growth and kill kinetics: the minimum inhibitory concentration versus stationary concentration.* Clin Pharmacokinet, 2005. **44**(2): p. 201-10.

15. Campion, J.J., et al., *Pharmacodynamic modeling of the evolution of levofloxacin resistance in Staphylococcus aureus.* Antimicrob Agents Chemother, 2005. **49**(6): p. 2189-99.
16. Meagher, A.K., et al., *Novel pharmacokinetic-pharmacodynamic model for prediction of outcomes with an extended-release formulation of ciprofloxacin.* Antimicrob Agents Chemother, 2004. **48**(6): p. 2061-8.
17. Nielsen, E.I., et al., *Semimechanistic pharmacokinetic/pharmacodynamic model for assessment of activity of antibacterial agents from time-kill curve experiments.* Antimicrob Agents Chemother, 2007. **51**(1): p. 128-36.
18. Nolting, A., et al., *Pharmacokinetic-pharmacodynamic modeling of the antibiotic effect of piperacillin in vitro.* Pharm Res, 1996. **13**(1): p. 91-6.
19. Budha, N.R., et al., *A simple in vitro PK/PD model system to determine time-kill curves of drugs against Mycobacteria.* Tuberculosis (Edinb), 2009. **89**(5): p. 378-85.
20. Patel, N., et al., *Determination of antibiotic dosage adjustments in patients with renal impairment: elements for success.* J Antimicrob Chemother, 2010. **65**(11): p. 2285-90.
21. Gonzalez, D., et al., *The effect of critical illness on drug distribution.* Curr Pharm Biotechnol, 2011. **12**(12): p. 2030-6.
22. Zeitlinger, M.A., et al., *Plasma concentrations might lead to overestimation of target site activity of piperacillin in patients with sepsis.* J Antimicrob Chemother, 2005. **56**(4): p. 703-8.
23. Mueller, M., A. de la Pena, and H. Derendorf, *Issues in pharmacokinetics and pharmacodynamics of anti-infective agents: kill curves versus MIC.* Antimicrob Agents Chemother, 2004. **48**(2): p. 369-77.
24. Rodvold, K.A., L. Yoo, and J.M. George, *Penetration of anti-infective agents into pulmonary epithelial lining fluid: focus on antifungal, antitubercular and miscellaneous anti-infective agents.* Clin Pharmacokinet, 2011. **50**(11): p. 689-704.
25. Mingeot-Leclercq, M.P. and P.M. Tulkens, *Aminoglycosides: nephrotoxicity.* Antimicrob Agents Chemother, 1999. **43**(5): p. 1003-12.
26. Joukhadar, C., H. Derendorf, and M. Muller, *Microdialysis. A novel tool for clinical studies of anti-infective agents.* Eur J Clin Pharmacol, 2001. **57**(3): p. 211-9.
27. Edginton, A.N., et al., *Defining the role of macrophages in local moxifloxacin tissue concentrations using biopsy data and whole-body physiologically based pharmacokinetic modelling.* Clin Pharmacokinet, 2009. **48**(3): p. 181-7.
28. Rowland, M., C. Peck, and G. Tucker, *Physiologically-based pharmacokinetics in drug development and regulatory science.* Annu Rev Pharmacol Toxicol, 2011. **51**: p. 45-73.
29. Gaohua, L., et al., *Development of a Multicompartment Permeability-Limited Lung PBPK Model and Its Application in Predicting Pulmonary Pharmacokinetics of Antituberculosis Drugs.* CPT Pharmacometrics Syst Pharmacol, 2015. **4**(10): p. 605-13.
30. Jumbe, N.L.n.S. and G.L. Drusano, *A Model-Based PK/PD Antimicrobial Chemotherapy Drug Development Platform to Simultaneously Combat Infectious*

Diseases and Drug Resistance, in *Clinical Trial Simulations: Applications and Trends*, C.H.H. Kimko and C.C. Peck, Editors. 2011, Springer New York: New York, NY. p. 251-279.
31. Upton, R.N. and D.R. Mould, *Basic concepts in population modeling, simulation, and model-based drug development: part 3-introduction to pharmacodynamic modeling methods.* CPT Pharmacometrics Syst Pharmacol, 2014. **3**: p. e88.
32. Greco, W.R., H.S. Park, and Y.M. Rustum, *Application of a new approach for the quantitation of drug synergism to the combination of cis-diamminedichloroplatinum and 1-beta-D-arabinofuranosylcytosine.* Cancer Res, 1990. **50**(17): p. 5318-27.
33. Greco, W.R., G. Bravo, and J.C. Parsons, *The search for synergy: a critical review from a response surface perspective.* Pharmacol Rev, 1995. **47**(2): p. 331-85.
34. Zhuang, L., et al., *Evaluation of in vitro synergy between vertilmicin and ceftazidime against Pseudomonas aeruginosa using a semi-mechanistic pharmacokinetic/pharmacodynamic model.* Int J Antimicrob Agents, 2015. **45**(2): p. 151-60.
35. Tam, V.H., *Suppressing Resistance Development*, in *Fundamentals of Antimicrobial Pharmacokinetics and Pharmacodynamics*, A.A. Vinks, H. Derendorf, and W.J. Mouton, Editors. 2014, Springer New York: New York, NY. p. 135-151.
36. Li, R.C., D.E. Nix, and J.J. Schentag, *Pharmacodynamic modeling of bacterial kinetics: beta-lactam antibiotics against Escherichia coli.* J Pharm Sci, 1994. **83**(7): p. 970-5.
37. Yang, Z., et al., *Mechanisms of protection against Clostridium difficile infection by the monoclonal antitoxin antibodies actoxumab and bezlotoxumab.* Infect Immun, 2015. **83**(2): p. 822-31.
38. Tam, V.H., A.N. Schilling, and M. Nikolaou, *Modelling time-kill studies to discern the pharmacodynamics of meropenem.* J Antimicrob Chemother, 2005. **55**(5): p. 699-706.
39. Jacobs, M., et al., *Distinguishing Antimicrobial Models with Different Resistance Mechanisms via Population Pharmacodynamic Modeling.* PLoS Comput Biol, 2016. **12**(3): p. e1004782.
40. Udekwu, K.I., et al., *Functional relationship between bacterial cell density and the efficacy of antibiotics.* J Antimicrob Chemother, 2009. **63**(4): p. 745-57.
41. Hengzhuang, W., et al., *High beta-lactamase levels change the pharmacodynamics of beta-lactam antibiotics in Pseudomonas aeruginosa biofilms.* Antimicrob Agents Chemother, 2013. **57**(1): p. 196-204.
42. Bulitta, J.B., et al., *Development and qualification of a pharmacodynamic model for the pronounced inoculum effect of ceftazidime against Pseudomonas aeruginosa.* Antimicrob Agents Chemother, 2009. **53**(1): p. 46-56.
43. Andes, D. and W.A. Craig, *In vivo pharmacodynamic activity of the glycopeptide dalbavancin.* Antimicrob Agents Chemother, 2007. **51**(5): p. 1633-42.
44. Drusano, G.L., et al., *Impact of burden on granulocyte clearance of bacteria in a mouse thigh infection model.* Antimicrob Agents Chemother, 2010. **54**(10): p. 4368-72.

45. Guo, B., et al., *Quantitative impact of neutrophils on bacterial clearance in a murine pneumonia model.* Antimicrob Agents Chemother, 2011. **55**(10): p. 4601-5.
46. Drusano, G.L., et al., *Use of preclinical data for selection of a phase II/III dose for evernimicin and identification of a preclinical MIC breakpoint.* Antimicrob Agents Chemother, 2001. **45**(1): p. 13-22.
47. Svensson, R.J. and U. Simonsson, *Application of the Multistate Tuberculosis Pharmacometric Model in Patients With Rifampicin-Treated Pulmonary Tuberculosis.* CPT Pharmacometrics Syst Pharmacol, 2016. **5**(5): p. 264-73.
48. Danhof, M., et al., *Mechanism-based pharmacokinetic-pharmacodynamic (PK-PD) modeling in translational drug research.* Trends Pharmacol Sci, 2008. **29**(4): p. 186-91.
49. Zumla , A., et al., *Tuberculosis.* New England Journal of Medicine, 2013. **368**(8): p. 745-755.
50. Organization, W.H., *Global tuberculosis report 2012*. 2012: World Health Organization.
51. Nguta, J.M., et al., *Current perspectives in drug discovery against tuberculosis from natural products.* International Journal of Mycobacteriology, 2015. **4**(3): p. 165-183.
52. Lee, R.E., et al., *Spectinamides: a new class of semisynthetic antituberculosis agents that overcome native drug efflux.* Nat Med, 2014. **20**(2): p. 152-8.
53. Liu, J., et al., *Structure–Activity Relationships of Spectinamide Antituberculosis Agents: A Dissection of Ribosomal Inhibition and Native Efflux Avoidance Contributions.* ACS Infectious Diseases, 2016.
54. Liu, J., et al., *The Structure-Activity Relationships of Spectinamide Antituberculosis agents; a Dissection of Ribosomal Inhibition and Native Efflux Avoidance Contributions.* ACS Infectious Diseases, 2016.
55. Malfatti, M.A., et al., *Use of microdosing and accelerator mass spectrometry to evaluate the pharmacokinetic linearity of a novel tricyclic GyrB/ParE inhibitor in rats.* Antimicrob Agents Chemother, 2014. **58**(11): p. 6477-83.
56. McLeay, S.C., et al., *Population pharmacokinetics of bedaquiline (TMC207), a novel antituberculosis drug.* Antimicrob Agents Chemother, 2014. **58**(9): p. 5315-24.
57. Rifat, D., D.A. Belchis, and P.C. Karakousis, *senX3-independent contribution of regX3 to Mycobacterium tuberculosis virulence.* BMC Microbiol, 2014. **14**: p. 265.
58. Dunphy, K.Y., et al., *Attenuation of Mycobacterium tuberculosis functionally disrupted in a fatty acyl-coenzyme A synthetase gene fadD5.* J Infect Dis, 2010. **201**(8): p. 1232-9.
59. Tischler, A.D., et al., *Mycobacterium tuberculosis requires phosphate-responsive gene regulation to resist host immunity.* Infect Immun, 2013. **81**(1): p. 317-28.
60. Kelley, C.L. and F.M. Collins, *Growth of a highly virulent strain of Mycobacterium tuberculosis in mice of differing susceptibility to tuberculous challenge.* Tuber Lung Dis, 1999. **79**(6): p. 367-70.
61. Ghosh, S., et al., *Phenotypic heterogeneity in mycobacterial stringent response.* BMC Syst Biol, 2011. **5**: p. 18.

62. Jacobs, W.R., et al., *Attenuated Mycobacterium tuberculosis vaccines*. 2010, Google Patents.
63. Ette, E.I., et al., *Analysis of animal pharmacokinetic data: performance of the one point per animal design.* J Pharmacokinet Biopharm, 1995. **23**(6): p. 551-66.
64. Mohamed, A.F., et al., *Pharmacokinetic-pharmacodynamic model for gentamicin and its adaptive resistance with predictions of dosing schedules in newborn infants.* Antimicrob Agents Chemother, 2012. **56**(1): p. 179-88.
65. Meibohm, B. and H. Derendorf, *Pharmacokinetic/pharmacodynamic studies in drug product development.* J Pharm Sci, 2002. **91**(1): p. 18-31.
66. Madhura, D.B., R. Lee, and B. Meibohm, *Pharmacokinetic profile of spectinomycin in rats.* Pharmazie, 2013. **68**(8): p. 675-6.
67. Ladigina, G.A. and M.A. Vladimirsky, *The comparative pharmacokinetics of 3H-dihydrostreptomycin in solution and liposomal form in normal and Mycobacterium tuberculosis infected mice.* Biomed Pharmacother, 1986. **40**(10): p. 416-20.
68. Walubo, A., et al., *The disposition of antituberculous drugs in plasma of elderly patients. II. Isoniazid, rifampicin and pyrazinamide.* Methods Find Exp Clin Pharmacol, 1991. **13**(8): p. 551-6.
69. Loos, U., et al., *Pharmacokinetics of oral and intravenous rifampicin during chronic administration.* Klin Wochenschr, 1985. **63**(23): p. 1205-11.
70. Tesseromatis, C., et al., *Acute-phase proteins: alpha-1-acid glycoprotein*. 2011: INTECH Open Access Publisher.
71. Mansor, S.M., et al., *Effect of Plasmodium falciparum malaria infection on the plasma concentration of alpha 1-acid glycoprotein and the binding of quinine in Malawian children.* Br J Clin Pharmacol, 1991. **32**(3): p. 317-21.
72. Piafsky , K.M., et al., *Increased Plasma Protein Binding of Propranolol and Chlorpromazine Mediated by Disease-Induced Elevations of Plasma α1 Acid Glycoprotein.* New England Journal of Medicine, 1978. **299**(26): p. 1435-1439.
73. Elsheikh, H.A., et al., *Effect of dehydration on the pharmacokinetics of oxytetracycline hydrochloride administered intravenously in goats (Capra hircus).* Gen Pharmacol, 1998. **31**(3): p. 455-8.
74. Regoes, R.R., et al., *Pharmacodynamic functions: a multiparameter approach to the design of antibiotic treatment regimens.* Antimicrob Agents Chemother, 2004. **48**(10): p. 3670-6.
75. Madhura, D.B., et al., *Tissue Penetration of a Novel Spectinamide Antibiotic for the Treatment of Tuberculosis.* AAPS J, 2016. **18**(3): p. 788-91.
76. Munoz-Elias, E.J., et al., *Replication dynamics of Mycobacterium tuberculosis in chronically infected mice.* Infect Immun, 2005. **73**(1): p. 546-51.
77. Gill, W.P., et al., *A replication clock for Mycobacterium tuberculosis.* Nat Med, 2009. **15**(2): p. 211-4.
78. Eldar, A. and M.B. Elowitz, *Functional roles for noise in genetic circuits.* Nature, 2010. **467**(7312): p. 167-73.
79. Zhang, Y., W.W. Yew, and M.R. Barer, *Targeting persisters for tuberculosis control.* Antimicrob Agents Chemother, 2012. **56**(5): p. 2223-30.

80. Manina, G., N. Dhar, and J.D. McKinney, *Stress and host immunity amplify Mycobacterium tuberculosis phenotypic heterogeneity and induce nongrowing metabolically active forms.* Cell Host Microbe, 2015. **17**(1): p. 32-46.
81. Manina, G. and J.D. McKinney, *A single-cell perspective on non-growing but metabolically active (NGMA) bacteria.* Curr Top Microbiol Immunol, 2013. **374**: p. 135-61.
82. Helaine, S. and E. Kugelberg, *Bacterial persisters: formation, eradication, and experimental systems.* Trends Microbiol, 2014. **22**(7): p. 417-24.
83. Silver, R.F., Q. Li, and J.J. Ellner, *Expression of virulence of Mycobacterium tuberculosis within human monocytes: virulence correlates with intracellular growth and induction of tumor necrosis factor alpha but not with evasion of lymphocyte-dependent monocyte effector functions.* Infect Immun, 1998. **66**(3): p. 1190-9.
84. Paul, S., P. Laochumroonvorapong, and G. Kaplan, *Comparable growth of virulent and avirulent Mycobacterium tuberculosis in human macrophages in vitro.* J Infect Dis, 1996. **174**(1): p. 105-12.
85. Jayaram, R., et al., *Pharmacokinetics-pharmacodynamics of rifampin in an aerosol infection model of tuberculosis.* Antimicrob Agents Chemother, 2003. **47**(7): p. 2118-24.
86. Chanwong, S., et al., *Intracellular growth and drug susceptibility of Mycobacterium tuberculosis in macrophages.* Tuberculosis (Edinb), 2007. **87**(2): p. 130-3.
87. Barry, C.E., 3rd, et al., *The spectrum of latent tuberculosis: rethinking the biology and intervention strategies.* Nat Rev Microbiol, 2009. **7**(12): p. 845-55.
88. Venisse, N., et al., *Mechanism-based pharmacokinetic-pharmacodynamic models of in vitro fungistatic and fungicidal effects against Candida albicans.* Antimicrob Agents Chemother, 2008. **52**(3): p. 937-43.
89. Dartois, V. and C.E. Barry, 3rd, *A medicinal chemists' guide to the unique difficulties of lead optimization for tuberculosis.* Bioorg Med Chem Lett, 2013. **23**(17): p. 4741-50.
90. Zhang, Y., *Persisters, persistent infections and the Yin-Yang model.* Emerg Microbes Infect, 2014. **3**(1): p. e3.
91. Zhang, Y., et al., *Mode of action of pyrazinamide: disruption of Mycobacterium tuberculosis membrane transport and energetics by pyrazinoic acid.* J Antimicrob Chemother, 2003. **52**(5): p. 790-5.
92. Hoiby, N., *Recent advances in the treatment of Pseudomonas aeruginosa infections in cystic fibrosis.* BMC Med, 2011. **9**: p. 32.
93. Azoicai, D. and S.A. Antoniu, *MP-376 (Aeroquin) for chronic Pseudomonas aeruginosa infections.* Expert Opin Investig Drugs, 2013. **22**(2): p. 267-76.
94. Antoniu, S.A. and I. Cojocaru, *Inhaled colistin for lower respiratory tract infections.* Expert Opin Drug Deliv, 2012. **9**(3): p. 333-42.
95. Muttil, P., C. Wang, and A.J. Hickey, *Inhaled drug delivery for tuberculosis therapy.* Pharm Res, 2009. **26**(11): p. 2401-16.
96. Sosnik, A., et al., *New old challenges in tuberculosis: potentially effective nanotechnologies in drug delivery.* Adv Drug Deliv Rev, 2010. **62**(4-5): p. 547-59.

97. Pinheiro, M., et al., *Liposomes as drug delivery systems for the treatment of TB.* Nanomedicine (Lond), 2011. **6**(8): p. 1413-28.
98. Dudley, M.N., J. Loutit, and D.C. Griffith, *Aerosol antibiotics: considerations in pharmacological and clinical evaluation.* Curr Opin Biotechnol, 2008. **19**(6): p. 637-43.
99. Gonzalez-Juarrero, M., et al., *Mouse model for efficacy testing of antituberculosis agents via intrapulmonary delivery.* Antimicrob Agents Chemother, 2012. **56**(7): p. 3957-9.
100. Cooper, A.E., D. Ferguson, and K. Grime, *Optimisation of DMPK by the inhaled route: challenges and approaches.* Curr Drug Metab, 2012. **13**(4): p. 457-73.
101. Hastedt, J.E., et al., *Scope and relevance of a pulmonary biopharmaceutical classification system AAPS/FDA/USP Workshop March 16-17th, 2015 in Baltimore, MD.* AAPS Open, 2016. **2**(1): p. 1-20.
102. Brown, R.A., Jr. and L.S. Schanker, *Absorption of aerosolized drugs from the rat lung.* Drug Metab Dispos, 1983. **11**(4): p. 355-60.
103. Cambier, C.J., et al., *Mycobacteria manipulate macrophage recruitment through coordinated use of membrane lipids.* Nature, 2014. **505**(7482): p. 218-22.
104. Nichols, D.J., et al., *Pharmacokinetics and fate of 3H-trospectomycin sulphate, a novel aminocyclitol antibiotic, in male and female rats.* Xenobiotica, 1991. **21**(7): p. 827-37.
105. Yokogawa, K., et al., *Influence of lipophilicity and lysosomal accumulation on tissue distribution kinetics of basic drugs: a physiologically based pharmacokinetic model.* Methods Find Exp Clin Pharmacol, 2002. **24**(2): p. 81-93.
106. Misra, A., P.B. Fourie, and A.J. Hickey, *Delivery Systems for Tuberculosis Prevention and Treatment*. 2016: John Wiley & Sons.
107. Odenholt-Tornqvist, I., *Pharmacodynamics of beta-lactam antibiotics. Studies on the paradoxical and postantibiotic effects in vitro and in an animal model.* Scand J Infect Dis Suppl, 1989. **58**: p. 1-55.
108. Craig, W., et al., *Key pharmacokinetic parameters of antibiotic efficacy in experimental animal infections.* J Drug Dev, 1988. **1**(Suppl 3): p. 7-15.
109. Benet, L.Z., F. Broccatelli, and T.I. Oprea, *BDDCS applied to over 900 drugs.* AAPS J, 2011. **13**(4): p. 519-47.
110. Lopez-Novoa, J.M., et al., *New insights into the mechanism of aminoglycoside nephrotoxicity: an integrative point of view.* Kidney Int, 2011. **79**(1): p. 33-45.
111. Suzuki, T., et al., *Megalin contributes to kidney accumulation and nephrotoxicity of colistin.* Antimicrob Agents Chemother, 2013. **57**(12): p. 6319-24.
112. Cox, J.W., et al., *Distribution and disposition of trospectomycin sulfate in the in vivo rat, perfused rat liver, and cultured rat hepatocytes.* Drug Metab Dispos, 1990. **18**(5): p. 726-31.
113. Paul, S.M., et al., *How to improve R&D productivity: the pharmaceutical industry's grand challenge.* Nat Rev Drug Discov, 2010. **9**(3): p. 203-14.
114. Riviere, J.E., et al., *Interspecies allometric analysis of the comparative pharmacokinetics of 44 drugs across veterinary and laboratory animal species.* J Vet Pharmacol Ther, 1997. **20**(6): p. 453-63.

115. Mahmood, I. and J.D. Balian, *Interspecies scaling: predicting clearance of drugs in humans. Three different approaches.* Xenobiotica, 1996. **26**(9): p. 887-95.
116. Jones, H. and K. Rowland-Yeo, *Basic concepts in physiologically based pharmacokinetic modeling in drug discovery and development.* CPT Pharmacometrics Syst Pharmacol, 2013. **2**: p. e63.
117. Baxter, L.T., et al., *Biodistribution of monoclonal antibodies: scale-up from mouse to human using a physiologically based pharmacokinetic model.* Cancer Res, 1995. **55**(20): p. 4611-22.
118. Hall, C., et al., *Interspecies scaling in pharmacokinetics: a novel whole-body physiologically based modeling framework to discover drug biodistribution mechanisms in vivo.* J Pharm Sci, 2012. **101**(3): p. 1221-41.
119. Bradshaw-Pierce, E.L., S.G. Eckhardt, and D.L. Gustafson, *A physiologically based pharmacokinetic model of docetaxel disposition: from mouse to man.* Clin Cancer Res, 2007. **13**(9): p. 2768-76.
120. Jamei, M., G.L. Dickinson, and A. Rostami-Hodjegan, *A framework for assessing inter-individual variability in pharmacokinetics using virtual human populations and integrating general knowledge of physical chemistry, biology, anatomy, physiology and genetics: A tale of 'bottom-up' vs 'top-down' recognition of covariates.* Drug Metab Pharmacokinet, 2009. **24**(1): p. 53-75.
121. Eissing, T., et al., *A computational systems biology software platform for multiscale modeling and simulation: integrating whole-body physiology, disease biology, and molecular reaction networks.* Front Physiol, 2011. **2**: p. 4.
122. Reisfeld, B., et al., *A physiologically based pharmacokinetic model for capreomycin.* Antimicrob Agents Chemother, 2012. **56**(2): p. 926-34.
123. Krauss, M., et al., *Bayesian Population Physiologically-Based Pharmacokinetic (PBPK) Approach for a Physiologically Realistic Characterization of Interindividual Variability in Clinically Relevant Populations.* PLoS One, 2015. **10**(10): p. e0139423.
124. Paine, S.W., et al., *Prediction of human renal clearance from preclinical species for a diverse set of drugs that exhibit both active secretion and net reabsorption.* Drug Metab Dispos, 2011. **39**(6): p. 1008-13.
125. Agasti, T., *Textbook of Anesthesia for Postgraduates*. 2010: JP Medical Ltd.
126. Hsu, C.H., et al., *Measurement of renal blood flow in the rat.* Proc Soc Exp Biol Med, 1975. **149**(2): p. 470-2.
127. Vaddady, V.N.R.P.K., *Pharmacokinetic and Pharmacodynamic Studies of a Novel Spectinamide Series of Antituberculosis Agents*. 2011.
128. Kato, Y., et al., *Gender difference in the urinary excretion of organic anions in rats.* J Pharmacol Exp Ther, 2002. **302**(2): p. 483-9.
129. Kusumi, R., C. Metzler, and R. Fass, *Pharmacokinetics of spectinomycin in volunteers with renal insufficiency.* Chemotherapy, 1981. **27**(2): p. 95-8.
130. Kojima, M., et al., *Single-dose treatment of male patients with gonococcal urethritis using 2g spectinomycin: microbiological and clinical evaluations.* Int J Antimicrob Agents, 2008. **32**(1): p. 50-4.

VITA

Chetan Rathi was born in 1985 in Kolkata, India. He obtained his Bachelor in Pharmacy degree from the Birla Institute of Technology, Mesra, India in 2008, and Masters of Science (Pharm.) from National Institute of Pharmaceutical Education and Research (NIPER), Rae Bareli in 2010. Following that he worked as a Trainee in Drug Metabolism Pharmacokinetics and Clinical Pharmacology division at Advinus Therapeutics, Bangalore, India. Then he received the French Government Scholarship to pursue an internship from the University of Poitiers, Poitiers, France from May - August 2011. Consequently, he joined the PhD Program in Pharmaceutical Science at the University of Tennessee Health Science Center (UTHSC) in fall of 2011 with Dr. Bernd Meibohm as his major advisor. While at UTHSC, he received a number of accolades including the following: Travelship awards to attend the Interscience Conference on Antimicrobial Agents and Chemotherapy at Denver in 2013 and American Conference on Pharmacometrics at Crystal City in 2015; Best poster presentation award in the Graduate Research Day organized by UTHSC, Memphis in 2014 and was inducted into the Rho Chi Pharmacy Honor Society for his academic excellence in 2014. In 2016, he won the Merck Biopharma Innovation Cup organized near Frankfurt, Germany and was also selected to participate at the "Journey through Science Day" organized by PepsiCo and New York Academy of Sciences. During his graduate school he published three book chapters and six peer-reviewed articles in scientific journals and also presented at a number of scientific meetings. During his PhD, he was involved with various leadership positions such as Chair of the American Association of Pharmaceutical Scientist (AAPS) Student Chapter at the University of Tennessee in 2014 and Student Representative for the Pharmacometrics Focus Group in AAPS.